



**Deutsche Geodätische Kommission**  
bei der Bayerischen Akademie der Wissenschaften

---

Reihe C

Dissertationen

Heft Nr. 621

**Mehdi Ravanbakhsh**

**Road Junction Extraction  
from High Resolution Aerial Images Assisted  
by Topographic Database Information**

**München 2008**

**Verlag der Bayerischen Akademie der Wissenschaften  
in Kommission beim Verlag C. H. Beck**

**ISSN 0065-5325**

**ISBN 978-3-7696-5033-4**

---

**Diese Arbeit ist gleichzeitig veröffentlicht in:  
Wissenschaftliche Arbeiten der Fachrichtung Geodäsie und Geoinformatik der Leibniz Universität Hannover  
ISSN 0174-1454, Nr. 273, Hannover 2008**





Deutsche Geodätische Kommission  
bei der Bayerischen Akademie der Wissenschaften

---

Reihe C

Dissertationen

Heft Nr. 621

Road Junction Extraction  
from High Resolution Aerial Images Assisted  
by Topographic Database Information

Von der Fakultät für Bauingenieurwesen und Geodäsie  
der Gottfried Wilhelm Leibniz Universität Hannover  
zur Erlangung des Grades  
Doktor-Ingenieur (Dr.-Ing.)  
genehmigte Dissertation

von

Dipl.-Ing. Mehdi Ravanbakhsh  
geboren am 12.05.1973 in Bojnord, Iran

München 2008

Verlag der Bayerischen Akademie der Wissenschaften  
in Kommission bei der C. H. Beck'schen Verlagsbuchhandlung München

ISSN 0065-5325

ISBN 978-3-7696-5033-4

---

Diese Arbeit ist gleichzeitig veröffentlicht in:  
Wissenschaftliche Arbeiten der Fachrichtung Geodäsie und Geoinformatik der Leibniz Universität Hannover  
ISSN 0174-1454, Nr. 273, Hannover 2008

Adresse der Deutschen Geodätischen Kommission:



Deutsche Geodätische Kommission

Alfons-Goppel-Straße 11 • D – 80 539 München  
Telefon +49 – 89 – 23 031 1113 • Telefax +49 – 89 – 23 031 -1283 / - 1100  
e-mail hornik@dgfi.badw.de • <http://www.dgk.badw.de>

Prüfungskommission

Vorsitzender: Univ.-Prof. Dr.-Ing. Steffen Schön  
Referent: Univ.-Prof. Dr.-Ing. habil. Christian Heipke  
Korreferenten: Univ.-Prof. Dr.-Ing. habil. Monika Sester  
Univ.-Prof. Dr.-Ing. habil. Helmut Mayer

Tag der mündlichen Prüfung: 09.06.2008

---

© 2008 Deutsche Geodätische Kommission, München

Alle Rechte vorbehalten. Ohne Genehmigung der Herausgeber ist es auch nicht gestattet,  
die Veröffentlichung oder Teile daraus auf photomechanischem Wege (Photokopie, Mikrokopie) zu vervielfältigen

## Summary

In this thesis a new approach for the automatic extraction of road junctions from high resolution aerial images by using an existing topographic database is presented. Road junctions are important components of a road network. However, they are usually not explicitly modeled in existing road extraction approaches. We model road junctions including roundabouts in detail as area objects with considering possible presence of traffic islands and develop an approach that combines a road extraction method with a novel snake model to capture the junction outline.

The information that is derived from the geospatial database includes geometric, radiometric, and topological characteristics of junctions. This information gives a rough idea of the junction and guides later processing steps.

Edges are detected and road segment hypotheses are generated using several geometric and radiometric criteria. Furthermore, road markings if present in the scene are detected in order to verify the obtained road segments. Road arms are obtained after road segments with similar geometric properties are linked. The resulting road arms supply initial conditions for our snake model.

We propose a novel snake model that employs the ziplock snake concept and whose external force field is a combination of the balloon force and the GVF (Gradient Vector Flow). Furthermore, the balloon force is associated with the junction shape features incorporated into our snake model implicitly. The GVF increases the capture range of snakes to draw deforming curves from far distances. The balloon force helps to overcome high variation of curvature in the junction border and lack of sufficient contrast between the junction central area and the surrounding. Before snake optimization starts, initial snakes are modified based on the junction geometrical shape to assure a close initialization. The junction outline is delineated without being overly affected by various kinds of disturbances due to the strong internal snake energy. The obtained junction outline defines an area within which possibly traffic islands exist.

A level set approach is used to detect islands. The initial level set function is constructed from the segmented image. In order to ensure that the evolved curves will converge to the island boundaries, some geometric and topological constraints are introduced based on the characteristics of traffic islands.

This type of initialization and evolution strategy, however, is not effective for roundabouts. Instead, the central island of a roundabout is detected using level sets with a hybrid evolution strategy. This hybrid strategy includes two steps: shrinking and iterative expansion curve evolution. Eventually, the central island is obtained after some post-processing. Since the shape of roundabouts is heavily affected by the shape of its central island, we need initially to detect the central island based on which the snake's external force field is modified. The snake's external force field is modified using the GVF of a signed distance function. The modified external force field is intended to pull the snakes toward the roundabout outline regardless of where they are located initially. The reason is that force arrows at any location on the modified force field point to the roundabout outline.

Many tests of the approach have been carried out using high resolution images taken over rural and suburban areas of Germany. The obtained results demonstrate the potential and suitability of the approach for the automatic extraction of road junctions.

**Keywords:** Road junction, active contours, topographic database, image analysis



## Zusammenfassung

In dieser Dissertation wird ein neuer Ansatz für die automatische Extraktion von Kreuzungen aus hochauflösenden Luftbildern mit Hilfe topografischer Daten präsentiert. Kreuzungen sind wichtige Komponenten eines Straßennetzes. Sie sind aber in aktuellen Straßenextraktionsansätzen in der Regel nicht explizit modelliert. Wir modellieren Kreuzungen und Kreisverkehre im Detail als Flächen-Objekte unter Berücksichtigung von Verkehrsinseln und entwickeln einen Ansatz, der eine Straßenextraktionsmethode mit einem neuartigen „Snake Model“ zur Erfassung der Kreuzung kombiniert, um äußere Grenzen von Kreuzungen zu extrahieren.

Die Informationen aus der geografischen Datenbank umfassen geometrische, radiometrische und topologische Eigenschaften der Kreuzungen. Diese Informationen ergeben eine grobe Vorstellung der Kreuzung und steuern spätere Arbeitsschritte.

Kanten werden detektiert und Straßensegment-Hypothesen werden mit Hilfe von verschiedenen geometrischen und radiometrischen Kriterien generiert. Außerdem werden Straßen-Markierungen extrahiert, wenn sie in der Szene existieren, um Straßensegmente zu überprüfen. Segmente mit ähnlichen geometrischen Eigenschaften werden miteinander zu Straßenarmen verknüpft. Die resultierenden Straßenarme liefern die Anfangsbedingungen für das „Snake Model“.

Wir schlagen ein neuartiges „Snake Model“ vor, welches das „Ziplock Snake“- Konzept verwendet und dessen äußeres Kraftfeld eine Kombination aus Ballonkraft und GVF (Gradient Vector Flow) ist. Außerdem ist die Ballonkraft verbunden mit den Kreuzungsformmerkmalen, die implizit in unserem „Snake Model“ enthalten sind. Das GVF erhöht die Erfassungsreichweite der „Snake“, um die Kurven aus größeren Abständen anzuziehen. Die Ballonkraft hilft bei hoher Variation der Krümmung am Rand der Kreuzung und bei Mangel an Kontrast zwischen der Kreuzungsmittle und der Umgebung. Bevor die Snake-Optimierung startet, werden die Start-Snakes basierend auf der geometrischen Form der Kreuzung modifiziert, um eine nahe Initialisierung sicherzustellen. Der Rand der Kreuzung wird wegen der starken inneren Energie der Snakes beschrieben, ohne durch die verschiedenen Störungen beeinflusst zu werden. Die resultierende Außenlinie grenzt eine Fläche ab, auf der möglicherweise Verkehrsinseln existieren.

Ein Level-Set-(Niveaumengen-)Ansatz wird verwendet, um Inseln zu detektieren. Die anfängliche Level-Set-Funktion wird aus dem segmentierten Bild abgeleitet. Um sicher zu stellen, dass die entwickelten Kurven sich um Inseln zusammen schließen, werden geometrische und topologische Bedingungen basierend auf Eigenschaften von Verkehrsinseln eingeführt.

Diese Initialisierungs- und Entwicklungsstrategie ist aber nicht effektiv für Verkehrskreisel. Stattdessen wird die Mittelinsel eines Kreisels durch Level Sets mit hybrider Entwicklungsstrategie detektiert. Diese hybride Strategie umfasst zwei Schritte: Schrumpfung und wiederholte Ausdehnung der Kurvenentwicklung. Schließlich wird nach einigen Nachverarbeitungsschritten die Mittelinsel erreicht. Da die Form eines Kreisels stark von der Form der Mittelinsel beeinflusst ist, müssen wir erst die Mittelinsel detektieren und darauf basierend das äußere Kraftfeld der Snakes modifizieren. Das äußere Kraftfeld der Snakes wird durch den GVF einer vorzeichenbehafteten Distanzfunktion modifiziert. Das modifizierte äußere Kraftfeld ist dazu bestimmt, die Snakes in Richtung des Kreiselsrands zu ziehen, ohne Rücksicht darauf, wo sie am Anfang sind. Der Grund ist, dass die Kraftpfeile in jeder Position des modifizierten Kraftfelds auf den Kreiselsrand zeigen.

Viele Tests des Ansatzes sind mit hochauflösenden Bildern von ländlichen und Stadtgebieten in Deutschland ausgeführt worden. Das erreichte Resultat demonstriert das Potenzial und die Angemessenheit des Ansatzes für die automatische Extraktion von Straßenkreuzungen.

**Stichworte:** Straßenkreuzung, aktive Konturen, topografische Datenbank, Bildanalyse

# TABLE OF CONTENTS

<b>1. Introduction .....</b>	<b>9</b>
1.1. Motivation.....	9
1.2. Objective and Focus .....	9
1.3. Organization of the Thesis and Main Contributions.....	10
<b>2. State of the Art.....</b>	<b>11</b>
2.1. Parametric Active Contours.....	11
2.1.1 Traditional Snake .....	11
2.1.2 Snake Growing.....	12
2.1.3 Balloon Snake .....	13
2.1.4 Ziplock Snake .....	14
2.1.5 GVF Snake.....	15
2.1.6 Discussion .....	16
2.2. Level Sets.....	17
2.2.1 Introduction.....	17
2.2.2 The Level Set Equation.....	18
2.2.3 Signed Distance Functions and Re-initialization.....	19
2.2.4 Variational Level Sets.....	20
2.3. Review of Road Junction Extraction .....	23
2.3.1 Road Junction as a Point Object .....	23
2.3.2 Road Junction as an Area Object.....	24
2.3.3 Discussion.....	25
<b>3. A New Approach to Road Junction Extraction .....</b>	<b>27</b>
3.1. Road Junction Classes .....	27
3.2. Road Junction Model.....	27
3.3. Workflow for Simple and Complex Junctions .....	27
3.3.1 Pre-analysis of Geospatial Database.....	29
3.3.2 Road Arm Extraction .....	29
3.3.3 Road Junction Reconstruction .....	32
3.3.4 Extraction of Islands .....	40
3.4. Workflow for Roundabout.....	48
3.4.1 Pre-analysis of Geospatial Database.....	48
3.4.2 Extraction of Central Island .....	49
3.4.3 Road Arm Extraction .....	54
3.4.4 Roundabout Reconstruction.....	54
<b>4. Results and Evaluation.....</b>	<b>59</b>
4.1. Test Images and Context .....	59
4.2. Extraction Results .....	59
4.2.1 Road Arms .....	59
4.2.2 Simple Junctions .....	59
4.2.3 Complex Junctions.....	67
4.3. Quantitative External Evaluation.....	79
4.3.1 Border of junctions .....	80
4.3.2 Islands .....	81
4.4. Summary.....	82

<b>5. Conclusions and Outlook</b> .....	<b>83</b>
5.1. Discussion and Conclusions .....	83
5.2. Outlook .....	85
<b>References</b> .....	<b>87</b>
<b>Acknowledgements</b> .....	<b>89</b>
<b>Curriculum Vitae</b> .....	<b>90</b>

# 1. Introduction

## 1.1. Motivation

The need for accurate, up-to-date and detailed geospatial databases is growing rapidly. This requires faster processing of high resolution image data by using efficient image analysis tools in order to supply high quality of topographic information. However, the traditional manual extraction of topographic information from high resolution imagery is costly and time-consuming. As a result, automation is seen as a promising solution to these problems. Although many automatic approaches have been developed for the extraction of man-made objects from aerial images, only some of them provide good quality results. The problem for automatic data extraction lies mostly in the complex content of aerial images. To ease the automation of an object extraction task, prior information coming from an existing geospatial database can be used.

Geospatial databases contain various man-made objects among which roads are of special importance as they are used in a variety of applications such as car navigation, traffic and fleet management, intelligent transportation systems, internet-based map services, etc. Road junctions are important components of a road network, so their detailed modeling and accurate extraction can contribute to road network extraction systems.

## 1.2. Objective and Focus

The primary objective of this thesis is the detailed modeling of road junctions and the development of an approach for their automatic extraction from high resolution aerial imagery by using an existing geospatial database. Junctions are mainly extracted in the context of automatic road extraction. Most of the existing approaches initially concentrate on road extraction for creating the road network. Subsequently, extraction of road junctions is achieved by perceptual grouping of road hypotheses. In such approaches, junctions are mostly regarded as a point object. In contrast, there are a few methods that treat junctions as planar objects without considering small traffic islands. In high resolution aerial images, sufficient information is provided to consider the junction as an area object. As is shown in Figure 1-1, the modeling of junctions as point objects does not always reflect the required degree of detail. As a result, detailed modeling of junctions is needed for data acquisition purposes in large scales. Since some junctions contain islands in their centre, a detailed junction model needs to consider the possible existence of these small islands.



Figure 1-1: Superimposition of vector data on a high resolution aerial image.

Although this work focuses on road junctions, crossing roads are first extracted in an area near the junction center in order to provide a rather close initialization for our snake method.

The extraction of road junctions is a complicated task [Mayer et al. 1998]. The reason is that fewer constraints can be applied on the junction shape than on roads, because the junction outline as well as traffic islands is of diverse geometrical shapes including various degrees of curvature. Furthermore, in the junction central area, a variety of disturbing features as well as small islands are often present, which precludes the application of radiometric constraints. In recent years, active contours have emerged as a powerful tool for semi-automated object modeling. They are especially useful for delineating objects that are difficult to be modeled with rigid geometric primitives. The potential usefulness of active contours to capture road junctions is a central goal pursued in this thesis.

In this thesis, road junctions and roundabouts are modeled in detail as area objects. Furthermore, the possible presence of islands is considered in our proposed junction model. We develop an approach that combines a road extraction method with a new snake model to capture the junction outline. Furthermore, a level set formulation in conjunction with a selection procedure is exploited to detect islands (Fig. 1-2).

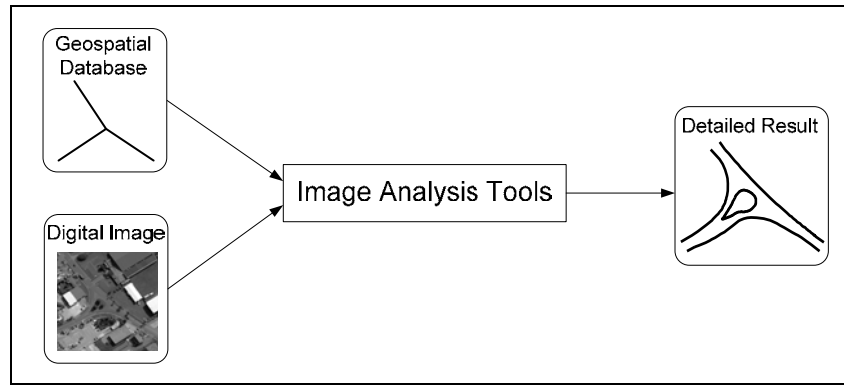


Figure 1-2: Diagram displaying input and output of the approach.

The difficulty of our task depends on the complexity of the scene. In urban areas, many disturbing factors exist often resulting in poor extraction results of junctions as well as roads. Therefore, we choose images taken from suburban and rural areas of Germany. We believe that these road junctions are sufficiently complex to illustrate the potential of our developed methods. It is not the purpose of this thesis to develop approaches to identify crossing roads that do not exist in the vector data. Therefore, geospatial database updating is not discussed. Furthermore, we model junctions as planar objects to avoid possible further complexity concerning the inclusion of three dimensional junctions. Hence, road interchanges are not considered in our work.

### 1.3. Organization of the Thesis and Main Contributions

In Chapter 2, we review the existing literature relating to our topic. We begin by discussing active contour models including snakes and level sets. Only those snake models used in our work are illustrated. The exploited level set formulation is described as well. We then review previous work on road junction extraction.

In Chapter 3, our strategy for automatic extraction of road junctions is described in detail. Road junctions are categorized and modeled, followed by the introduction of the workflow designed for simple and complex junctions. Then, we also propose a new snake-based approach for detecting road junction borders using the road arm extraction results. Furthermore, a level set method combined with a procedure to select the converged curves to islands is introduced, with the aim to capture small islands appearing in complex junctions. Finally, we present our workflow for the extraction of roundabouts as a subclass of complex junctions and introduce a modified external force field designed to capture the roundabout outline. In Chapter 4, extensive tests of our approach are reported and the effect of various kinds of disturbances on the results is illustrated. Furthermore, the exploited evaluation scheme is introduced and applied to road junction components separately. The last chapter, Chapter 5, gives conclusions about the developed approach, and finally recommendations for further research are given.

The main contributions presented in this thesis are as follows:

- Use of an existing geospatial database to guide the extraction process  
Vector data is analyzed and the information used to guide the extraction of road arms is derived. Furthermore, the search space is restricted and the number of crossing roads is determined.
- Development of a novel snake-based method to capture road junction outline  
Our snake method integrates the ziplock snake with a new external force field. The external force field is a combination of the Gradient Vector Flow (GVF) and the Balloon force. The Balloon force is activated in association with the shape information of junction borders. Furthermore, various kinds of disturbances in the junction central area and on the outline of the junction are resolved using strong internal snake energy.
- Development of a level set method with a region-based initialization to detect traffic islands in complex junctions  
A level set method whose initialization is based on segmented regions is used. The main features of this region-based initialization are efficiency in practice and speed in convergence.
- Development of a hybrid evolution strategy to capture central islands in roundabouts  
The level set evolution strategy is carried out in a combined shrinking and iterative expansion manner to detect central islands. The advantages are elimination of disturbing effects such as vehicles, and other obstacles inside the central island hindering the curve's movement
- Shape-based modification of the external force field  
The external force field in the snake method is modified based on the shape of central islands by introducing a signed distance function. The modified external force field helps to overcome various kinds of disturbances and to delineate the roundabout outline also in presence of a high variation of curvature

## 2. State of the Art

### 2.1. Parametric Active Contours

Parametric active contours or snakes are curves that deform within digital images to recover object shapes. All properties and the behavior of snakes are specified through a function called energy functional. A partial differential equation controlling the snake causes it to evolve so as to reduce its energy. Snakes have been successful in performing a variety of image analysis tasks such as edge detection, corner detection, motion tracking, and stereo matching. Active contour models can be classified according to several different criteria. In this work, they are classified as either parametric active contours (this section) or level sets (section 2.2) according to their representation and implementation. In particular, parametric active contours are represented explicitly as parameterized curve.

#### 2.1.1 Traditional Snake

Snakes were first introduced by Kass, Witkin and Terzopoulos [1988] as an active contour model for segmentation. They represent a contour in two dimensions as an explicit polygon or spline. This contour is physically modeled as a collection of points connected by springs and thin plates. Spring forces ensure that the control points remain well-spaced while thin-plate spline forces ensure that the contour itself is smooth. External forces derived from the image move the contour toward nearby edges.

Traditional snakes are defined as parametric curves  $v(s) = (x(s), y(s))$  where  $s$  is the curve length and  $x$  and  $y$  are the image coordinates of the 2D-curve. In the simplest way the image or external energy can be written as the image intensity itself with  $E_{img}(v(s)) = I(v(s))$  where  $I$  represents the image. In the literature, the image energy is often defined as

$$E_{img}(v(s)) = -|\nabla I(v(s))|^2 \quad (2.1)$$

where  $|\nabla I(v(s))|$  is the norm or magnitude of the gradient image at the coordinates  $x(s)$  and  $y(s)$ . Often the image energy  $E_{img}(v(s))$  is computed by the values  $|\nabla I(v(s))|$ , taken from pre-computed gradient magnitude images along the line segments that connect the vertices of the contour. The image energy is designed to attract the contour toward nearby edges or other features of interest.

The internal energy is given by

$$E_{int}(V(s)) = \frac{1}{2} \left[ \alpha(s) |v_s(s)|^2 + \beta(s) |v_{ss}(s)|^2 \right] \quad (2.2)$$

where  $|v_s(s)|^2$  represents the spring force as the contour is stretched or compressed, and  $|v_{ss}(s)|^2$  represents the spline force causing the contour to become smooth.  $\alpha$  and  $\beta$  are weights controlling the effect of these terms on the regularity of the contour at each point. Kass et al. [1988] proposed the following energy functional for image segmentation using snakes:

$$\begin{aligned} E_{snake} &= \int_0^1 E_{snake}(v(s)) ds \\ &= \int_0^1 E_{int}(v(s)) + E_{img}(v(s)) + E_{con}(v(s)) ds \end{aligned} \quad (2.3)$$

where  $E_{int}$  is the internal energy of the snake including contour spacing and smoothing,  $E_{img}$  represents the information derived from the image and  $E_{con}$  is the external constraint energy imposed during user interaction. In this thesis, only internal and image energy,  $E_{int}$  and  $E_{img}$ , are exploited.

The substitution of (2.1) and (2.2) into the equation of the snake's total energy (2.3) excluding  $E_{con}$  results in

$$E_{snake} = \int_0^1 \frac{1}{2} \alpha |v_s|^2 + \frac{1}{2} \beta |v_{ss}|^2 - |\nabla I(v(s))|^2 ds \quad (2.4)$$

A minimum of the total energy in Equation (2.4) can be derived by solving the Euler equation:

$$-\frac{\partial}{\partial s}(\alpha v_s) + \frac{\partial^2}{\partial s^2}(\beta v_{ss}) + \frac{\partial E_{img}(v(s))}{\partial v(s)} = -\alpha v_{ss}(s) + \beta v_{ssss}(s) + \frac{\partial E_{img}(v(s))}{\partial v(s)} = 0 \quad (2.5)$$

where  $v(s)$  stands for either  $x(s)$  or  $y(s)$ .  $v_{ss}$  and  $v_{ssss}$  denote the second and fourth derivative of  $v$  respectively. The derivatives are approximated with finite differences since they can not be computed analytically. Converted to vector notation with  $v_i = (x_i, y_i)$  and  $\partial E_{img}(v(s)) / \partial v(s) = P_v(v)$  the Euler equations read as follows:

$$\begin{aligned} &\alpha_i(v_i - v_{i-1}) - \alpha_{i+1}(v_{i+1} - v_i) + \beta_{i-1}(v_{i-2} - 2v_{i-1} + v_i) \\ &- 2\beta_i(v_{i-1} - 2v_i + v_{i+1}) + \beta_{i+1}(v_i - 2v_{i+1} + v_{i+2}) + P_v(v) = 0 \end{aligned} \quad (2.6)$$

These equations can be rewritten in matrix form as

$$Kv + P_v(v) = 0 \quad (2.7)$$

where  $K$  is a pentadiagonal matrix whose band is:

$$[\beta_{i-1}; -\alpha_i - 2\beta_{i-1} - 2\beta_i; (\alpha_i + \alpha_{i+1}) + \beta_{i-1} + 4\beta_i + \beta_{i+1}; -\alpha_{i+1} - 2\beta_i - 2\beta_{i+1}; \beta_{i+1}] \quad (2.8)$$

As it can be seen,  $K$  depends only on the functions  $\alpha$  and  $\beta$ .

Equation (2.7) can be solved iteratively by introducing a step size  $\gamma$  multiplied with the negative time derivatives  $\partial v / \partial t$ , which are discretized by  $v_t - v_{t-1}$ . It is assumed that  $P_v(v)$  is constant during a time step, i.e.  $P_v(v_t) \approx P_v(v_{t-1})$ , yielding an explicit Euler step regarding the image energy. In contrast, the internal energy is an implicit Euler step due to its specification by the banded matrix  $K$ . The resulting equation reads

$$Kv_t + P_v(v_{t-1}) = -\gamma(v_t - v_{t-1}) \quad (2.9)$$

The time derivatives vanish at equilibrium ending up in Equation (2.10):

$$v^{[t]} = (K + \gamma I)^{-1} * (\gamma v^{[t-1]} - \kappa P_v|_{v^{[t-1]}}) \quad (2.10)$$

where  $I$  is the identity matrix and  $\kappa$  is an additional parameter in order to control the weight between internal and image energy.

Snakes may model both open and closed geometric objects. They may be used to represent contours in two or more dimensions or surfaces in three dimensions. Unfortunately, it is difficult to model topological changes in snakes. Existing methods must either explicitly detect self-intersections of the contour, which becomes increasingly complicated in higher dimensions, or maintain a binary array labeling each image point as inside or outside of the contour. Furthermore, traditional snakes are sensitive to noise and need a close initialization. To overcome these limitations several approaches were proposed like snake growing [Berger and Mohr 1990], balloon forces [Cohen 1991] and ziplock snakes [Neuenschwander et al. 1997].

### 2.1.2 Snake Growing

Berger and Mohr [1990] proposed a method eliminate the initialization and convergence problem based on local features whereas the traditional snakes take into account a global point of view. This method is based on an open snake model with free extremities. The outlining process starts with a short snake which already lies in the influence area of a contour. The snake boundary conditions are set in such a way that both end points are free. At the endpoints, two new snake segments are attached, hence increasing the snake length. This new snake is then subject to a fixed number of traditional optimization steps. Let  $S_0$  be the initial snake, a short description of the approach follows:

When  $S_0$  lies in the vicinity of the contour, the iterative method will converge quickly, especially if  $S_0$  is short whereas longer segments are located farther from the contour. Therefore a created sequence  $S_1, \dots, S_n$  of snakes will yield contours  $Cont_1, \dots, Cont_n$  whose lengths are increasing. Since only smoothed edges are searched, it seems natural to take as  $S_{i+1}$  the curve inferred from  $Cont_i$  by lengthening its extremities in the direction of the tangents. In each sequence the traditional Euler equations are iteratively solved leading to convergence toward contours.

The major advantage of snake growing is that at each step, the iterative method reaches equilibrium. Furthermore, the snake growing method allows to detect easily rectilinear edges and contours which present small curvature variations, as lengthening is quite close to the contour. We implemented the idea of the snake growing to explore its potential for

delineation of road junctions with the exception that the end point of each snake segment that is close to an already optimized snake is fixed (Fig. 2-1).

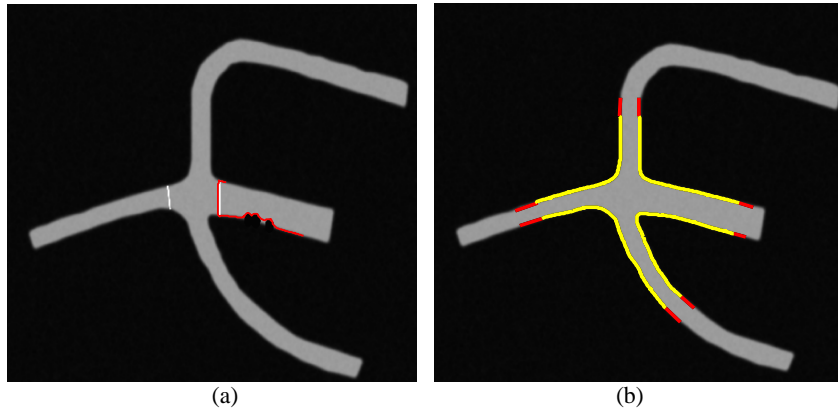


Figure 2-1: The snake growing method for road junction detection. (a) The result of snake growing optimization, which is trapped by shadows and misled by road markings to the wrong direction. (b) A correct result when disturbing features are not present. Red lines represent road sides which are fixed. Yellow curves represent the optimized snakes to the boundaries.

As can be seen snake growing can be easily confused by artificially created shadows and road markings which are often present in the image, whereas in areas with no disturbing factors a good result can be obtained. Another drawback of this method is that no stop mechanism exists when the snake goes in a false direction.

### 2.1.3 Balloon Snake

Resolving the formulation described in traditional snakes (Eq. 2.10) leads to two difficulties caused by time and space discretization due to the image energy. These problems can occur even if the initial guess is close to an edge. If the time discretization step is too large, the curve may move too far across the desired boundary and never come back. This problem can be avoided by manually tuning the time step but this is not very practical in large scale applications. On the other hand, if we choose the time step to be small enough, for example never larger than one pixel, then the problem is avoided, but only very few high gradient points will attract the curve and the small values of the image force field will not affect the curve much. One way to improve the model was proposed by Cohen [1991]. Instead of acting on the time step, he modified the force field  $P_v$  by normalizing it, taking  $P_v = -k \frac{\nabla E_{image}}{|\nabla E_{image}|}$ , where the product of the time step

and  $k$  is on the order of the pixel size. Since the magnitude of  $P_v$  is about one pixel, when a point of the curve is close to an edge point, it is attracted to the edge and stabilized there. Thus smaller and larger gradients have the same influence on the curve. However, it happens often that, due to noise, some isolated points are gradient maxima and can stop the curve when it passes by. To solve the problems just mentioned, Cohen [1991] added another force which makes the contour have a more dynamic behavior. The curve is considered as a balloon (in 2D) that is inflated. He added to the previous forces a pressure force pushing outside. The force now becomes

$$P_v = k_1 \vec{n}(s) - k_2 \frac{\nabla E_{image}}{|\nabla E_{image}|} \quad (2.11)$$

where  $\vec{n}(s)$  is the normal unit vector to the curve at point  $v(s)$  pointing outward and  $k_1$  is the amplitude of the force. Now, the curve expands until it is stopped by edges as before, but since there is a pressure force, if the edge is too weak, the curve can pass through this edge. If the curve runs into an isolated point, it tends to create a tangent discontinuity at this point. The smoothing effect with the help of the inflation force removes the discontinuity and the curve passes through these points (Fig. 2-2). The balloon force can be applied on open and closed snakes. In case of an open curve, the balloon force pushes the curve in the direction of normal vector until it is stopped by strong edge points.

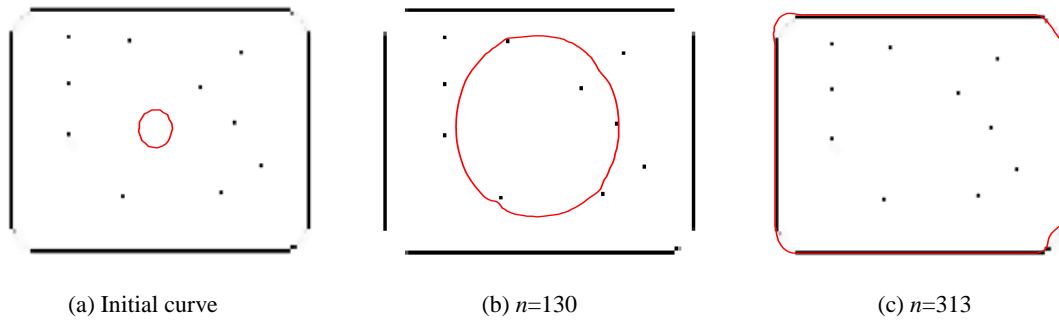


Figure 2-2: Evolution of the balloon curve to detect a rectangle. (a) Initial curve as a circle. (b) Intermediate curve. (c) The curve after inflating the balloon.  $n$  denotes the number of iterations here and in all figures in this thesis.

### 2.1.4 Ziplock Snake

Like the growing snake, the ziplock snake [Neuenschwander et al. 1997] was proposed to solve the problem of poor initialization encountered with the traditional snake. It allows for an initialization of the snake by only its endpoints. Starting with correctly initialized endpoints of a searched contour, the optimization progresses from these points toward the center of the snake propagating the edge information along the curve in the following manner:

A ziplock snake consists of two parts: an active part and a passive part (Fig. 2-3). The two parts are separated by moving force boundaries, and the active part is further divided into two segments, indicated as head and tail respectively. The initial positions of the head and tail segments are specified by an operator or a preprocessing module. Unlike the procedure for a traditional snake, the external force derived from the image is turned on only for the active parts. Thus, the movement of passive vertices is not affected by any image forces. Starting from two short pieces, the active part is iteratively optimized to image features, and the force boundaries are progressively moved toward the center of the snake. Each time that the force boundaries are moved, the passive part is re-interpolated using the position and direction of the end vertices of the two active segments. Optimization is stopped when force boundaries meet each other.

We call the external force used in the ziplock snake *traditional force field*. Ziplock snakes need far less initialization effort and are less affected by the shrinking effect from the internal energy term ( $|v_s(s)|^2$  in Equation 2.2). Furthermore, the computational process is more robust because the active part whose energy is minimized is always quite close to the contour being extracted.

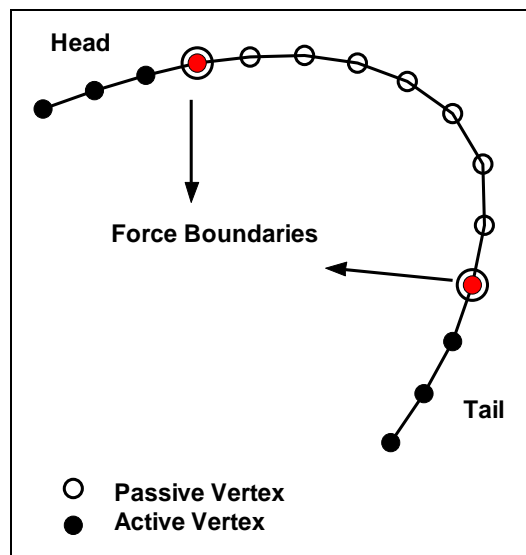


Figure 2-3: Evolution of a ziplock snake. A ziplock snake, fixed at head and tail, consists of two parts, the active and the passive vertices. These parts are separated by moving force boundaries. The active parts of the snake consist of head and tail segments.

Both the growing snake and the ziplock snake adopt a local adaptation technique in order to deform the snake model to keep it on the pre-selected contour. Nevertheless, there are two clear advantages for the ziplock. Viewing both systems as differential equation solvers, the growing snakes are clearly formulated as an initial value problem, while the ziplock snakes solve a boundary value problem. With essentially the same underlying differential equation, a boundary value solution is expected to be significantly more stable numerically [Neuenschwander et al. 1997]. Secondly, the decision procedure adopted by the growing snake model to determine when it must be extended is both complex and arbitrarily tuned, with a number of adjustable thresholds. By contrast, there are only two decision procedures in the ziplock snake

process: the first to decide when to move the force boundary, and the second to decide when the final fully active snake has been stabilized.

### 2.1.5 GVF Snake

The energy model proposed by Cohen [1991] solved some of the problems of the original model but not all. If the object to be segmented has a concavity, neither of the previously proposed models manages to force the snake into the concavity. As can be seen in Fig. 2-4-e, although the image forces point correctly toward the object boundary, the range of the force field is small. Therefore, the curve is “pulled apart” but not made to progress into the concavity.

The problem is not solved by Cohen’s model since it only changes the magnitude and not the range of the force. Xu and Prince [1998] suggested a new force to solve the problem. The underlying mathematical premise for this new force comes from the Helmholtz theorem, which states that each general static vector field can be decomposed into two components: an irrotational field and a solenoidal component. The traditional force field used for snakes is irrotational since it is the gradient of a scalar potential function derived from the image.

Xu and Prince [1998] proposed to generate a more general field by allowing the possibility that it comprises both an irrotational component and a solenoidal component. This new force has both the desired properties of both a large capture range and the presence of forces that point into boundary concavities. The GVF field points toward the object boundary when very near to the boundary, but varies smoothly over homogeneous image regions, extending to the image border (Fig. 2-4-c).

The GVF is defined to be the vector field  $G(x, y) = (u(x, y), v(x, y))$  that minimizes the energy functional:

$$E = \iint \mu(u_x^2 + u_y^2 + v_x^2 + v_y^2) + |\nabla f|^2 |G - \nabla f|^2 dx dy \quad (2.12)$$

where  $f(x, y)$  is derived from the image having the property that it is larger near the image edges. It is seen that when  $|\nabla f|$  is small, the energy is dominated by sum of the squares of the partial derivatives of the vector field, yielding a slowly-varying field when minimizing  $E$ . On the other hand, when  $|\nabla f|$  is large, the second term dominates the integrand and is minimized by setting  $G = \nabla f$ . This produces the desired effect of keeping  $G$  nearly equal to the gradient of the edge image when it is large, but forcing the field to be slowly-varying in homogeneous regions. The parameter  $\mu$  is a regularization parameter governing the tradeoff between the first term and the second term in the integrand. It should be set according to the amount of noise present in the image. More noise requires a larger  $\mu$ .

Using the *calculus of variation* [Courant and Hilbert 1953], it can be shown that the GVF can be found by solving the following Euler equations:

$$\begin{aligned} \mu \nabla^2 u - (u - f_x)(f_x^2 + f_y^2) &= 0 \\ \mu \nabla^2 v - (v - f_y)(f_x^2 + f_y^2) &= 0 \end{aligned} \quad (2.13)$$

where  $\nabla^2$  is the Laplacian operator.

It is noted that in homogeneous regions, the second term of both equations is zero as the gradient of  $f(x, y)$  is zero. Therefore, within these regions,  $u$  and  $v$  are each determined by Laplace's equation. This results in a type of “filling-in” of information taken from the boundaries of the region.

Equations (2.13) can be solved by treating  $u$  and  $v$  as functions of time [Xu et al. 1998]

$$\begin{aligned} u_t(x, y, t) &= \mu \nabla^2 u_{t-1}(x, y, t) - (u_{t-1}(x, y, t) - f_x(x, y)) \cdot (f_x(x, y)^2 + f_y(x, y)^2) \\ v_t(x, y, t) &= \mu \nabla^2 v_{t-1}(x, y, t) - (v_{t-1}(x, y, t) - f_y(x, y)) \cdot (f_x(x, y)^2 + f_y(x, y)^2) \end{aligned} \quad (2.14)$$

The steady-state solution (as  $t \rightarrow \infty$ ) of these linear parabolic equations is the desired solution of the Euler equations (2.13).

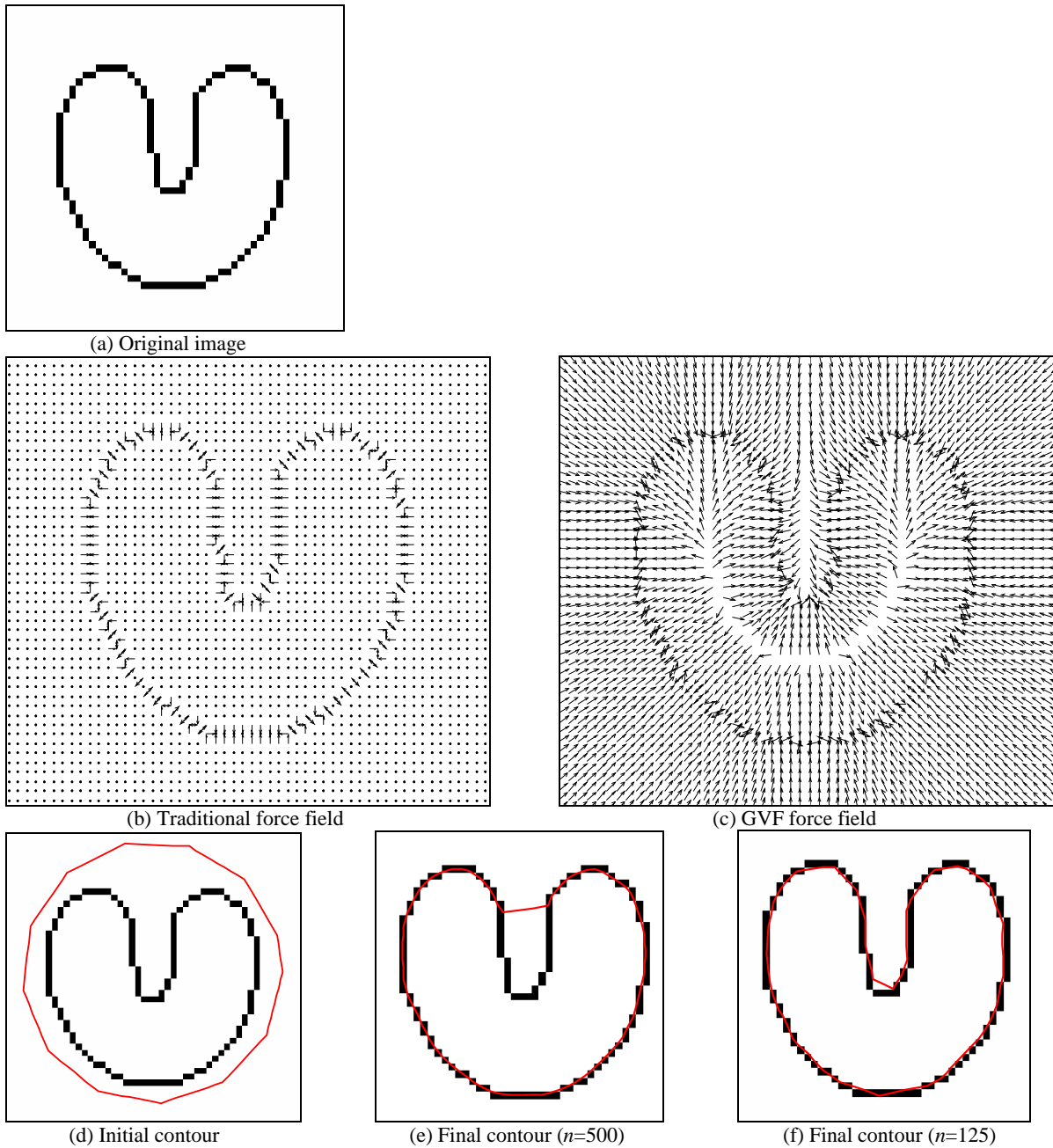


Figure 2-4: Comparison between the traditional force field and the GVF field. (a) Shows the original image. (b) Tradition force field computed by taking the gradient of the edge image  $f$ . (c) GVF vectors are depicted, which are present in concave region and in regions far from the boundaries. (d) Initial contour enclosed the object of interest. (e) The result of applying a snake with the traditional force field. The curve is unable to move into concave boundary region. (f) The result when GVF force field is used. The curve moves into the concave boundary region with smaller number of iterations.

After  $G(x, y)$  including its constituents  $u$  and  $v$  are computed, it is replaced with the external force field in Equation (2.10), yielding

$$v^{[t]} = (K + \gamma I)^{-1} * (\gamma v^{[t-1]} - \kappa G|_{v^{[t-1]}}) \quad (2.15)$$

The parametric curves solving the above dynamic equation are called *GVF snakes*.

### 2.1.6 Discussion

We started from the model of Kass et al. [1988] whose evolution equations are based on a Lagrangian formulation, i.e. a parametric formulation of curve evolution. This model is sensitive to noise and a close initialization is necessary to detect boundaries correctly. The snake growing method [Berger and Mohr 1990] was proposed which allows detecting boundaries without providing a close initialization by considering local features. It is, however, sensitive to noise and

post-processing is necessary to stop the evolution, whereas in the ziplock approach [Neuenschwander et al. 1997], the most similar to the growing snake, this step is eliminated and termination of the evolution occurs when two force boundaries meet. Nevertheless both approaches are sensitive to disturbing features.

Cohen [1991] proposed to introduce a constant force in the direction normal to boundaries to remove the effect of noise and image anomalies. The two main reasons to use the balloon force are to significantly increase the speed of convergence towards the steady state solution and to allow the detection of non-convex objects. In addition to Cohen [1991], Xu et al. [1998] proposed a new external force field called Gradient Vector Flow (GVF) which allows the active contour to progress into concave boundary regions. Furthermore, the GVF contains a much larger capture range which attracts the snake even from far distances. Another drawback of the snake segmentation model is the dependence of the energy functional  $E_{snake}$  to the parameterization of the curve  $S$ , in other words,  $E_{snake}$  is not intrinsic. This means that different parameterizations of the curve may give different solutions for the same initial condition, which is not satisfactory. Furthermore, parametric active contours do not allow changes of topology in the case of closed curves, since the final curve has the same topology as the initial one. In other words, it is not possible to detect more than one object as we can see in Figure 2-5.

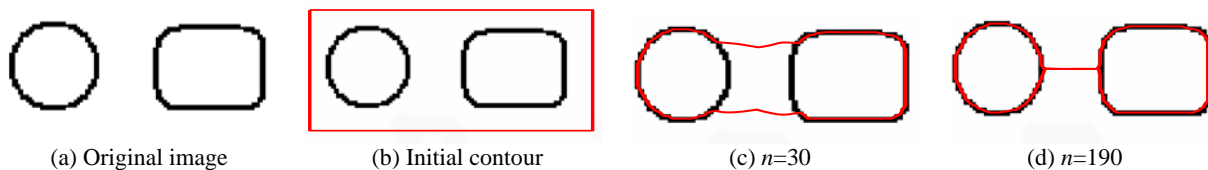


Figure 2-5: (a) Original image. (b) Initial closed contour situated around two objects. (c) Intermediate contour during the evolution. (d) Final curve that is converged to boundaries. It is proved that the snake model can not naturally change its topology during the evolution process since the final contour has captured only one object.

## 2.2. Level Sets

To overcome the problem of the changes of topology, Osher and Sethian [1988] proposed the *level set method*. This method has become a popular theoretical and numerical framework within image processing, fluid mechanics, graphics, computer vision etc. The level set method is basically used for tracking moving fronts by considering the front as the zero level set of an embedding function, called the level set function. In physics, numerous phenomena can be modeled with moving fronts propagated using a curvature dependent speed such as for example flame and wave propagation. Other applications are optimal path planning and noise removal. In image analysis it has become a widely used tool for segmentation. Depending on how the propagation speed of the front is defined, many features can be considered simultaneously such as edges, region statistics and shape and any kind of multidimensional data. Consideration of priori knowledge of shape for segmentation of partly occluded objects [Bresson et al. 2004] and texture segmentation [Bresson et al. 2005] are some other recent and very interesting approaches.

### 2.2.1 Introduction

The level set method is a theoretical and numerical tool for moving any kind of implicitly represented surfaces or interfaces. The core idea of the level set method is to implicitly represent an interface  $C$  as the set of zero values of an embedding function  $\phi$  (Detailed information about  $C$  and  $\phi$  can be found in the next section (2.2.2)). Such an implicit representation has numerous advantages over a parametrical approach. The most striking example is topological changes occurring during the propagation, typically when two flames burn together the evolving interfaces merge into one single propagating front. In Figure 2-6 it is shown how the level set method handles topology changes.

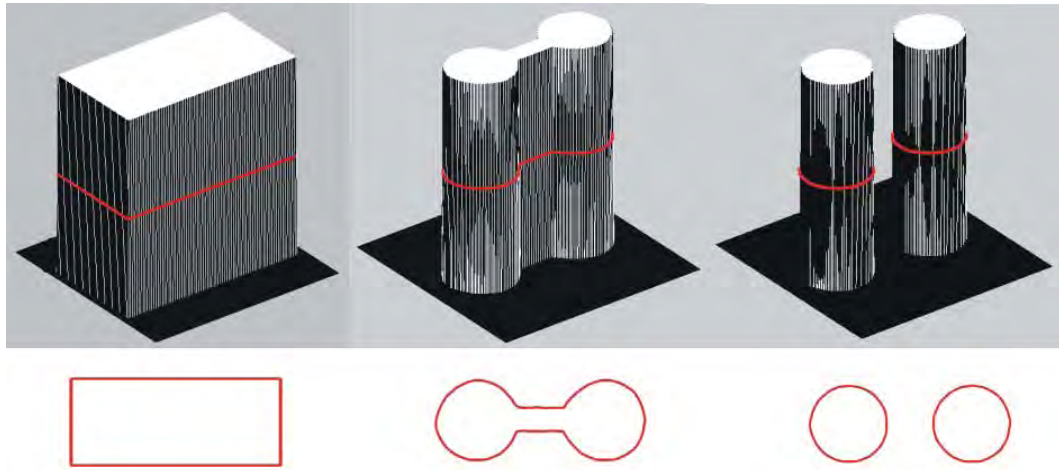


Figure 2-6: Natural change of topology in the level set framework. The top row presents the evolution of the embedding function ( $\phi$ ) and the bottom row shows the evolution of the associated curve or interfaces ( $C$ ).

The level set method can be applied to any kind of problem where an interface is moving with a certain speed defined on every point.

### 2.2.2 The Level Set Equation

Let an interface  $C$  be a curve as a boundary between two regions, one inside the boundary and another one outside the boundary. A level set function is constructed around the interface that constitutes the zero value of the embedding function,  $\phi$ , as can be seen in Figures 2-7-a and b. All other points of the level set function have the value of the Euclidean distance from that point to the closest point on the boundary  $d(x)$ . The distance is positive if this point is situated outside the bounded area and negative if it is situated inside. The definition is illustrated:

$$\phi(x) = \begin{cases} +d(x) & \text{if } x \text{ is outside } C \\ -d(x) & \text{if } x \text{ is inside } C \end{cases} \tag{2.16}$$

The use of the distance  $d(x)$  assures us that  $\phi$  does not become too flat or too steep near  $C$  and subsequently it can be differentiated across the interface with significantly higher confidence.

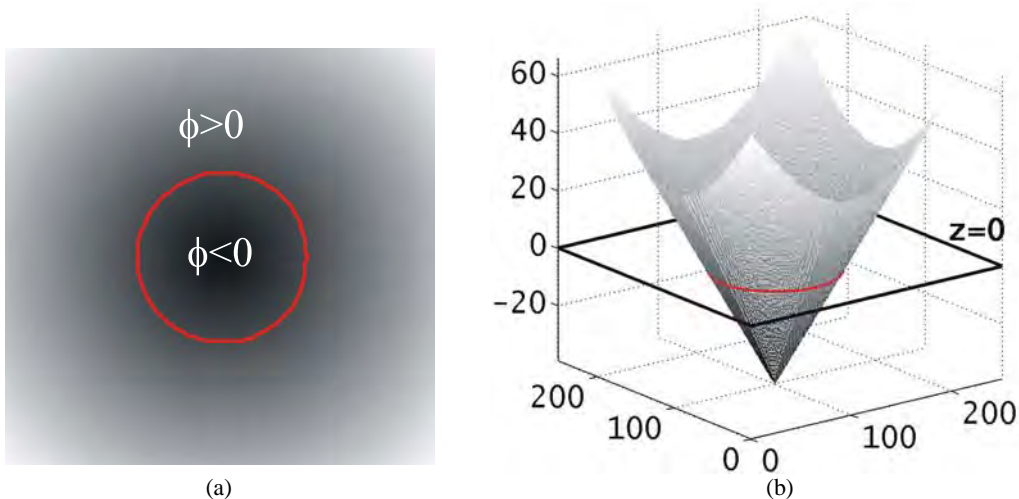


Figure 2-7: Illustrating level sets. (a) The level set function is constructed around the interface (red) such that it is negative inside and positive outside the curve. (b) A surface at zero level ( $z=0$ ) intersects the level set function, of which the interface is obtained.

The level set function will change with time according to the speed  $V$  and the interface is always constituted by the points where the level set function equals zero. The interface, embedded by the level set function,  $\phi$ , can be expressed as:

$$C = \{x \mid \phi(x) = 0\} \quad (2.17)$$

Introducing an artificial evolution time parameter  $t$ , we obtain the level set equation over time:

$$\phi(x(t), t) = 0 \quad (2.18)$$

where  $x(t)$  are the points of the level set function  $\phi$  at time  $t$ . The level set function is negative for the points lying inside the interface and positive for the points lying outside the interface.

Taking the time derivative of the level set, we obtain

$$\frac{\partial \phi}{\partial t} + \nabla \phi(x(t), t) \cdot \frac{dx}{dt} = 0 \quad (2.19)$$

Generally, the simplest way to move every point on the interface is to solve the ordinary differential equation

$$\begin{cases} \frac{\partial x}{\partial t} = V(x, t) \\ V(x, t) = V_n N + V_t T \end{cases} \quad (2.20)$$

where  $T$  and  $N$  are respectively the unit tangential and the outward/inward (arbitrary choice) unit normal to the curve in point  $x$  and  $V_n$  and  $V_t$  are respectively the normal and tangential velocities. In [Epstein and Gage 1987], it is shown that the geometry of the curve deformation is not affected by the tangential velocity  $V_t$ . This results to the fact that the tangential velocity does not change the geometry of the curve. Hence, the term related to  $V_t$  is omitted from Equation (2.20). Putting the velocity into Equation (2.19), we obtain:

$$\frac{\partial \phi}{\partial t} + \nabla \phi(x(t), t) \cdot (V_n N) = 0 \quad (2.21)$$

Since

$$\nabla \phi \cdot N = \nabla \phi \cdot \frac{\nabla \phi}{|\nabla \phi|} = \frac{|\nabla \phi|^2}{|\nabla \phi|} = |\nabla \phi| \quad (2.22)$$

We can rewrite Equation (2.21) as

$$\frac{\partial \phi}{\partial t} + V_n |\nabla \phi| = 0 \quad (2.23)$$

This Partial Differential Equation (PDE) is known as level set equation. It defines the motion of the interface by the evolution of the zero level set of  $\phi(t)$ .

Equation (2.23) assumes that the level set function  $\phi(t)$  is continuous with well defined gradients everywhere in the computational domain  $\Omega$ . However, to use these mathematical expressions on a computer, we need to discretize the function, only computing values at discrete points. These points are situated on a fixed coordinate system since the level set is a parameterization free formulation.

### 2.2.3 Signed Distance Functions and Re-initialization

As stated in the previous section, the level set function needs to be continuous with well defined gradients, in order to solve Equation (2.23). However, because of the spatial discretization, this requirement can be relaxed. More specifically, we require  $\phi$  to be *Lipschitz continuous*, satisfying the following condition:

$$\frac{|\phi(x_0) - \phi(x_1)|}{|x_0 - x_1|} \leq K \quad (2.24)$$

where  $K \geq 0$ . This means that the gradients of  $\phi$  can be discontinuous, if the rate of change of  $\phi$  is bounded by the finite *Lipschitz* constant  $K$ . This constant is affected by the numerical schemes used to solve the discretized equations. In order to assure stability,  $K$  needs to be approximately unity. As a result, Equation (2.24) can be rewritten

$$|\nabla\phi|=1 \quad (2.25)$$

Intuitively, this means that the level sets of  $\phi$  have a uniform density. In other words, as one walks in a direction orthogonal to the level set interface, the distance increases one unit each step. Combined with Equation (2.16), this means that  $\phi$  is a signed distance function. If  $|\nabla\phi|$  drifted away from one, the speed of the information flow would increase, implying that we need to evolve the PDE with smaller time steps. However, it is often more efficient to keep the time step fixed while making sure  $\phi$  approximately satisfies Equation (2.25). This process is called re-initialization and should be performed more or less frequently depending on how sensitive the discretization of the particular PDE is to numerical fluctuations. Re-initialization has been extensively used as a numerical remedy for maintaining stable curve evolution [Caselles et al. 1997, Malladi et al. 1995, Caselles et al. 1993]. Many proposed re-initialization schemes have an undesirable side effect of moving the zero level set away from its original location. It still remains a serious problem when and how to apply the re-initialization [Gomes and Faugeras 2000].

## 2.2.4 Variational Level Sets

Early level sets [Osher and Sethian 1988] are derived using Eulerian formulation that yields a certain evolution PDE of a parameterized curve. As an alternative, the evolution PDE of the level set function can be directly derived from the problem of minimizing certain energy functional defined on the level set function. This type of variational methods is known as variational level set methods [Vemuri and Chen 2003, Chan and Vese 2001]. Compared with pure PDE driven level set methods, the variational level set methods are more convenient and natural for incorporating additional information, such as region-based information [Chan and Vese 2001] and shape-prior information [Vemuri and Chen 2003], into energy functionals that are directly formulated in the level set domain, and therefore produce more robust results.

In this thesis, we use the variational formulation that forces the level set function to be close to a signed distance function, and therefore completely eliminates the need of the costly re-initialization procedure. This variational energy functional consists of an internal energy term and an external energy term, respectively. The internal energy term penalizes the deviation of the level set function from a signed distance function, whereas the external energy term drives the motion of the zero level set to the desired image features such as object boundaries. The resulting evolution of the level set function is the gradient flow that minimizes the overall energy functional.

It was shown in section (2.2.3) that a signed distance function must satisfy the property of  $|\nabla\phi|=1$  represented in Equation (2.25). Therefore, the following formula is proposed [Li et al. 2005]

$$P(\phi) = \int_{\Omega} \frac{1}{2} (|\nabla\phi| - 1)^2 dx dy \quad (2.26)$$

as the internal energy term, which penalizes the deviation of  $\phi$  from a signed distance function.  $P(\phi)$  is a metric to characterize how close a function  $\phi$  is to a signed distance function in an specified computational domain  $\Omega \subset R^2$ . Along with the functional  $P(\phi)$ , the following variational formulation is proposed

$$E(\phi) = \mu P(\phi) + E_m(\phi) \quad (2.27)$$

where  $\mu > 0$  is a parameter controlling the effect of penalizing the derivation of  $\phi$  from a signed distance function, and  $E_m(\phi)$  is a certain external energy that drives the motion of the zero level curve of  $\phi$ . Let  $I$  be an image, and  $g$  be the *edge indicator function* defined by

$$g = \frac{1}{1 + |\nabla G_{\sigma} * I|^2} \quad (2.28)$$

where  $G_{\sigma}$  is the Gaussian kernel with standard deviation  $\sigma$ .

An external energy for a function  $\phi(x, y)$  is defined by

$$E_m(\phi) = \lambda L_g(\phi) + \nu A_g(\phi) \quad (2.29)$$

where  $\lambda > 0$  and  $\nu$  is constant.  $E_m(\phi)$  is a function of parameters  $g$ ,  $\lambda$  and  $\nu$ .  $L_g(\phi)$  is a length term obtained by taking the *surface integral* (line in  $R^2$ ) of function  $g$  over the interface  $C$  :

$$L_g(\phi) = \int_{\Omega} g \hat{\delta}(\phi) dx dy \quad (2.30)$$

and  $A_g(\phi)$  is as an area term obtained by computing the *volume integral* (area in  $R^2$ ) of function  $g$  over the interior region  $\Omega_{\phi}^- = \{(x, y) | \phi(x, y) < 0\}$  [Osher and Fedkiw 2002] :

$$A_g(\phi) = \int_{\Omega} g H(-\phi) dx dy \quad (2.31)$$

where  $\hat{\delta}$  denote the *Dirac delta function*, and  $H$  is the *Heaviside function*.

The Heaviside function,  $H$ , is a discontinuous function whose value is zero for negative argument and one for positive argument

$$H(\phi) = \begin{cases} 0 & \text{if } \phi < 0 \\ 1 & \text{if } \phi \geq 0 \end{cases} \quad (2.32)$$

where  $\phi$  is a discrete variable.

By definition, the directional derivative of the Heaviside function  $H$  in the normal direction  $\vec{N}$  is the Dirac delta function

$$\hat{\delta} = \nabla H(\phi(x)) \cdot \vec{N} \quad (2.33)$$

which is a function of the multidimensional  $x$ . Note that this distribution is nonzero only on the interface  $\partial\Omega$  where  $\phi = 0$ . We can rewrite Equation (2.33) as

$$\hat{\delta}(x) = H'(\phi(x)) \nabla(\phi(x)) \cdot \frac{\nabla\phi(x)}{|\nabla\phi(x)|} = H'(\phi(x)) |\nabla\phi(x)| \quad (2.34)$$

using the chain rule to take the gradient of  $H$ , the definition of the normal  $\vec{N} = \frac{\nabla\phi}{|\nabla\phi|}$  and the fact that

$\nabla\phi(x) \cdot \nabla\phi(x) = |\nabla\phi|^2$ . In one spatial dimension, the *delta function* is defined as the derivative of the one-dimensional Heaviside function:

$$\delta(\phi) = H'(\phi) \quad (2.35)$$

where  $H(\phi)$  is defined in Equation (2.32) above. The delta function  $\delta(\phi)$  is identically zero everywhere except at  $\phi = 0$ . This allows us to rewrite Equations (2.33) and (2.34) as

$$\hat{\delta} = \delta(\phi) |\nabla\phi| \quad (2.36)$$

As a result, Equation (2.30) is rewritten as

$$L_g(\phi) = \int_{\Omega} g \delta(\phi) |\nabla\phi| dx dy \quad (2.37)$$

Since  $\delta(\phi) = 0$  almost everywhere except at  $(x, y) = (0, 0)$ , the energy functional  $L_g(\phi)$  measures the total effect of  $g$  over the interface  $C$ . When the interface locates image boundaries,  $L_g(\phi)$  has its minimum value. To understand the geometric meaning of the energy  $L_g(\phi)$ , we suppose that the zero level set of  $\phi$  can be represented by a differentiable parameterized curve  $C(p)$ ,  $p \in [0, 1]$ . It is well known [Vemuri and Chen 2003] that the energy functional  $L_g(\phi)$  in (2.30) computes the length of the zero level curve of  $\phi$  in the conformal metric  $ds = g(C(p)) |C'(p)| dp$ .

The energy functional  $A_g(\phi)$  in (2.31) is introduced to speed up curve evolution. Note that, when the function  $g$  is constant ( $g=1$ ), the energy functional in (2.31) is the area of the region  $\Omega_{\phi}^-$ .

Now, the following total energy functional is defined

$$\begin{aligned} E(\phi) &= \mu P(\phi) + E_m(\phi) \\ &= \mu \int_{\Omega} \frac{1}{2} (|\nabla \phi| - 1)^2 dx dy + \lambda \int_{\Omega} g \delta(\phi) |\nabla \phi| dx dy + \nu \int_{\Omega} g H(-\phi) dx dy \end{aligned} \quad (2.38)$$

The external energy  $E_m$  drives the zero level curve toward the object boundaries, while the internal energy  $\mu P(\phi)$  penalizes the deviation of  $\phi$  from a signed distance function during its evolution.

The following evolution equation:

$$\frac{\partial \phi}{\partial t} = - \frac{\partial E}{\partial \phi} \quad (2.39)$$

is the gradient flow that minimizes the functional  $E$ .

Using the *calculus of variation* [Courant and Hilbert, 1953], the Gateaux derivative (first variation) of the functional  $E$  in (2.34) can be written as

$$\frac{\partial E}{\partial \phi} = -\mu[\Delta \phi - \operatorname{div}\left(\frac{\nabla \phi}{|\nabla \phi|}\right)] - \lambda \delta(\phi) \operatorname{div}\left(g \frac{\nabla \phi}{|\nabla \phi|}\right) - \nu g \delta(\phi) \quad (2.40)$$

where  $\Delta$  is the Laplacian operator.

The function  $\phi$  that minimizes this functional satisfies the Euler-Lagrange equation  $\frac{\partial E}{\partial \phi} = 0$ . The steepest descent process for minimization of the functional  $E$  is the following gradient flow [Li et al. 2005]:

$$\frac{\partial \phi}{\partial t} = \mu[\Delta \phi - \operatorname{div}\left(\frac{\nabla \phi}{|\nabla \phi|}\right)] + \lambda \delta(\phi) \operatorname{div}\left(g \frac{\nabla \phi}{|\nabla \phi|}\right) + \nu g \delta(\phi) \quad (2.41)$$

This gradient flow is the evolution equation of the level set function used in our approach.

### 2.2.4.1 Implementation

Since  $\delta(\phi) = 0$  almost everywhere except for zero level curves, it seems unlikely that any standard numerical approximation will give a good approximation to Equation (2.37). Thus, in practice, the accurate smeared-out approximation of the Dirac function  $\delta(x)$  is defined

$$\delta_{\varepsilon}(x) = \begin{cases} 0 & |x| > \varepsilon \\ \frac{1}{2\varepsilon} \left[ 1 + \cos\left(\frac{\pi x}{\varepsilon}\right) \right] & |x| \leq \varepsilon \end{cases} \quad (2.42)$$

where  $\varepsilon$  is a tunable parameter that determines the size of the bandwidth of numerical smearing. We used the regularized Dirac  $\delta_{\varepsilon}(x)$  with  $\varepsilon = 1.5$ , for all the experiments in this thesis, i.e. numerical computations are done within a stripe of three grid cells around the zero level curves. The approximation of (2.41) by the difference scheme can be simply written as

$$\frac{\phi_{i,j}^{k+1} - \phi_{i,j}^k}{\tau} = L(\phi_{i,j}^k) \quad (2.43)$$

where  $L(\phi_{i,j})$  is the approximation of the right hand side in (2.41) by the spatial difference scheme. The difference equation (2.43) can be expressed as the following iteration:

$$\phi_{i,j}^{k+1} = \phi_{i,j}^k + \tau L(\phi_{i,j}^k) \quad (2.44)$$

It was found experimentally that the time step  $\tau$  and the coefficient  $\mu$  must satisfy  $\tau\mu < \frac{1}{4}$ , in order to maintain a stable level set evolution. Using a larger time step can speed up the evolution, but may cause errors in the boundary location. Unlike the traditional level set methods in which the level set function  $\phi$  is initialized to a signed distance function  $\phi_0$ , in the presented formulation, the level set function  $\phi$  is no longer required to be initialized as a signed

distance function because the internal energy compensates the deviation of  $\phi$  from a signed distance function. Instead the initial level set function  $\phi_0$  is defined as

$$\phi_0(x) = \begin{cases} +\rho & \text{if } x \text{ is outside } C \\ -\rho & \text{if } x \text{ is inside } C \end{cases} \quad (2.45)$$

where  $\rho > 0$  is a constant. It is suggested to choose  $\rho$  larger than  $2\varepsilon$ , where  $\varepsilon$  is the width of the definition of the regularized Dirac Delta function  $\delta_\varepsilon$  in Equation (2.42).

The used variational level set formulation has two main advantages over the traditional level set formulations. First, a significantly larger time step can be used for numerically solving the evolution partial differential equation, and therefore speeds up the curve evolution. Second, the need of costly re-initialization procedure is completely eliminated because the internal energy forces the level set function to be close to a signed distance function [Li et al. 2005]. The described variational level set method is applied on a sample image displayed in Fig. 2-8. The initial level set  $\phi_0$  is computed from the region enclosed by the quadrilateral, as shown in Fig. 2-8-a. We used time step  $\tau = 5.0$ , which is significantly larger than the time step used for the traditional level set methods.

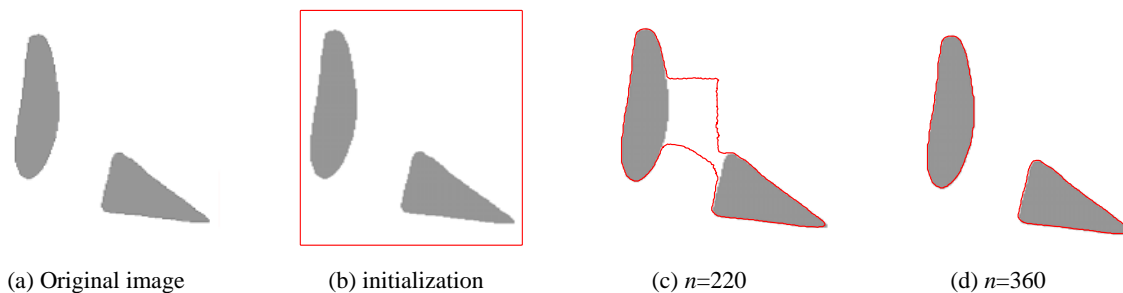


Figure 2-8: Result of shrinking curve evolution. (a) The interface as a quadrilateral. (b) Initial zero level curve or interface. (c) Intermediate result after 220 iterations. (d) The evolved curve after 360 iterations with  $\lambda = 0.5$ ,  $\mu = 0.04$ ,  $\nu = 3.0$ , and the time step  $\tau = 5.0$ .

## 2.3. Review of Road Junction Extraction

Junctions are mainly extracted in the context of automatic road network extraction. Most of the existing approaches initially concentrate on road extraction. Subsequently, the extraction of road junctions is realized by perceptual grouping of road hypotheses. In the literature, there are only a few approaches which are dedicated to this task. We classify these approaches based on whether they consider road junctions as point or area objects. In this work, road junctions are modeled as area objects. Therefore, similar approaches are described in more detail in order to identify challenges and possibilities to develop a robust and reliable method.

### 2.3.1 Road Junction as a Point Object

There are a large number of approaches on road extraction which extract roads as line features. These approaches are either automatic or semi-automatic. Furthermore, automatic methods may use a GIS or geospatial database as additional external information. They are usually applied on low resolution images of less than 0.5 m ground resolution in which case roads are treated as lines and road junctions as points. Such approaches employ varying techniques for the extraction of roads. Nevertheless, they lack a precise and explicit junction model. Therefore, junctions are modeled implicitly as the intersection of linear crossing roads. Since roads are extracted as lines, the perceptual grouping of these linear features results in a point. This point can be obtained through the calculation using the endpoint coordinate of connecting roads [Zhang 2003] or through a simple extension of neighboring roads [Wiedemann and Hinz 1999, Baumgartner 1998]. In [Gautama et al. 2004], a differential ridge detector combined with region growing is used to detect junctions. Since the ridge model does not hold in the vicinity of junctions, its performance is extended using a region growing method so that the road segments obtained initially are extended to the junction regions that contain similar gray values. Finally, junctions are detected and verified using morphological thinning followed by shape analysis. The evaluation was conducted on high resolution remotely-sensed imagery with a ground resolution of about 1 m.

Unlike the publications just outlined in that junctions are reconstructed using the branching roads already captured, in [Koutaki et al. 2005, Zhang and Couloigner 2004] road network is assumed to be constructed based on detected road junctions by connections between them, i.e. junctions are detected independently from branching roads. In [Koutaki et al. 2005], an explicit junction model based on which a strategy is developed are proposed. Furthermore, in [Zhang and

Couloigner 2004], once the preliminary road network is constructed, junctions are reinvestigated based on the extracted branching roads. As a result, the initial road network is modified after some junctions are added or deleted.

[Zhang and Couloigner 2004] proposed a wavelet approach to extract roads from satellite imagery. The approach makes use of a multi-resolution analysis scheme in combination with a road junction method. The road junctions are detected automatically based on the local analysis of the wavelet coefficients in a neighborhood of 7 by 7 pixels in size. Using the junction detection information, road centerlines are extracted through a road following algorithm. Road junctions are again investigated using the obtained road network features. This approach was applied on IRS and IKONOS images.

In [Koutaki et al. 2005], road junctions are initially detected followed by a road tracking method to generate connection hypotheses between two adjoining junctions. A model for typical junctions such as 4-arms junctions, T-junctions and Y-junctions was proposed in which two or three elongated rectangles with different or same widths meet at a certain point. The proposed strategy for the detection of junctions is based on matching the defined model to the image features obtained from an ISODATA clustering method. The matching process uses a coarse-to-fine strategy to reduce computational complexity. This method was evaluated in rural and suburban areas on images with a ground resolution of 0.5 m.

There are a few publications which exclusively address the junction extraction issue and propose a junction model.

In [Boichis et al. 1998], a top-down strategy for the automatic extraction of road junctions is presented. They model junctions using a knowledge database and reconstruct junctions based on the “main road” idea. Using several radiometric and geometric properties, the main road is reconstructed first on which secondary roads are later projected. Roads are detected by Hough Transform and the results are evaluated with fuzzy functions. This method cannot handle disturbances and does not exploit the image information to validate the obtained junction point. They extended their approach later to extract roundabouts [Boichis et al. 2000]. It is assumed that a vector representation of roundabouts in the geospatial database is similar to road junctions, so a circle detector (the parametric Hough Transform) is used to verify the existence of a roundabout and to extract the roadway. First, linear roads and then divergent and circulating roads are extracted before the complete reconstruction. The reconstruction is performed by connecting three kinds of extracted roads using radiometric and geometric constraints.

In [Wiedemann 2002] a method is developed to improve the road junction extraction results obtained by [Hinz and Wiedemann 1999]. Their road extraction approach delivers sometimes cycles instead of crossing points. Wiedemann [2002] makes use of main and branching road properties to model commonly used junction types. Subsequently, all cycles within the crossing area are detected and replaced by a node. Then, the road segments in the vicinity of a junction are combined and described by parameterized cubic curves. The junction is evaluated by introducing several attributes combined by a linear fuzzy function of which the maximum score is stored as the best result. The external evaluation of results is carried out using the buffer method [Heipke et al. 1998] and some quality measures such as completeness, correctness, redundancy, and RMS difference.

[Barsi et al. 2002] presented a method to detect road junctions in orthoimages with 0.4 m ground resolution in the context of rural areas. The junction model is created using a neural network trained with some collected junction. Several parameters describing junctions are thus obtained, including grey value statistics and edge information in the junction areas. The neural network is then applied to detect road junction in images. While the results are encouraging, a disadvantage of the method is the high false alarm rate.

### 2.3.2 Road Junction as an Area Object

In the following publications, road junctions are not explicitly modeled, but they are extracted in the context of road extraction. In [Heipke et al. 1995] a strategy is proposed to extract roads in two different scales: a coarse one with 2 m per pixel and a fine one with 0.25 m per pixel. In the fine resolution, roads are modeled as an area object and in coarse resolution as a line object. Results from both resolutions are merged using a rule based system. To delineate the junction area, segments next to accepted road segments are recursively investigated for homogeneity of the adjacent area. They are accepted if the same homogeneity criteria applied for road segments is fulfilled.

In [De Guenst 1996], a knowledge based interpretation strategy for updating road maps was proposed. Gray value profiles perpendicular to the existing roads are evaluated to generate hypotheses for a newly constructed road. The junction where the recognized link road intersects the existing road is reconstructed using the specialized road model. The specialized road model uses the standards for road construction. This approach can extract only a special type of junction. Furthermore, it heavily depends on the knowledge obtained from road markings and their spatial relationships, which limits its application. The author states that more knowledge needs to be included into the system to improve its performance.

In [Laptev et al. 2000, Mayer et al. 1998, Laptev 1997], a snake model is used to delineate junctions. In [Laptev 1997], a method based on the ziplock snake is presented to detect road junctions. The initial snake is supplied by two far endpoints sharing the same junction border. These endpoints are previously obtained by a snake-based approach designed to extract intersecting roads. Since initial curves are straight and lie often outside the junction area, junction borders must be strong enough to prevent leakages to the surrounding area. In [Laptev et al. 2000, Mayer et al. 1998], instead of ziplock snakes, a closed snake is initialized inside the junction central area and expanded until it delineates the junction borders. These snake-based methods have a high flexibility to detect junctions of various shapes and

topology if the central area of junctions is homogeneous with a good contrast to the surrounding area. Disturbing features are not considered in this method.

[Péteri et al. 2004] proposed a multi-resolution snake for urban road extraction from IKONOS and QuickBird images. They employ a multi-resolution analysis to increase the convergence of the algorithm by minimizing the problem of noise including vehicles, ground marking, etc. After the extraction of roads close to the junction, open snakes are initialized to detect junction boundaries. Two constraints applied on snakes are that the snakes' extremities are fixed and that they are limited lie inside a circle defined around the junction center. However, the authors did not specify the how large the circle can be. Furthermore, even inside the defined circle snakes can converge to undesirable features.

[Niu 2006] used geometric deformable models for semi-automatic extraction of highways and vehicles simultaneously in rural and suburban areas. He assumes that highways have a good contrast to the surroundings and their surface is radiometrically quite homogenous. Then, geometric active contours are initialized as seed points and evolved. To prevent leakages during the evolution, he adds region-based information into the geometric active contours. Although this approach is basically developed to extract highways, highway junctions where two highways are merged into a single highway are also extracted. However, no model for either highway junctions or vehicles is developed. Furthermore, the method might fail when disturbances like large shadow areas and a truck with its shadow block the curve movement towards the highway boundary.

### 2.3.3 Discussion

We reviewed and discussed publications dealing with road junctions, directly or indirectly, of which most treat road junctions as point objects. In this category, the result of junction extraction is often used to construct the road network. Some of them [Zhang 2003, Wiedemann and Hinz 1999, Baumgartner 1998], however, first focus on roads and next junctions are detected using road extraction results whereas some others [Koutaki et al. 2005, Zhang and Couloigner 2004], in which a junction model is also proposed, initially detect junctions, and subsequently roads are extracted using junction information. There exist only a few publications in which junctions are explicitly modeled [Barsi et al. 2002, Wiedemann 2002, Boichis et al. 1998/ 2000].

Junctions are considered as planar objects in approaches making use of high resolution aerial or satellite imagery. In such publications, different methodologies to attack the problem were proposed.

One kind of methodology is based on road markings and the spatial relationships between them [Shi et al. 2004, De Guent 1996], which often is used in city areas or for expressways. In urban areas, however, road markings can be occluded by various kinds of disturbing sources such as traffic boards, traffic lights, street lights, vehicles, trees and their associated shadows, which make their extraction difficult. Furthermore, junctions include a variety of road marking configurations resulting in different spatial relationships between them. As a result, a general approach to handle various kinds of junctions based on road markings is almost impossible.

Another kind of methodology is based on energy minimizing techniques called active contours or snakes. Snake-based methods for junction extraction achieve some degree of success due to the flexibility that snakes offer in tackling geometric variability in junction shapes. Nevertheless, the initialization method used in these approaches is suitable for junctions that are of special characteristics within a certain context. For example, in [Laptev et al. 2000, Mayer et al. 1998], snake segments are initialized as a small circle in the junction center and then expanded until they converge to junction boundaries. This method can fail when there are islands, strong road markings and vehicles in the central area of the junction. Furthermore, in case that tree shadows occlude junction borders, the snakes delineate the boundary of shadows. Since expanding snakes can pass over weak junction borders, sufficient contrast of the desired boundaries is a necessary precondition for a successful delineation. Also, the authors do not propose a mechanism to overcome leakages into surrounding areas occurring when junction boundaries are weak.

Unlike [Laptev et al. 2000, Mayer et al. 1998] where initial snake segments are located inside the junction, in [Péteri et al. 2004] they are often situated outside the junction, because initialization is supplied by straight lines connecting adjacent road end points. This kind of initialization can be appropriate for junctions with mild change of curvature in their borders because less curvature contributes to a closer initialization. Nevertheless, in junctions with sharp changes of curvature, initial curves may be located too far from the answer. Furthermore, the area outside the junction contains various kinds of features hindering the curve movement towards the junction borders. Therefore, except for junctions that are surrounded by farm land and that contain a smooth change of curvature in their borders, this method is likely to fail. Disturbances inside the junction, however, have no influence on the performance.

In [Niu 2006] geometric class of active contours is used to delineate highways and their intersections. He proposed a radiometric constraint to overcome the leakage problem which usually occurs in weak boundaries. However, his approach cannot handle shadows and disturbances.

Approaches developed based on active contours are suitable for medium resolution images ( $>0.2$  m) where fine features are not apparent and road markings do not strongly affect the snake movement. Furthermore, current snake-based methods are very sensitive to disturbances. These issues emphasize the need for an advanced snake model with the ability to overcome disturbances existing inside and outside the junction. Furthermore, a close initialization is crucial for the success of the snake performance. Snake-based approaches enjoy the advantage of being independent from road markings and their spatial relationship, so they are applicable to junctions of various geometrical shape and topology.

Furthermore, islands as important components of junctions also need to be considered in a precise and detailed junction model. None of existing publications has yet taken islands into consideration.

### 3. A New Approach to Road Junction Extraction

#### 3.1. Road Junction Classes

For road traffic, various kinds of junctions have been designed. Different types of junctions have different properties and construction specifications. We classified junctions into three main classes: simple, complex, and motorway (Fig. 3-1). Simple junctions contain three or more road arms without islands in the centre. In contrast, complex junctions do contain islands in the centre. A road model for simple and complex junctions complies with the classic road model in which roads are defined as quadrilateral objects with parallel edges and a constant width. In the complex class, however, the width of roads might increase when approaching the road junction. The main difference between motorway junctions and the two other classes is that crossing roads do not have the same height. In other words, simple and complex junctions are defined in two-dimensional space, whereas motorway junctions are defined in three-dimensional space. Roundabouts include the same properties as complex junctions with the exception that their central island is very large. Therefore, they are regarded as a subclass of complex junctions. In this thesis, we focus on simple and complex junctions only.



Figure 3-1: Junction classes. (a) Simple junction. (b) Complex junction. (c) Roundabout as a subclass of complex junction. (d) Motorway junction.

#### 3.2. Road Junction Model

The conceptual model of simple and complex road junctions is represented and described in Fig. 3-2. According to the model, a road junction area is composed of two parts: the road junction itself and the road arms. The road junction, where road arms are connected, is composed of the junction border and its central area where either traffic islands in complex junctions or central islands in roundabouts may be located. A road arm is composed of one or more road segments. Disturbances such as occlusions and shadows are not explicitly included in the model.

#### 3.3. Workflow for Simple and Complex Junctions

In this work, we make use of prior knowledge derived from a geospatial database to extract only those parts of the object which are consistent with the corresponding content of the geospatial database. Our strategy consists of four parts (Fig. 3-3):

1. Pre-analysis of geospatial database
2. Extraction of road arms
3. Road junction reconstruction
4. Island extraction

In part 1, the geospatial database is analyzed resulting in a rough idea of the junction appearance in the image. In part 2, road arms are extracted within a limited area around the initial junction position. A road arm is a long straight road segment connected to the road junction. The snake-based approach by means of which the road junction is reconstructed is presented in part 3. Part 4 illustrates a level set method used to delineate islands that lie in the junction central area.

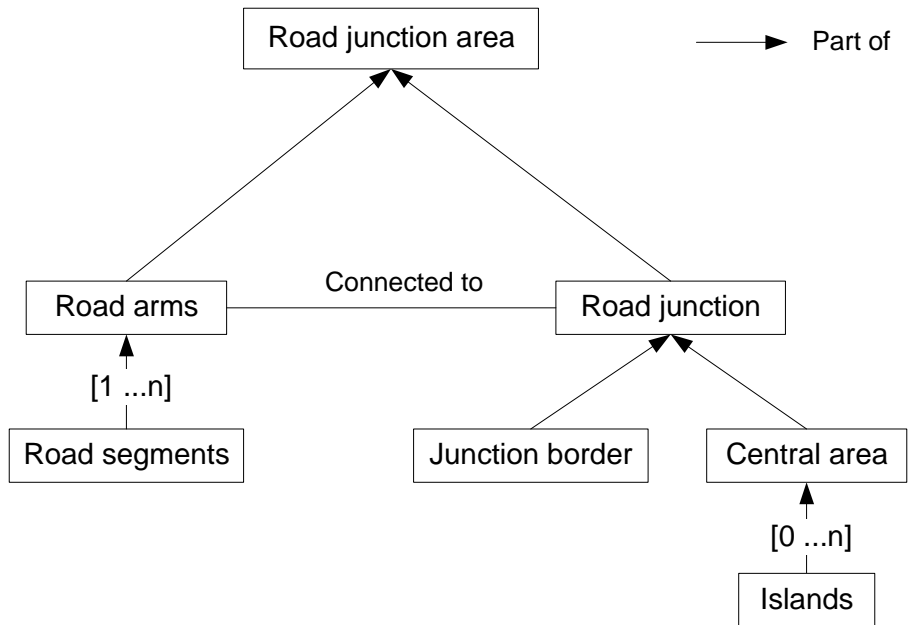


Figure 3-2: Road junction model

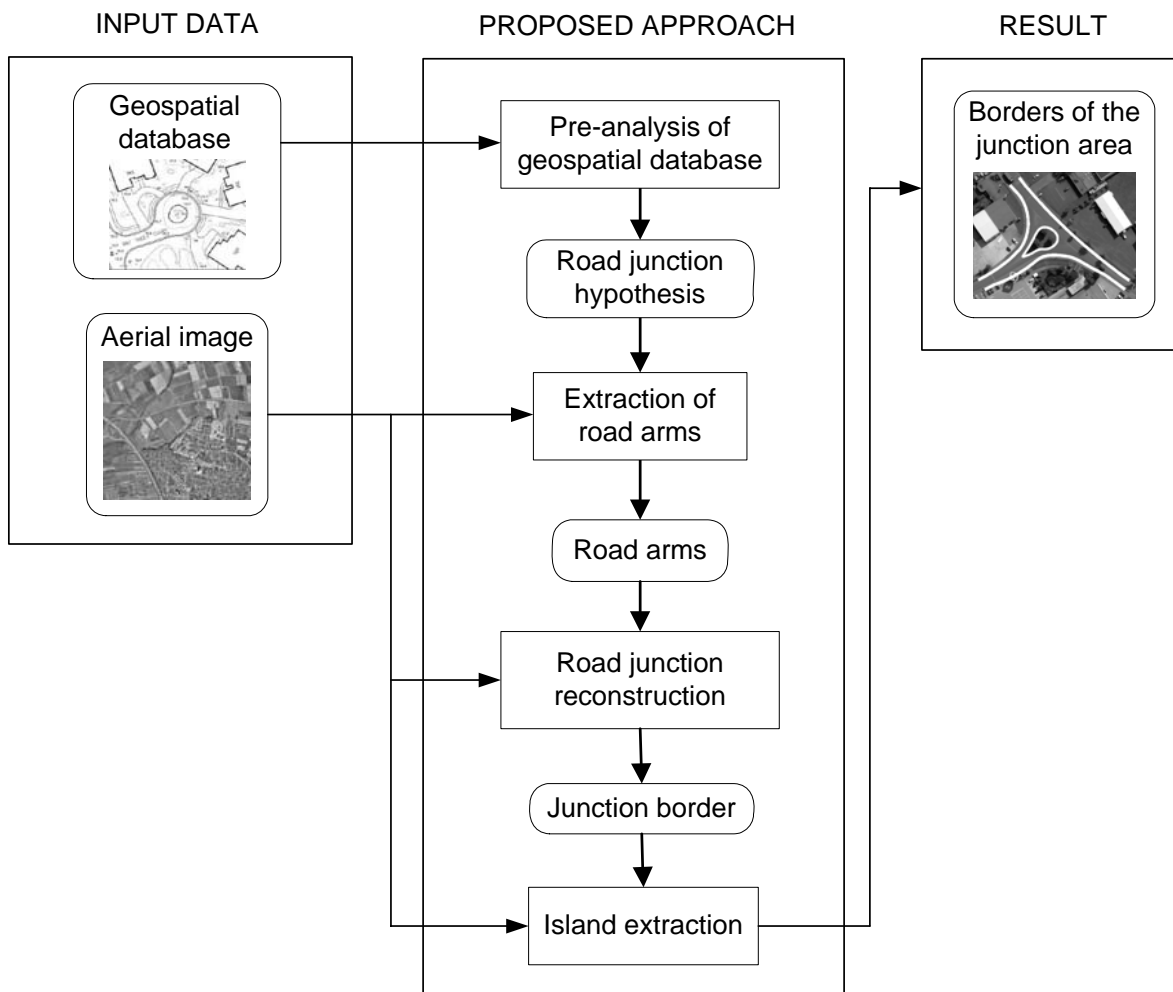


Figure 3-3: Proposed approach organization

### 3.3.1 Pre-analysis of Geospatial Database

The geospatial database we used contains explicit geometric and implicit topologic and radiometric information about road junctions. Topologic information determines the number of roads connected to the junction centre and geometric information provides us with the approximate location of the junction and the width of the connected roads. A road junction in the geospatial database is composed of a centre point at which a few lines or polylines meet. Using vector coordinates of lines, we compute road directions. In the road extraction step, geometric and topologic information are used to construct road segments. Furthermore, the geospatial database contains information about the road surface material, from which radiometric property of roads can be estimated.

### 3.3.2 Road Arm Extraction

A correct result of road arm extraction is crucial to the success of our approach. Road arms provide initial values such as points and directions required to initialize the snakes.

#### 3.3.2.1 Road Model

A road arm is defined in terms of geometry and radiometry as follows:

- **Geometry:** A road arm is a rectilinear object which is represented as a ribbon with a constant width and two parallel edges.
- **Radiometry:** A road arm is considered to be a homogeneous region with a high contrast to its surroundings. The absolute brightness depends on the surface material.

#### 3.3.2.2 Strategy

Roads can bend in different ways, for instance, in a simple curved form, serpentine curve or in a state with changing width. However, in the area close to the junction centre they are normally straight partly because of traffic safety regulations. This observation leads us to extract long and straight road segments near the junction centre, which we call road arms (Fig. 3-4). Since in high resolution images the surface of roads is not quite homogeneous and many edges are usually detected around road sides, the process is performed at a somewhat reduced resolution equivalent to about 0.2 m ground resolution and the results are subsequently transferred into the original image. In order to apply the geometric part of the road model, edges are extracted from the image using the Deriche edge detector.

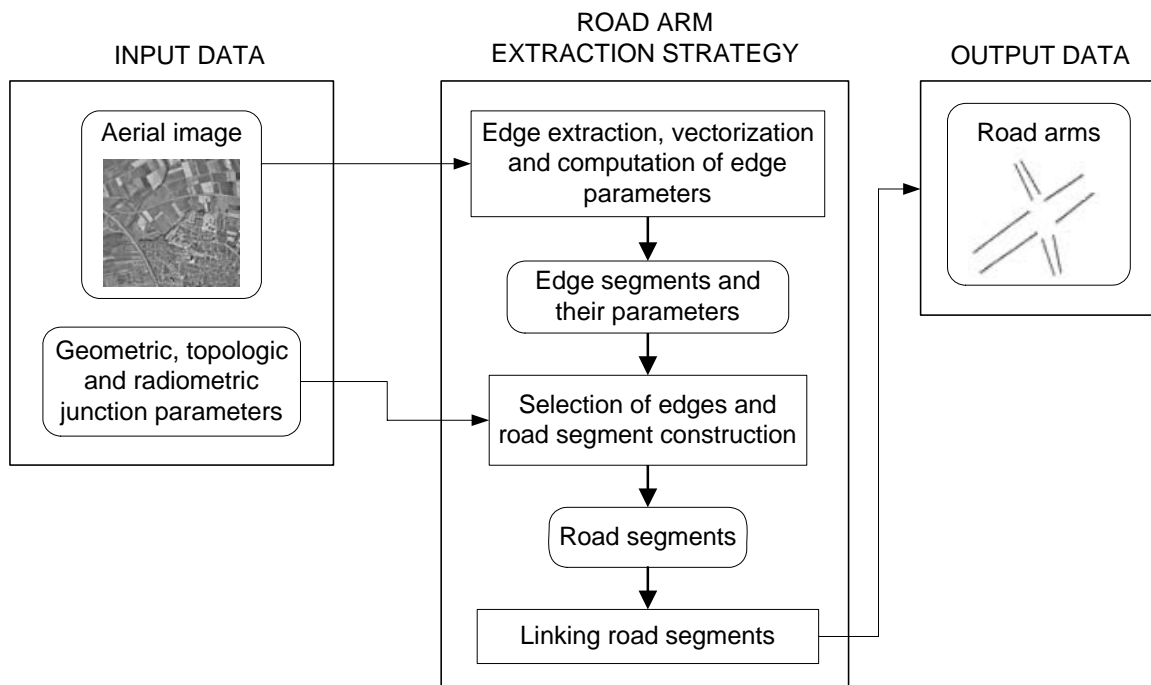


Figure 3-4: Road arm extraction

Subsequently, a thinning operation is applied, yielding one pixel wide edges. The edges are approximated by polygons to facilitate further processing (Fig. 3-5-b). We call the result of this step *edge segments*. They are grouped based on one radiometric and two geometric criteria: homogeneity, parallelism, overlap. As roads are defined as homogeneous surfaces, radiometric homogeneity is subsequently checked for quadrilateral areas within the parallel and overlapping

edge segments. This means the variance within an area must be smaller than a predefined threshold. Threshold values for all used parameters are specified in Table 3-1. As a result of these two steps, irrelevant edge segments are eliminated (Fig. 3-5-c). Edge segment information like image coordinates of endpoints, length and direction are computed. The direction is calculated so that it lies within the radian range of 0 to  $\pi$ , i.e. all direction angles are projected to a half circle. These parameters are used later for the road segment construction. We then group edge segments based on the direction of connected roads from the geospatial database. The number of groups corresponds to the number of connected roads (Fig. 3-5-d). Since road directions derived from the geospatial database are regarded as reference directions (Fig 3-5-a), each group should contain parallel edge segments having a direction similar to their reference direction. It is noted that the direction difference between edge segments in each group must be below a predefined threshold.

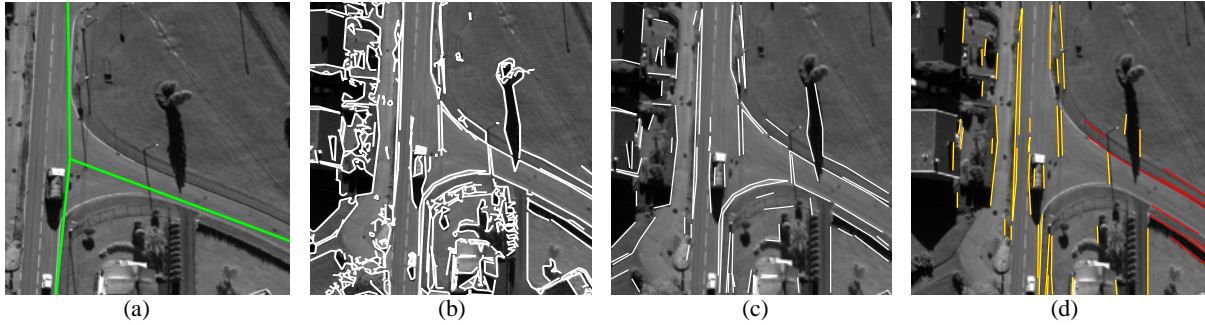


Figure 3-5: (a) Vector data superimposed on the clipped image. (b) Edge segments. (c) Grouped edge segments. (d) Two groups of edge segments in red and yellow. Yellow edge segments contain two groups since the related roads are collinear.

Before applying rules leading to the construction of road segment short edge segments are eliminated as they are not usually related to roads. For example, image noise, shadows or occlusions can generate short edge segments. Thus, cases involving short straight edge segments are not considered.

Road segments are generated using selected edge segments that have overlapping parts. The overlap property can be described by classifying it into four types. In Figure 3-6, four possible cases in which edge segments overlap are illustrated. In all four cases, road segments are constructed from four endpoints.

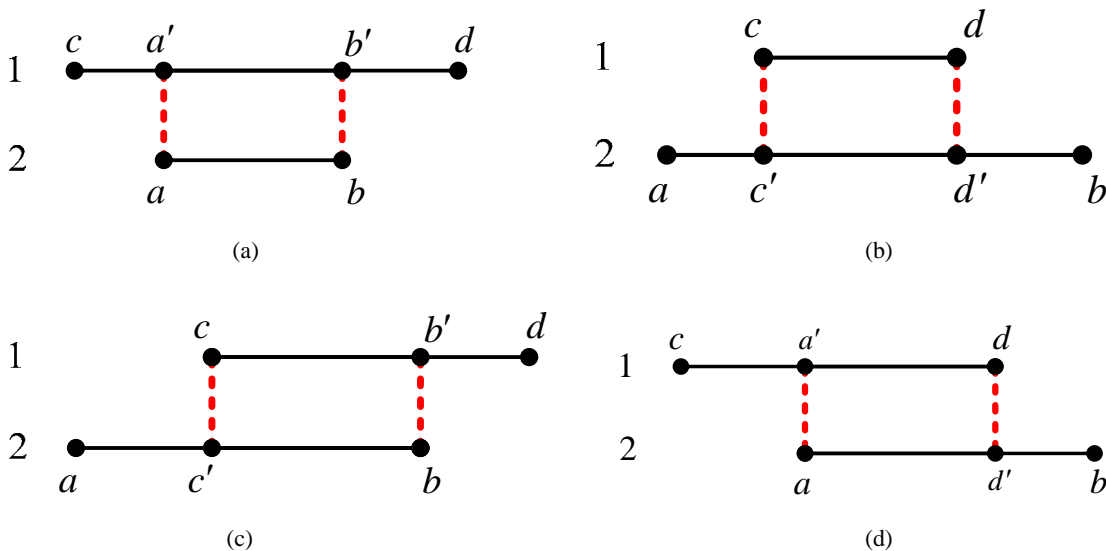


Figure 3-6: Illustrating four possible cases for road segment construction. (a) The entire edge segment 2, when projected on edge segment 1, is located between  $c$  and  $d$ . (b) Edge segment 1 is shorter than 2 and its orthogonal projection is placed between  $a$  and  $b$ . In (c) and (d), one endpoint of each edge segment is projected on its related edge segment.

Road segments are constructed from the selected overlapping edge segments that fulfill some preconditions defined in terms of geometry and radiometry. We introduce some criteria in order to generate reliable road segments as follows:

1. **Anti-parallelism:** Two image gradient vectors taken at two overlapping edge segments are in approximately opposite directions. Furthermore, they are approximately parallel with each other and orthogonal to the edge segment. We check this criterion through an image in which gradient directions along edge segments are depicted as gray values.

Points with edge amplitude 0 in homogeneous areas are assigned the gray value 255 (Fig. 3-7-b). Mean gray value along each edge segment is calculated and subtracted from that of others. Finally, we select only those edge segments whose difference gray value is equal to the angle difference of approximately  $180^\circ$ .

2. **Width:** This property is derived from the geometric part of the road model. Road width is known from the geospatial database. We define a width range by introducing some tolerance around the road width. Road segment hypothesis are generated using edge segments having a width within the defined range. A prerequisite for the width characteristic is that two edge segment candidates must overlap and must have opposite gradient directions (anti-parallelism condition) (Fig. 3-7-c). The result of this step is shown in Figure 3-8-a.

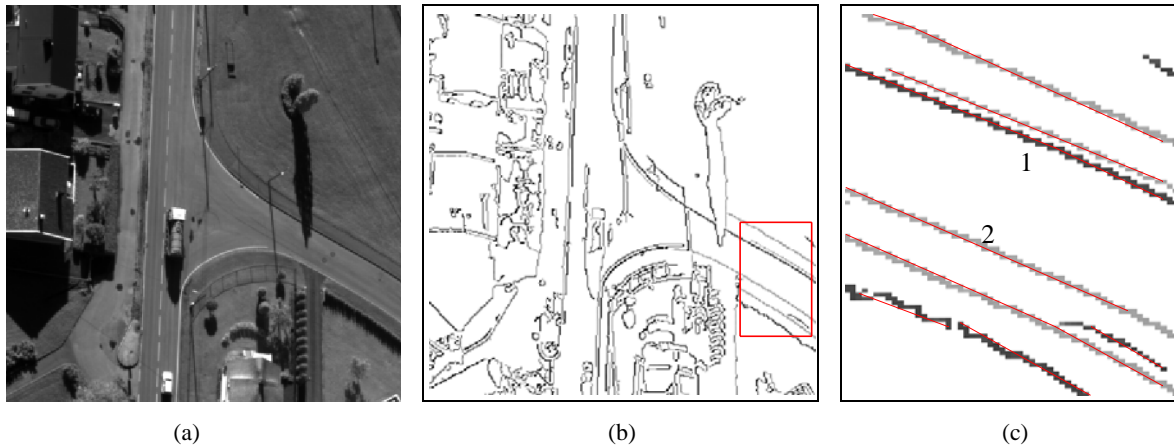


Figure 3-7: (a) Original image. (b) Gradient direction image. (c) Edge segments are superimposed on the cut-out from the gradient direction image. 1 and 2 are two possible choices for generating road segment.

3. **Contrast:** Radiometric property of the resulting road segments must be investigated in order to eliminate wrong hypotheses. The mean gray value of the quadrilaterals can be roughly estimated using the information about the road surface material. This information is available from the geospatial database. The mean gray value within each segment area must fall into a predefined range. Thresholds used are specified in Table 3-1. Applying contrast constraint, some hypothesized road segments are removed, as is shown in Figure 3-8-b.

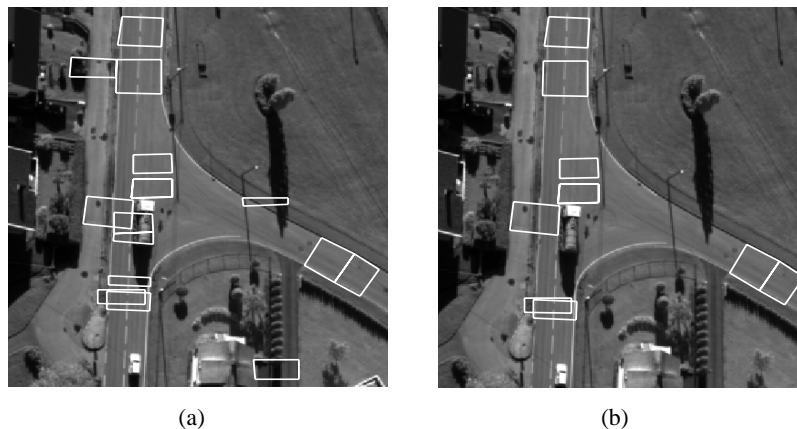


Figure 3-8: Illustrating road segment construction. (a) Resulting road segments after applying geometric width and anti-parallelism constraints. (b) Obtained road segments after applying radiometric contrast constraint.

As can be seen, some resulting road segments from this stage might overlap. We decided to select the longer segment in each group of overlapping road segments as a shorter segment is more likely to be generated from edge fragments of features close to road sides (Fig. 3-9-a). The remaining road segments are verified using lane lines if found in the image [Steger 1998], otherwise road centre lines extracted in the image with a reduced resolution of 2 m [Steger 1998] are used for the verification. Road segments are verified if road centre lines or lane lines are located within the road segments [Heipke et al. 1995] (Figs. 3-9-b and c).

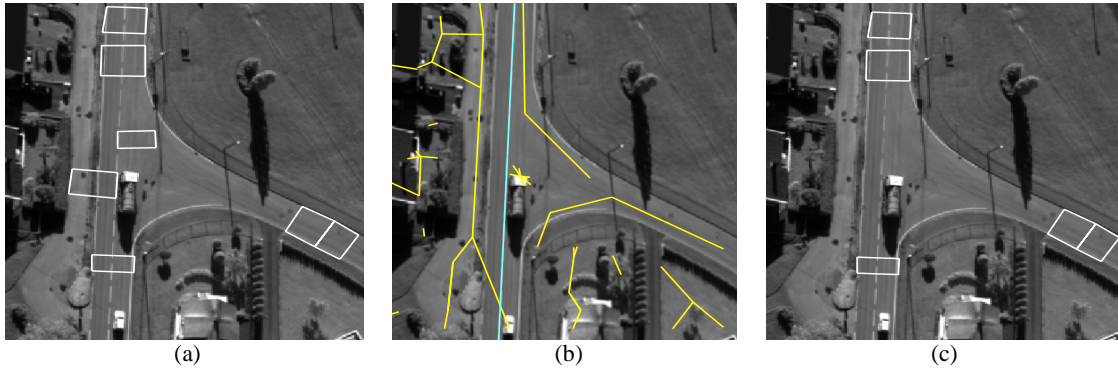


Figure 3-9: Illustrating road segment verification. (a) Resulting road segments after removing overlapping road segments. (b) Cyan line represents the extracted lane line and yellow lines depict the result of line extraction in the image with ground resolution of about 2 m. (c) Verified road segments.

Although we have so far extracted groups of road segments, what is needed is one road arm per group. To achieve this purpose, road segments within each group are linked. The linking between road segments is achieved when they are collinear and have a similar width (Fig. 3-10). Next, the orientation of each resulting road arm is investigated with the aim to decide which end point faces the junction. This information could be taken from the geospatial data base, but in order to be more independent, we compute the distance between the endpoints of pairs of road arms, and subsequently select the endpoints sharing the shortest distance.

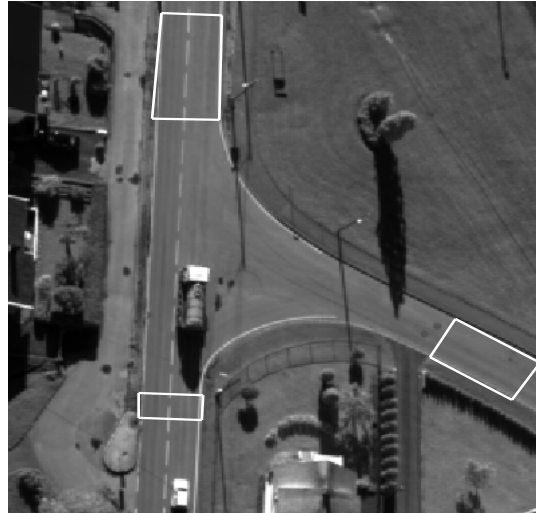


Figure 3-10: Extracted road arms

### 3.3.3 Road Junction Reconstruction

In the reconstruction step, junction borders are located using our proposed snake model and connected to the associated road arm sides. In the following sections, the snake model and issues related to its implementation as well as the incorporation of junction shape information into the snake method is illustrated and discussed.

#### 3.3.3.1 Balloon-guided GVF Ziplock Snake

Traditional snakes [Kass et al. 1988], or parametric active contours are polygonal curves with which is associated an objective function that combines an image term, external energy, measuring the edge strength and a regularization term, internal energy, minimizing the tension and curvature. The curve is deformed so as to optimize the objective function and, as a result, to extract the image edges. Traditional snakes are sensitive to noise and need a close initialization. Since the junction border is composed of open curves with various degrees of curvature, close initialization often cannot be provided. As a result, traditional snakes get stuck in an undesirable local minimum. To overcome these limitations, the ziplock snake model was proposed [Neuenschwander et al. 1997]. We call the external force used in the ziplock snake *traditional force field*. Ziplock snakes need far less initialization effort and are less affected by the shrinking effect from the internal energy term. Furthermore, the computation process is more robust because the active part whose energy is minimized is always quite close to the contour being extracted.

Table 3-1: Road model parameters and their associated thresholds

Road model parameters	Threshold
The difference between the direction of each group of edge segments ( $dir_E$ ) and the reference direction ( $dir_R$ ) must be below a predefined threshold ( $Th_{dir}$ ).	$ dir_E - dir_R  < Th_{dir}$ , $Th_{dir} = 0.2$ radians or 15 degrees
Parallelism: Road segments are generated by parallel edge segments ( $seg1, seg2$ ). Edge segments are considered parallel if direction difference between them is below a predefined threshold ( $Th_{dir}$ ).	$ dir_{seg1} - dir_{seg2}  < Th_{dir}$ , $Th_{dir} = 0.3$ radians or 17 degrees
Standard deviation of road segment gray values $\sigma_{gv}$ must be below a predefined threshold ( $Th_{\sigma}$ ).	$\sigma_{gv} < Th_{\sigma}$ , $Th_{\sigma} = 40$
Road width: The width of extracted road segments ( $W_E$ ) must fall within the range defined by the road width derived from the geospatial database ( $W_R$ ).	$W_R + T_w > W_E > W_R - T_w$ , $T_w = 2$ m where $T_w$ denotes the width tolerance
Mean gray value of road segments ( $GV$ ) must fall within the gray value range defined by the reference gray value $GV_R$ estimated from the geospatial database.	$GV_R + T_{gv} > GV > GV_R - T_{gv}$ , $T_{gv} = 40$ where $T_{gv}$ denotes the gray value tolerance

A ziplock snake is an appropriate method to delineate the junction border if precise initial points and directions could be provided. We assume that these fixed values can be obtained from the road arm extraction result. Nevertheless, ziplock snakes are easily confused by disturbances caused by various features such as trees and their shadows, different kinds of road markings and the shadows from buildings, traffic lights, street lights, power lines and traffic boards. A strong internal energy can considerably decrease the effect of disturbing features. Furthermore, a global initialization is introduced to assure that snake vertices are distributed along the entire object boundary. The global initialization is provided by pairs of lines, each of which is defined by close endpoints and the intersection point of their related road sides (Fig. 3-11). They are called *intersection lines*. These lines are divided up into equidistance vertices surrounding the junction borders which usually appear in curve form.

We tested the ziplock snake method on several samples of which one is shown in Figure 3-12. As opposed to low-resolution images where the road surface is quite homogeneous and road markings have less disturbing effects, in high-resolution images, there are various disturbing features destabilizing active parts of the ziplock and subsequently hinder their motion. Furthermore, disturbing features, such as some types of road markings as are shown in Figure 3-12, besides destabilizing the active parts, i.e. no convergence occurs, pull the contour away from the desired boundaries. However, if the external force has a large capture range, it draws the contour back toward the object boundaries even from far distances. Since a traditional force field has a small capture range, the Gradient Vector Flow (GVF) as an alternative external field is used. In Figure 3-13, the large capture range of the GVF can be compared with the traditional force field in a real image.

The formulation for the motion of the GVF ziplock snake can be written in the form (Section 2.1.5):

$$v^{[t]} = (K + \gamma I)^{-1} * (\gamma v^{[t-1]} - \kappa G|_{v^{[t-1]}}) \quad (3.1)$$

where  $\gamma$  stands for the viscosity factor (step size) determining the rate of converges and  $t$  is the iteration index.  $\kappa$  alters the strength of the external force. The pentadiagonal matrix  $K$  contains the internal energy functions ( $\alpha, \beta$ ) and  $G$  is the GVF external force field.

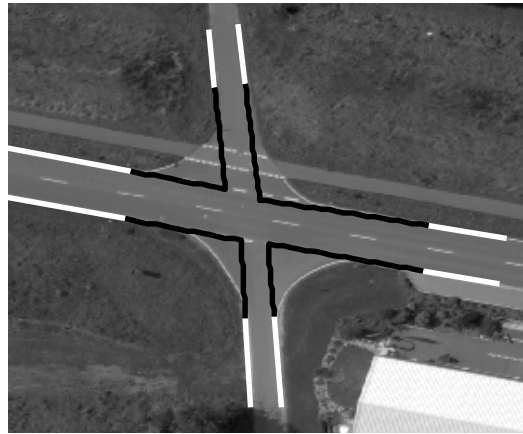


Figure 3-11: Illustrating the global initialization. Intersection lines in black colour are defined by two close endpoints and the intersection point of their respective road sides.



Figure 3-12 : Optimization results of the ziplock snake using tradition force field. Black curves are the result of snake optimization. White lines are the extracted road arms. Since the capture range of the external force field is small, the iterations are stopped near the initial positions.

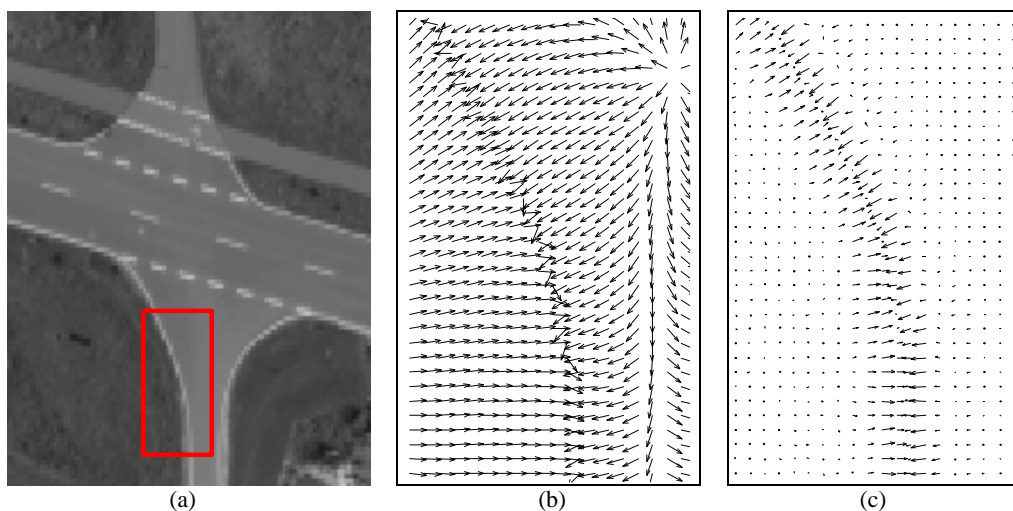


Figure 3-13: (a) A small part of a test image. In (b) and (c), the GVF and traditional force field of the box marked in (a) are shown respectively.

With the GVF ziplock snake, we can overcome most of the limitations encountered with the original ziplock snake. However, this model might fail to detect the correct boundaries in the following cases:

- High variation of curvature at the junction border resulting in too poor initialization at some of its parts. Consequently the snakes become and remain straight (Fig. 3-14-a).

- The central area of the junction lacks sufficient contrast with the surrounding causing the curve converge to the nearby features (Fig. 3-14-b).



Figure 3-14: Illustrating examples where GVF snake fails to detect junction borders due to a high variation of curvature (a) and poor contrast (b).

### Role of curvature

Curvature is a measure of the rate of change in orientation at each point along a curve. Let a plane curve be given parametrically as  $V(s) = (x(s), y(s))$ , then the curvature  $k$  is defined by

$$k = \frac{x_s y_{ss} - y_s x_{ss}}{(x_s^2 + y_s^2)^{3/2}} \quad (3.2)$$

where  $x_s = \partial x / \partial s$  and  $y_s = \partial y / \partial s$  are first derivatives and  $x_{ss} = \partial^2 x / \partial s^2$  and  $y_{ss} = \partial^2 y / \partial s^2$  are the second derivatives.

In road junctions, the curvature of the contours changes smoothly. As can be seen in Figures 3-15-a, b, c and d the curvature is either increasing or decreasing from endpoints toward the curve center point where the curvature has its extremum. Although junctions are diverse in shape, they usually have at least one extremum in the curvature graph along each junction border. When a high variation of curvature exists along the curve, as it is the case in some junctions (Fig. 3-15-e) and in roundabouts (Fig. 3-18-f), more than one extremum can be found in the curvature graph. By experiments, we found that during the snake optimization, the overall curvature, which is defined to be the sum of absolute curvature values along the curve, of the active and passive parts must not be below a certain threshold. Active and passive parts possess a low value of curvature when they become straight. It means that the passive part, which usually contains the extremum curvature value, is not close to the junction border any more.

Using such shape description parameter as curvature computed from the snake vertices, we added another force to the GVF force field which gives the contour a more dynamic behavior [Cohen 1991], thereby solving the two problems described in Figures 3-14-a, b. This new force has an effect of inflation what we applied to our contour to localize the concave part of the road junction. This force, which makes the contour act like a balloon, can be written (see section 2.1.3):

$$F = k_1 \vec{n}(s) \quad (3.3)$$

where  $\vec{n}(s)$  is the normal unitary vector of the curve at point  $v(s)$  pointing toward the junction center and  $k_1$  is the amplitude of this force. Thus, the snake's motion equation (3.1) is modified:

$$v^{[t]} = (K + \gamma I)^{-1} * (\gamma v^{[t-1]} - \kappa G|_{v^{[t-1]}} - k_1 \vec{n}(s)) \quad (3.4)$$

The balloon force is activated when active and passive parts of the snake are approximately straight, i.e. their overall curvature is below a certain threshold (<0.9). It is applied only on the passive part of the curve which is regarded to lie exterior to the junction border, because in the active parts, the snakes are assumed to be on the right track.

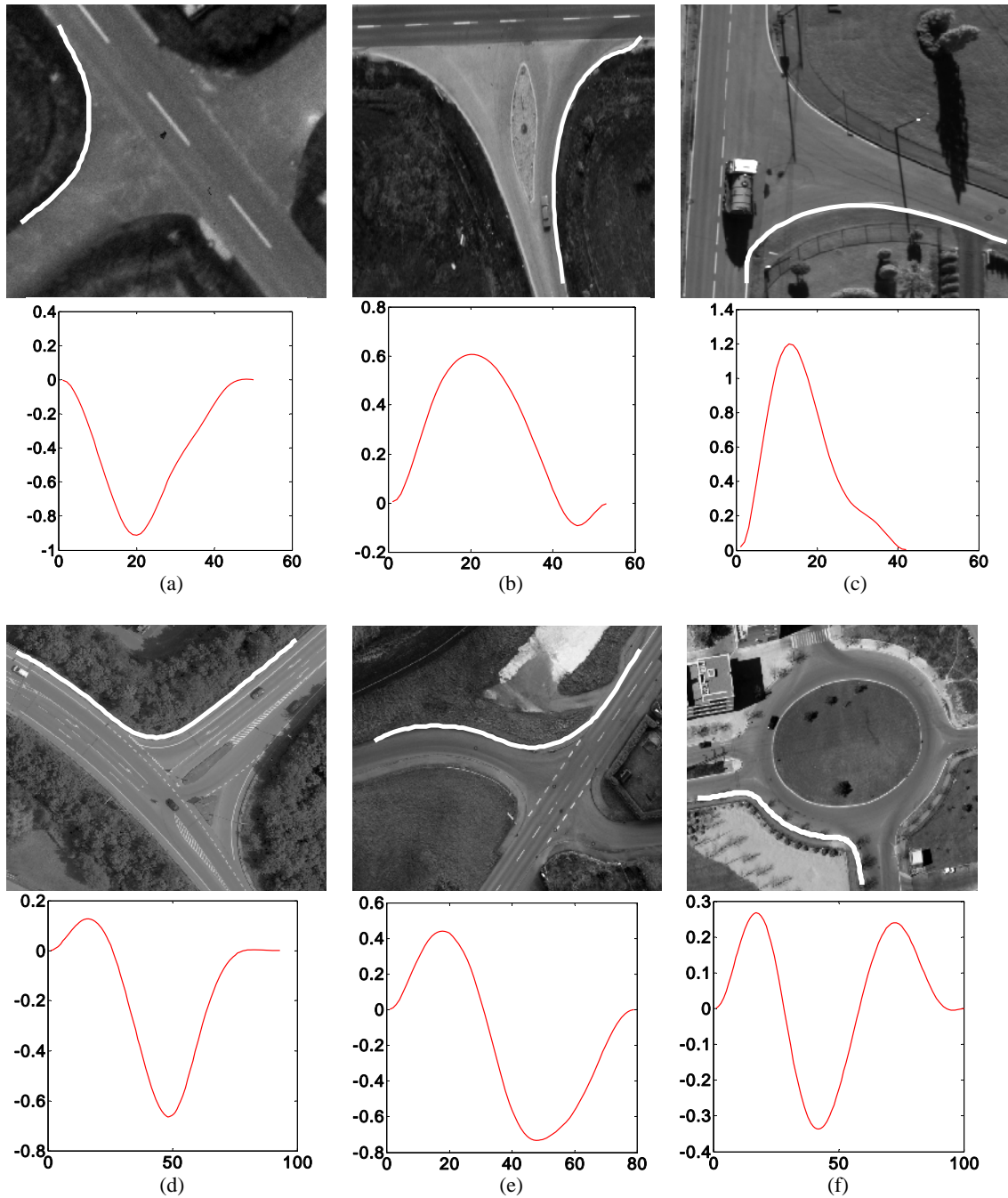


Figure 3-15 : Illustration of the curvature behaviour in different types of junctions. In the graphs, curve vertices (horizontal axis) against the curvature value (vertical axis) are plotted. Graphs in the bottom layer are related to the images at the top row. Graphs in (a), (b), (c) and (d) show examples where only one curvature extremum exists. In (e) the graph contains two extrema as two times the orientation changes and in (f) three extrema exist.

In Figure 3-16, time instances when the balloon force is applied and the change of curvature in active and passive parts are shown individually. In Figures 3-16-a, b, the curvature in left-right active curves increase constantly, while in the passive part, depicted in Figure 3-16-c, the graph picks when for the first time the balloon force is applied and subsequently starts falling as the length of the passive curve decreases.

The effect of the balloon force when applied for the first time during the evolution is displayed in further samples in Figure 3-17. The improved results of the cases shown earlier in Figure 3-14 are depicted in Figures 3-18 where the balloon force has been applied. Although the balloon force is applied on the passive part of the snake, active snake vertices that are close to the passive part are deformed accordingly to allow a smooth transition between the active and passive parts. This smoothness constraint is assured by the second term of the internal energy (rigidity). This characteristic is shown in Figure 3-19 where a sequence illustrates successive steps in which the balloon force is applied. The direction in which the balloon force is applied can be estimated by analyzing the spatial direction of adjacent road sides in relation to each other. In every case, the balloon force must apply toward the junction central

area. It is noted that when two adjacent road arm sides are collinear, related junction border is reconstructed by connecting the end points of the road arm sides. Therefore, our snake model does not apply to this part (Fig. 3-20).

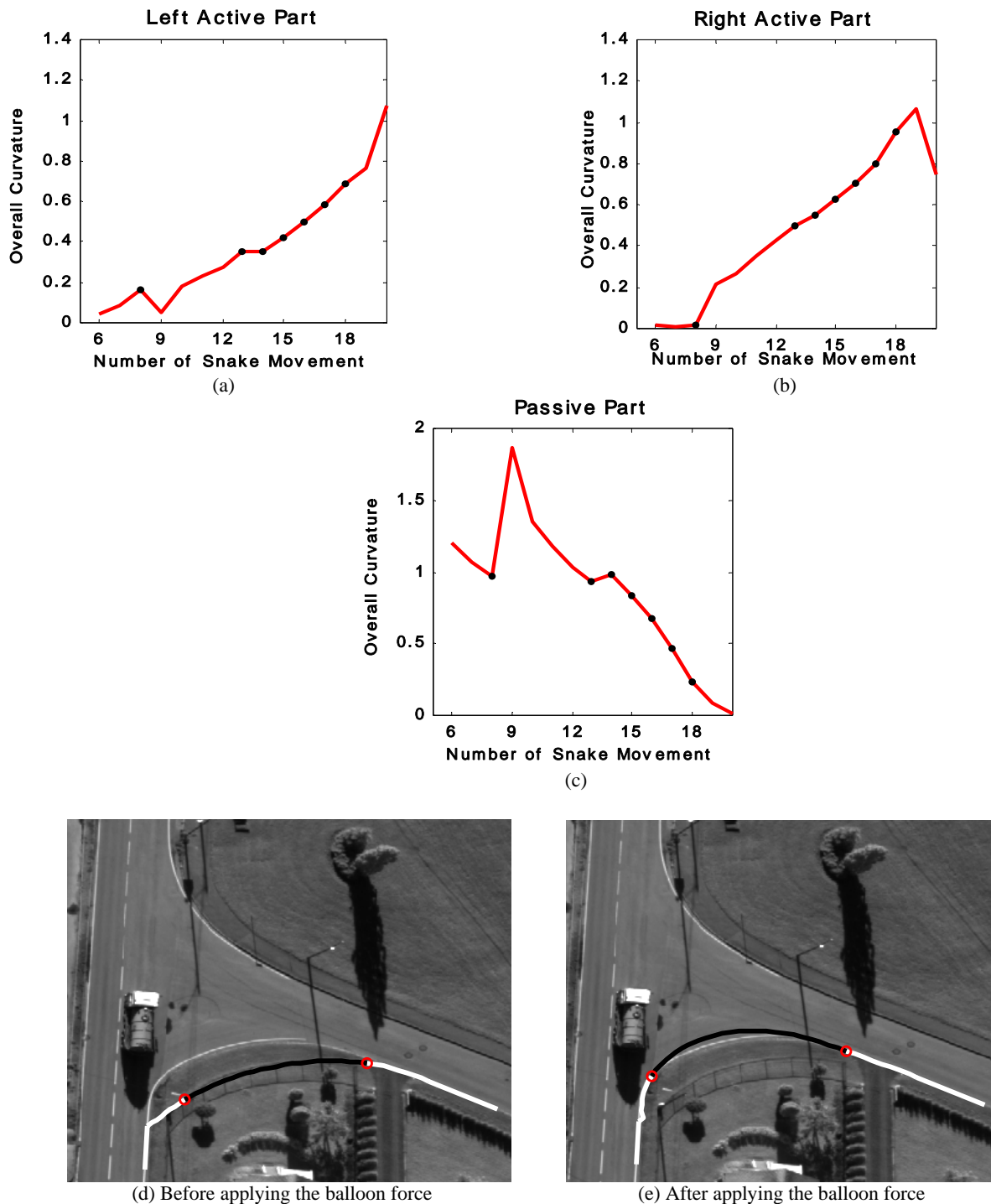


Figure 3-16 : Describing when and how the balloon force is applied. Curvature fluctuation in active and passive parts occurred during the snake optimization is shown in (a), (b) and (c). Black points on the graphs indicate the time instances when the balloon force is applied. When the number of the snake movement is 8, for the first time the balloon force is applied. This results in the inflation in the snake passive and active curves though for the active curve the amount of inflation is far smaller. In (d) and (e), this characteristic is shown on the related image.

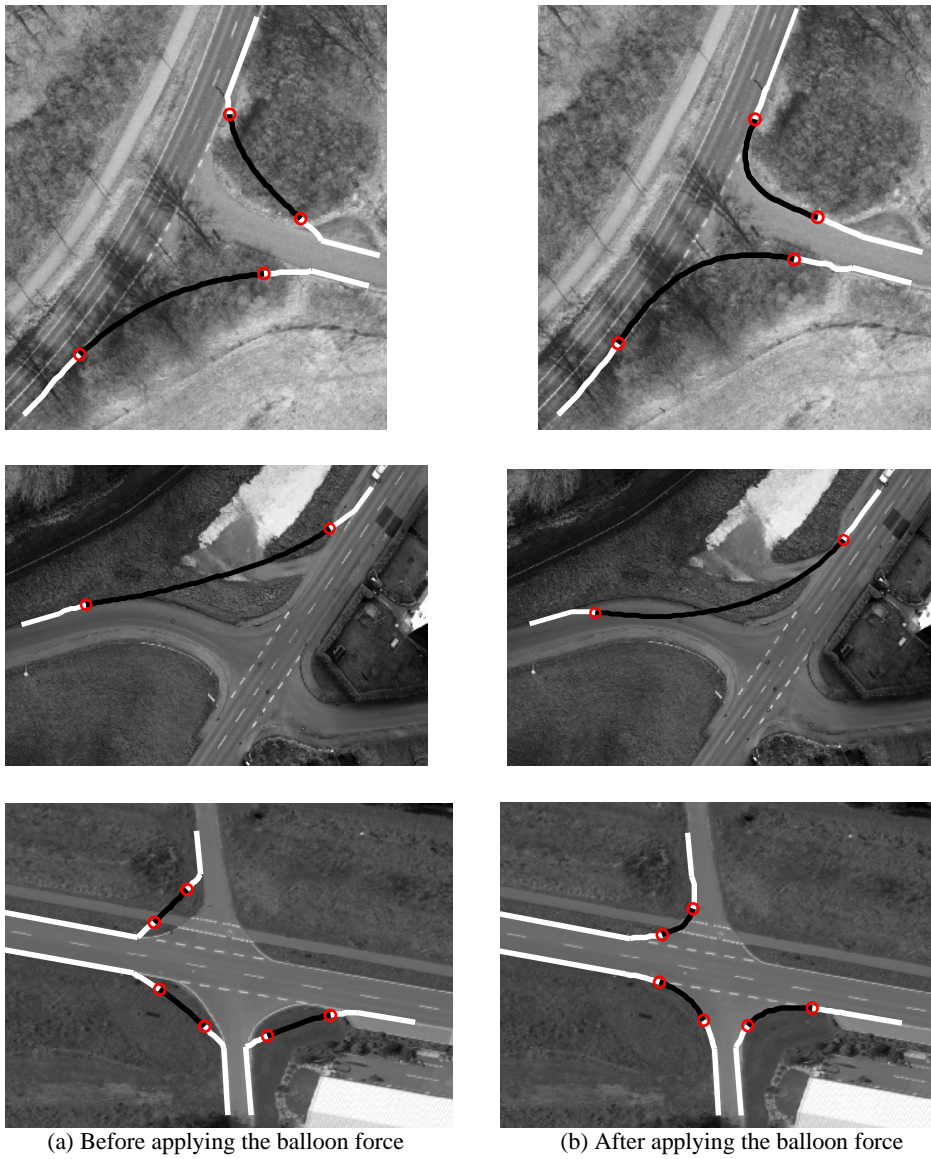


Figure 3-17 : (a) Snake optimization before the balloon force is applied. Active curves (white) and the passive part (black) are approximately straight. (b) The effect of the balloon force on the passive and active parts is shown after the balloon force is applied for the first time.

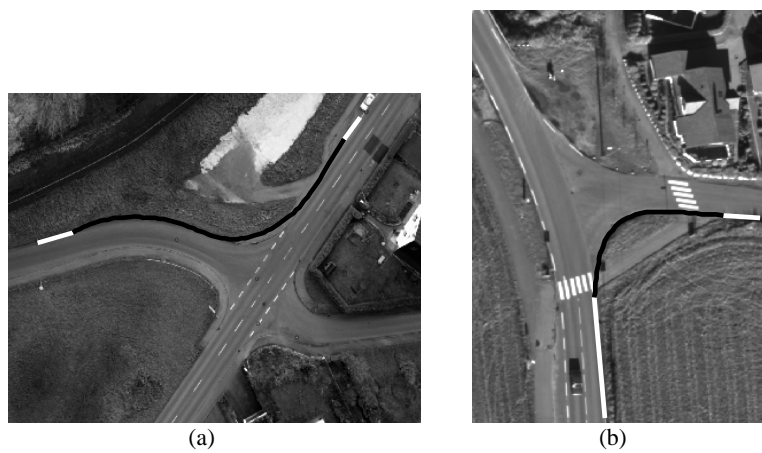


Figure 3-18: Illustrating the effect of the balloon force to overcome high variation of curvature on junction borders (a) and poor contrast (b).

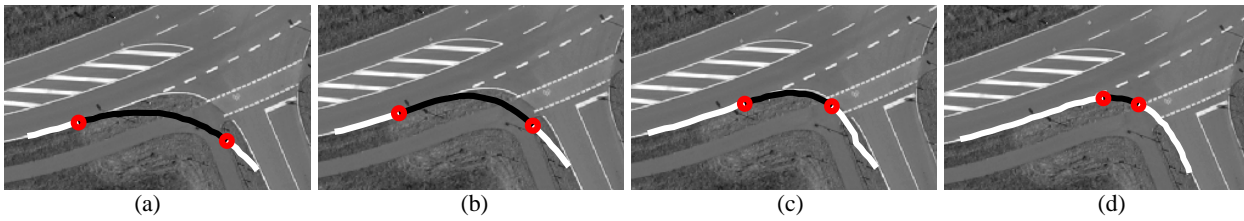


Figure 3-19: The effect of the balloon force in four successive steps. In (a), for the first time the balloon force is applied. (b) The intermediate result of applying the balloon force. In (c), a slight deformation of the bottom-right active part close to the passive part can be observed and in (d) both active and passive parts captured the junction boundary correctly.

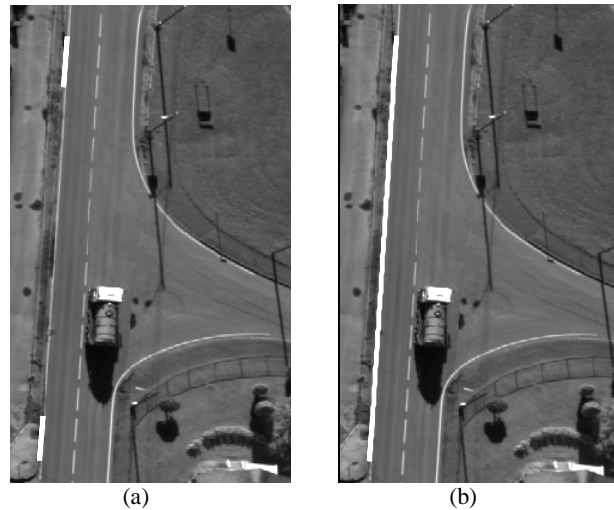


Figure 3-20: Detection of the junction border when associated road arm sides are collinear. (a) Collinear road arm sides. (b) Detected junction border.

### 3.3.3.2 Implementation Issues

In our implementation, we chose  $\alpha = 0.0001$  because a larger value forces the snake to become and then stay straight. By experiment,  $\beta = 3$  was chosen to let the contour become smooth. To reduce the effect of disturbances, we set  $\kappa = 0.1$ , i.e. giving more weight to the internal force than to the external. The amplitude of the balloon force ( $k_1 = 0.025$ ) needs to be set smaller than the amplitude of the GVF ( $\kappa$ ) so that edge points can stop the balloon force [Cohen 1991]. Each force boundary is moved individually but at most one vertex per iteration.

A force boundary is advanced when we can verify that the motion of the corresponding active part has stabilized. We do this by testing at each iteration step whether the mean change in image coordinates of active vertices is below 1/200 pixel. This threshold in places where boundaries with poor contrast or disturbances exist may not be met, in which case the threshold value is increased incrementally from 1/200 to 1/100 pixel allowing the snake optimization to continue. Snake spacing refers to the distance between the sampled snake vertices. Denser snake vertices are more likely to be trapped by such features as vehicles and road markings (Fig. 3-21-a). Conversely, when snake vertices are too sparse, concave object boundaries, as it is the case in road junctions, cannot be delineated correctly (Fig. 3-21-b). We noticed that the latter problem when not severe can be solved by balloon forces. The snake spacing was set to be 10 pixels so that the movement of snake vertices is less likely to be blocked by trees, single cars and road markings such as stop lines and cross walks. Likewise, the disturbing effect of the shadow cast by traffic lights and power lines are easily resolved. However, rows of cars standing behind the traffic light, and every large body of shadow from a row of buildings or trees might mislead the snake to converge to wrong boundaries, because in such cases, a large number of vertices are trapped in the disturbing object. This situation affects the motion of neighboring vertices and eventually results in the delineation of the disturbing object boundaries or the leakage into either the road junction area or the surroundings. Another problem which can occur frequently in roundabouts and less likely in simple and complex junctions is that a close global initialization cannot be provided when the angle between a pair of intersection lines is sharp ( $<40^\circ$ ). As a result, the snake is unable to converge to the junction border. A close global initialization is supplied by decreasing the length of the intersection lines by half (Fig. 3-22). In our proposed approach, the force boundary is advanced one vertex per iteration when we can verify that the motion of the corresponding active part has stabilized. We evaluate each active part individually by testing if the displacement in x and y direction are less than a predefined threshold. Once two force boundaries collide, the viscosity factor is increased and the optimization is repeated simultaneously on all vertices since we found experimentally that this additional step improves the quality of the final result at places where there is a small deviation from the object boundaries.

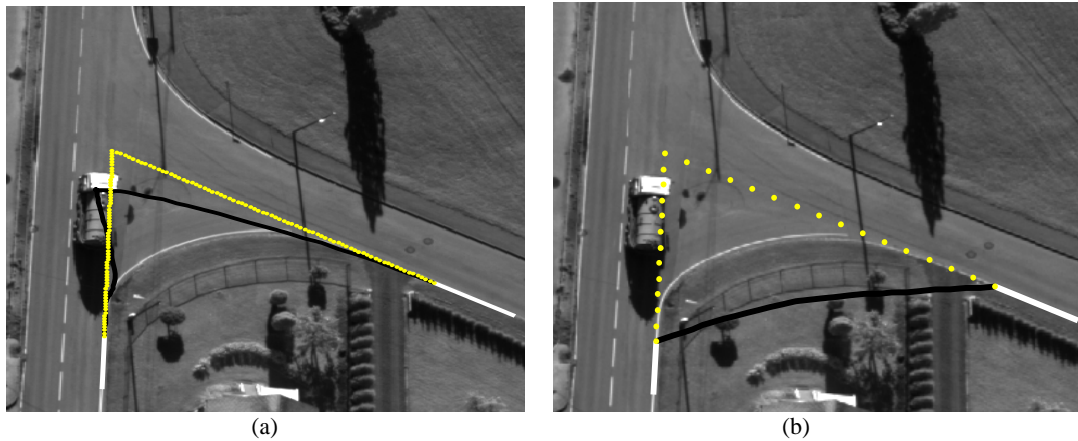


Figure 3-21 : Illustrating the snake behaviour with two different snake spacing values. (a) Snake spacing is 3 pixels, which signifies dense initial vertices (yellow), and the convergence threshold is  $1/200$  pixel. Here, the snake is caught by the truck and its shadow (black line). (b) Snake spacing is 15 pixels with the same convergence threshold. The optimized active contour cannot delineate the junction border even if the balloon force is active.

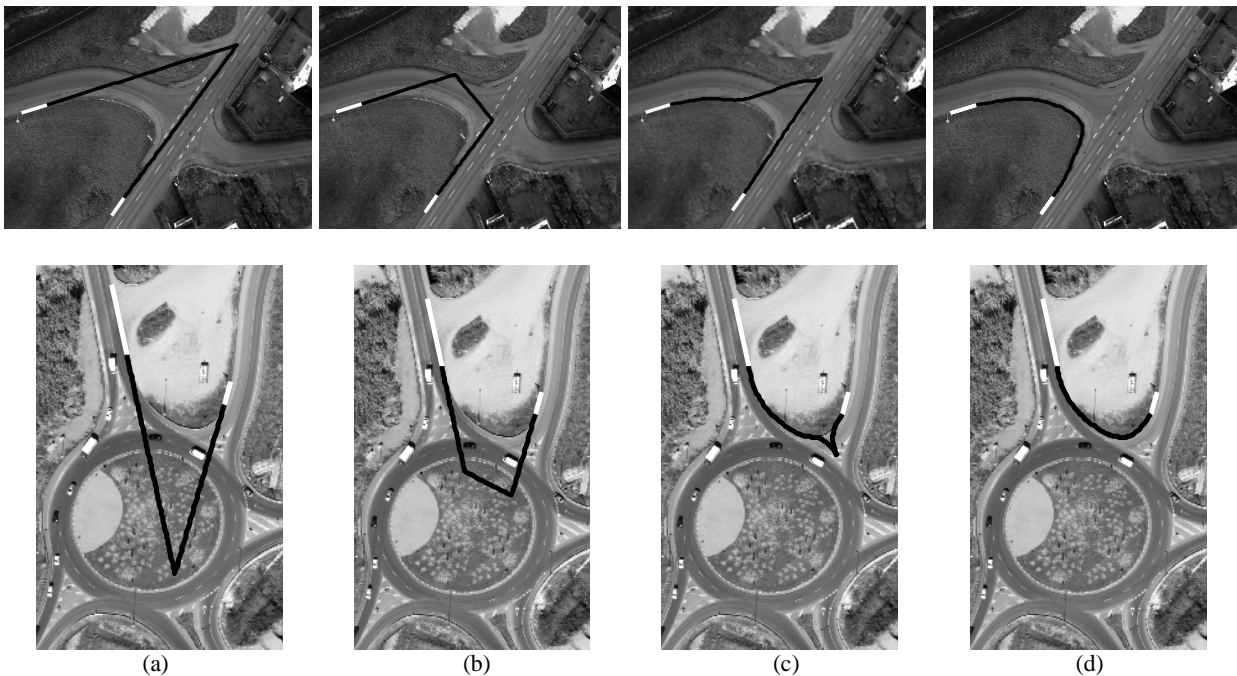


Figure 3-22 : (a) Intersection lines when their intersection angle is sharp (Intersection angles in the top row and bottom row examples are  $35^\circ$  and  $27^\circ$  respectively). (b) Intersection lines whose lengths are modified. Column (c) and (d) show the results of the snake optimization for (a) and (b) respectively.

### 3.3.3.3 Discussion

A close initialization is of significant importance to the success of our snake model. We make use of road arms and shape information of the junction to achieve this goal. Road arms are used to initialize the snakes along the junction border. Furthermore, the angle between crossing roads is used to reduce the length of intersection lines, thereby improving the quality of the initialization. We described in several examples how the curvature of the junction border can be exploited to design an efficient snake model by incorporating the balloon force into the GVF external force. The internal force is decided to be strong enough to overcome various kinds of disturbances. This useful property, however, causes the snake to become straight early and sometimes pass over weak junction borders. The balloon force in such cases is helpful so that it pushes the snake back until the snake localizes the desired boundary.

### 3.3.4 Extraction of Islands

By definition, a complex road junction can contain several small islands located in its central area and enclosed by the junction border (see section 3.1). The number of islands varies in different junctions depending on the number of crossing roads and the junction functionality. Islands are of diverse geometrical shape. Furthermore, they might be

partially occluded by shadows from traffic lights, traffic signs and vehicles. These properties imply that the extraction of islands is a challenging problem in aerial image analysis. Furthermore, the number of islands in the junction is unknown. Therefore, it is crucial to be able to handle a change of topology of the curve that is to delineate islands. Geometric active contours provide a solution to the problem of the required change of topology.

### 3.3.4.1 Island Model

Generally, islands whose surface is covered with bush or grassland appear darker than the surrounding surface. In contrast, they appear lighter when covered with only soil. In both cases, there is a sufficient contrast between the surrounding area within the junction and the island surface. This is a pre-condition in our approach for a successful detection of islands. Although islands have various geometrical shapes, their boundary is smooth, i.e. only a few peaks of curvature along their boundaries exist.

### 3.3.4.2 Workflow for island extraction

When extracting islands, we make use of the junction outlines obtained using our snake-based approach. This component together with the aerial imagery is regarded as input. Our strategy comprises three steps (Fig. 3-23). The obtained result consists of the extracted islands.

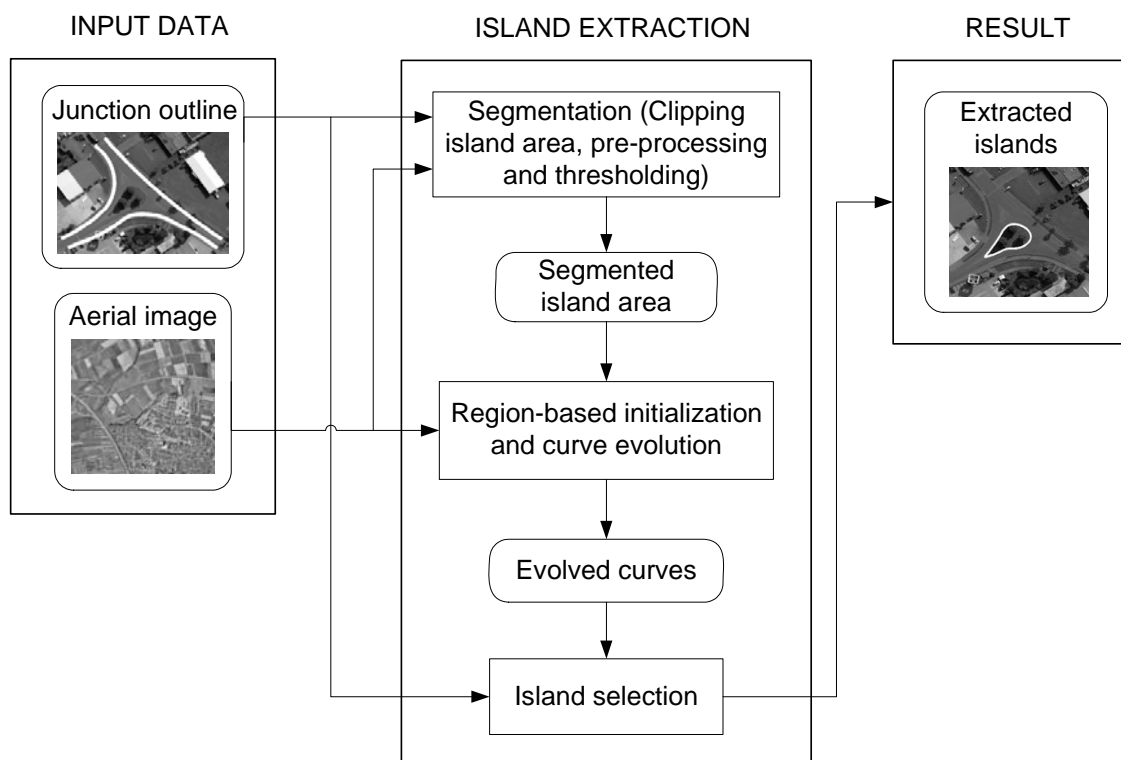


Figure 3-23: Work flow of island extraction

### Segmentation

First, the image area in which islands are located is clipped from the image. The search space for islands is further restricted to an area around the estimated junction centre point called *island area* (Fig. 3-24-a). To begin the island extraction by curve evolution, the initial level set function needs to be constructed. It is computed within the island area. Prior segmentation of this area is carried out to derive a rough idea of island regions from which the initial level set function is constructed. Skipping the segmentation step results in a much larger number of iterations, furthermore, many undesirable features can be delineated when the evolving curve moves towards islands.

Since we work in suburban or rural regions we assume that most of the junction area shows a rather homogeneous grey value distribution. This assumption is equivalent to expecting that there are not too many disturbances such as cars or shadows in the junction. Under these circumstances, the histogram of the pre-processed image shows one main peak which is related to the surface material of the road and potentially a few smaller peaks related to the islands and various disturbances (Fig. 3-24-e). To start pre-processing morphological opening is applied in order to remove distortions such as road markings (Fig. 3-24-b). Subsequently, closing with the same structuring element is performed to eliminate small shadows etc. (Fig. 3-24-c). Next, Gaussian smoothing is applied to the image (Fig. 3-24-d) followed by thresholding the histogram (Fig. 3-24-f). The threshold value is computed by applying the Iterative Self-Organizing Data Analysis

Technique Algorithm (ISODATA) [Ridler and Calvard 1978] on the histogram of the island area. At this stage, we consider convex areas inside the junction to be potential islands.

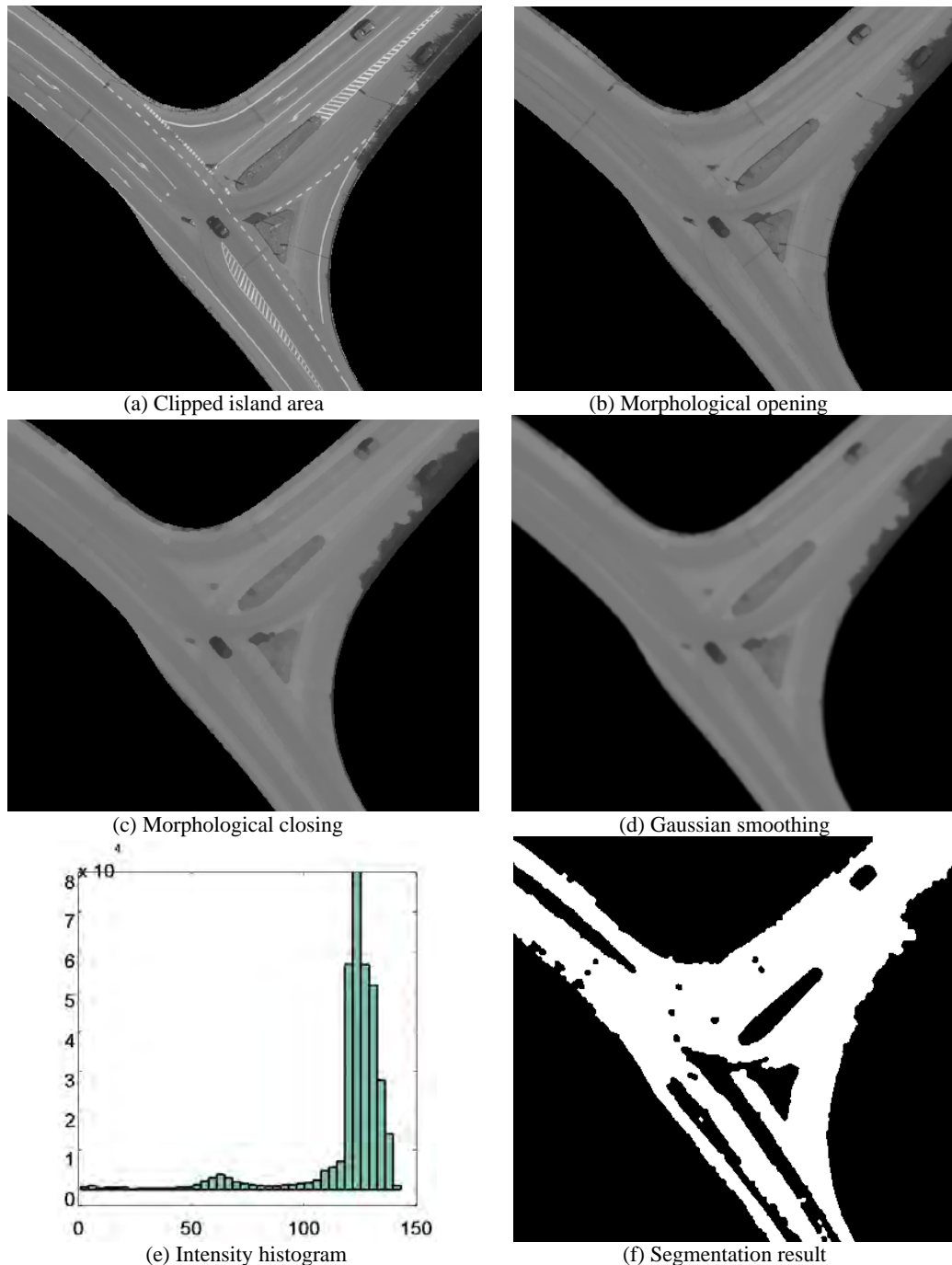


Figure 3-24: Illustration of the segmentation steps. (a) Clipped island area. In (b) and (c), a disk structuring element of size 5 is used for morphological operations. (d) Smoothed image. (e) Intensity histogram with two distinct peaks, of which the higher belongs to the asphalt area and the shorter to the islands. In (f), the threshold value is calculated to be 121 and the image is segmented.

### Region-based Initialization and Curve Evolution

The initial level set function is constructed from the segmented image (Fig. 3-25-a) so that areas in white are assigned a negative constant value and black areas take a positive constant value of the same magnitude. The zero level curves of the initial level set function are shown in Figure 3-25-b.

The curves usually enclose the island border either entirely or in part, so they need to move toward the island boundaries. To achieve this goal, the coefficient of the weight  $\nu$  of the area term in Equation (2.29) needs to be positive if the island surface is brighter than the surrounding asphalt area, and negative otherwise. In synthetic images in Figure 3-26 the problem is described. When the island appears on a darker background (Fig. 3-26-a top), it becomes a white area after thresholding (Fig. 3-26-b top). Therefore, the initial curve needs to evolve from black areas toward white

areas, which means a positive value of  $\nu$  is needed. Conversely, when the island appears darker than the background (Fig. 3-26-a bottom), it becomes a black area after thresholding (Fig. 3-26-b bottom).

Therefore, the initial curve needs to evolve from white areas toward black areas, which means a negative value of  $\nu$  is needed. Thus, depending on whether the island surface is brighter or darker than the background, the sign of  $\nu$  should be changed properly. In principle, the evolution of the zero level curve from black areas toward white areas is known as shrinkage curve evolution (positive  $\nu$ ) (Fig. 3-26-d top), whereas the evolution from white areas toward black areas refers to expansion curve evolution (negative  $\nu$ ) (Fig. 3-26-d bottom). The question of whether islands appear darker or brighter than the background is answered using the intensity histogram of the island area (Fig. 3-24-e) in such a way that shorter peak belongs to islands.

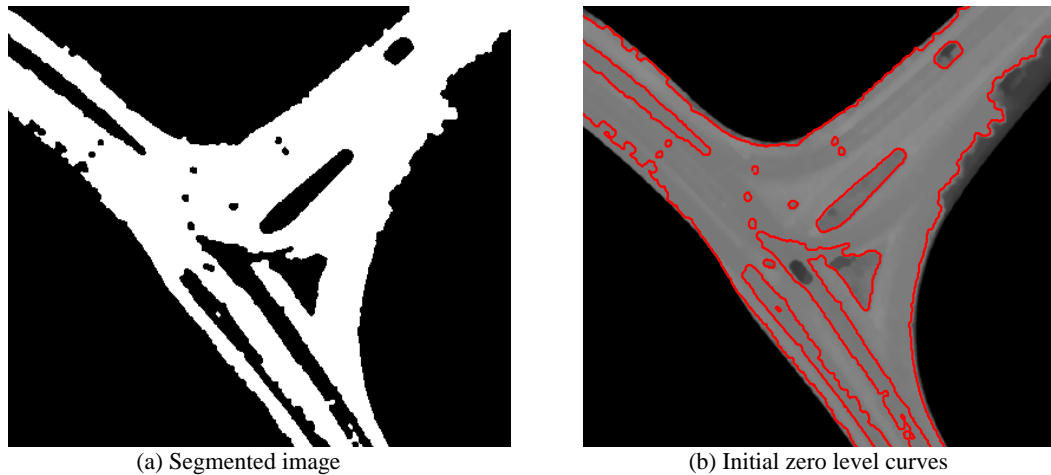


Figure 3-25: Illustration of initial level set function construction. (a) The same as depicted in Figure 3-24-f. (b) Initial zero level curves or interfaces.

In examples where among existing islands some are darker and some others brighter than the background, only one group of islands can be detected with our method. Since this problem originates from the segmentation, a suitable segmentation method can solve the problem.

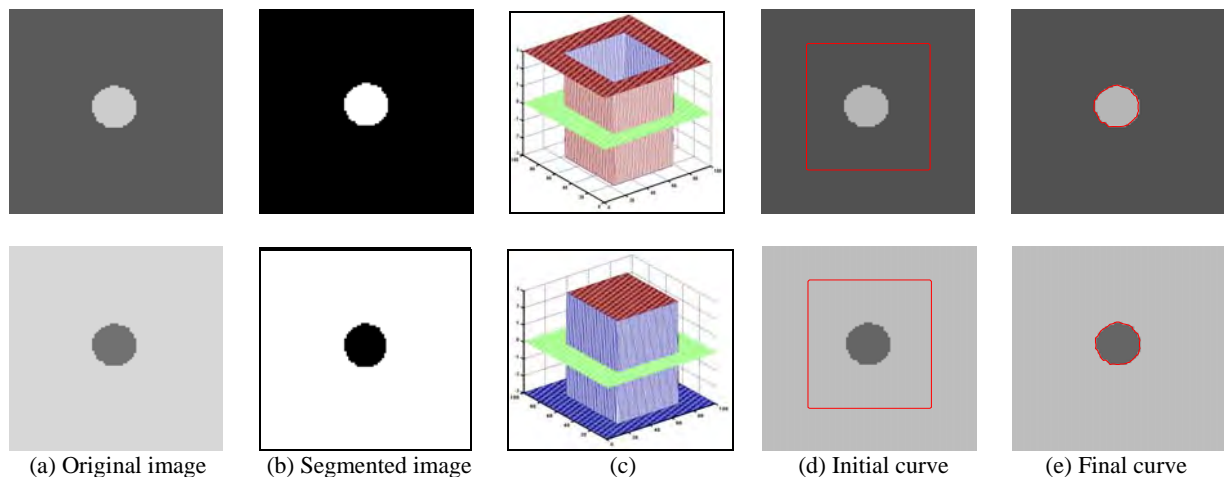


Figure 3-26 : Two sequences illustrating the choice of a proper curve evolution. (a) Original image. (b) Segmentation result. (c) Initial level set functions are displayed. They are designed so that the initial zero level curves derived from them lie outside the island area in (d). In (d), the curves need to shrink in order to converge to the object boundary. (e) Evolved curves have detected the islands.

In Figures 3-27 and 3-28, we have illustrated this property using real images when islands appear brighter and darker than the background. Then, the initial level set function will evolve according to the evolution Equation (2.41), with its zero level curve converging to the exact boundary of the islands (Fig. 3-29).

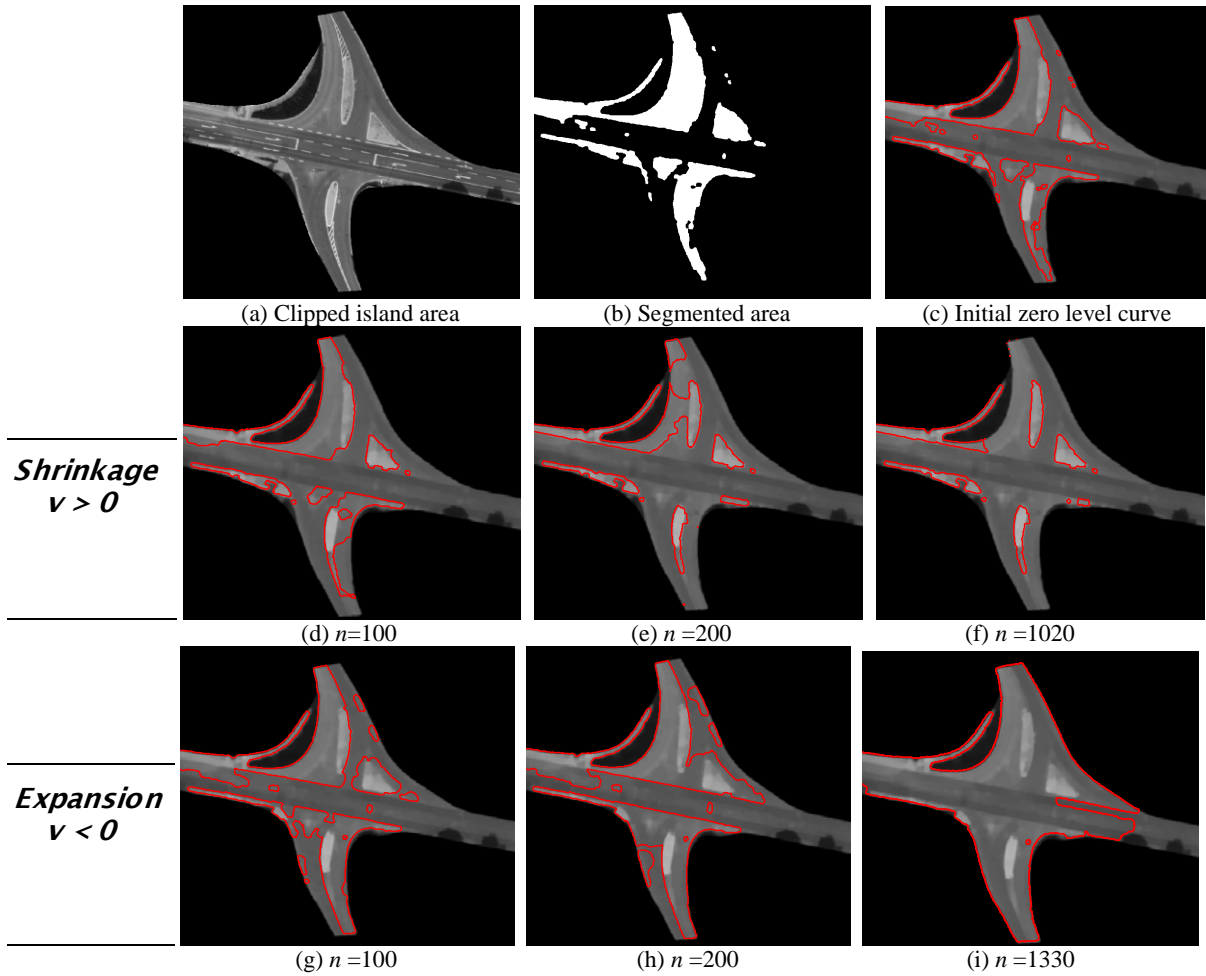


Figure 3-27: Comparison between the shrinkage and expansion curve evolution results when islands appear brighter than the background. In all figures,  $n$  is the number of iterations. (a) Clipped island area. (b) Segmentation results. (c) Initial zero level curves overlaid on the image. (d) and (e) are intermediate results when shrinkage evolution is applied and (f) displays the evolved curve. (g) and (h) are intermediate results when expansion curve evolution is applied on initial zero level curves in (c). (i) Evolved curves.

### Stop Criterion

The curve evolution is terminated when the overall change in the evolving curve positions per iteration is within sub-pixel range (Fig. 3-30). On the graph, Root Mean Square (RMS) of the change of curve coordinates is decreasing sharply from iteration 1 to iteration 265, from which point on only a slight change in the curve's movement (0.03 pixels) is reported after a high number of iterations (430 iterations). At iteration 695, RMS is reached its lowest value 0.04 and then remains unchanged. A similar behavior in RMS values of evolving curves is observed in all experiments. Since a small change of RMS (0.03) occurs from iteration 265 on, which in our work is almost negligible, we decided to take the RMS value 0.07 pixels as a threshold and consequently stop the evolution when the RMS of the evolving curve is smaller than the defined threshold. A smaller threshold considerably increases the computation cost, although the quality of the final result is the same.

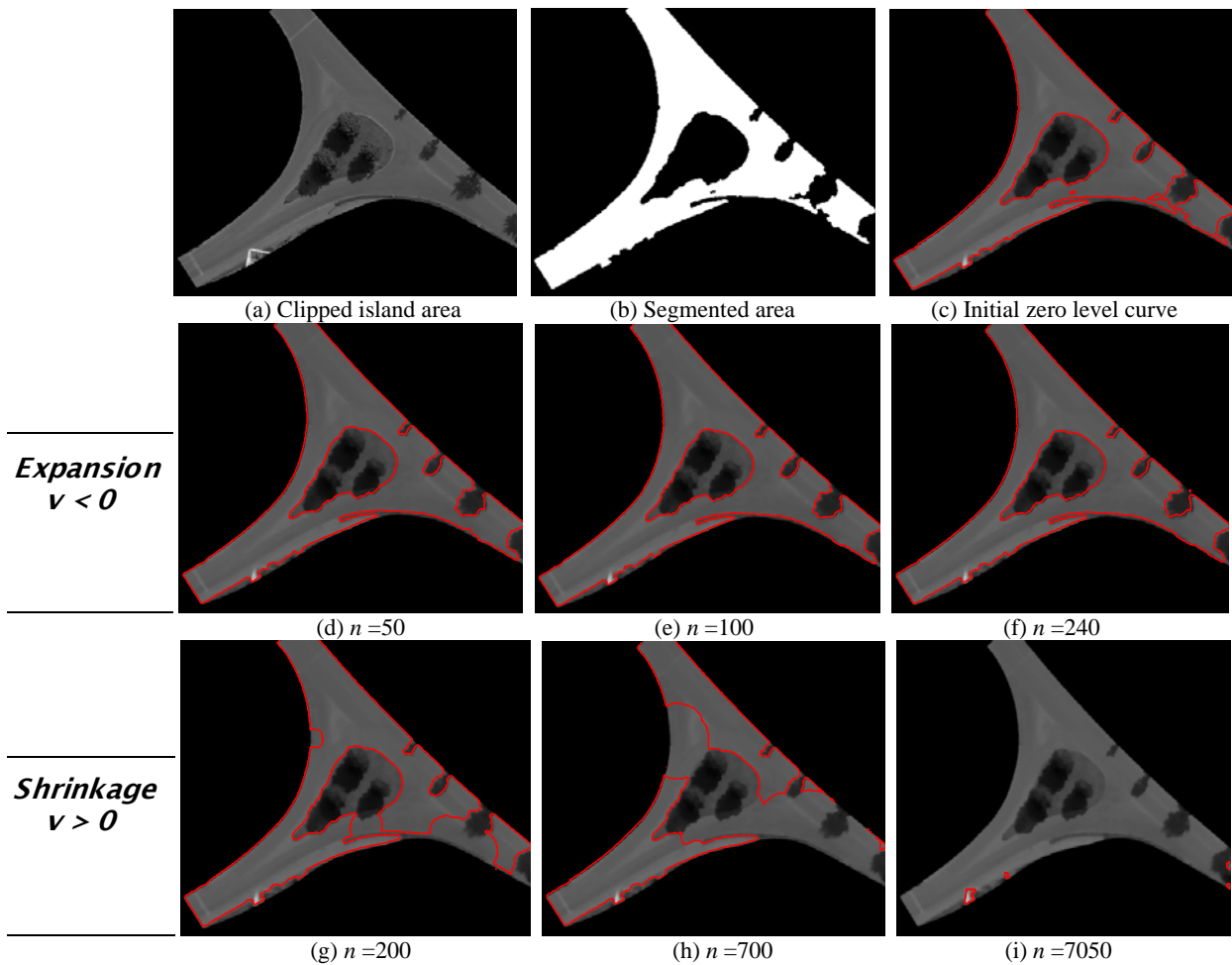


Figure 3-28: Comparison between the expansion and shrinkage evolution results when islands appear darker than the background. In all figures,  $n$  is the number of iterations. (a) Clipped island area. (b) Segmentation results. (c) Initial zero level curves overlaid on the image. (d) and (e) are intermediate result when expansion evolution is applied and (f) displays the evolved curve. (g) and (h) are intermediate results when shrinkage evolution is applied on initial zero level curves in (c). (i) Evolved curves.

### Selection of islands

In order to select the curves converged to the island boundaries, some geometric and topological constraints are introduced based on the properties of islands, because, in addition to the islands, some undesirable features such as vehicles and large shadow areas might be extracted as island candidates (Fig. 3-31-a). Small closed areas such as cars are easily removed as their areas are below a certain threshold (Fig. 3-31-b).

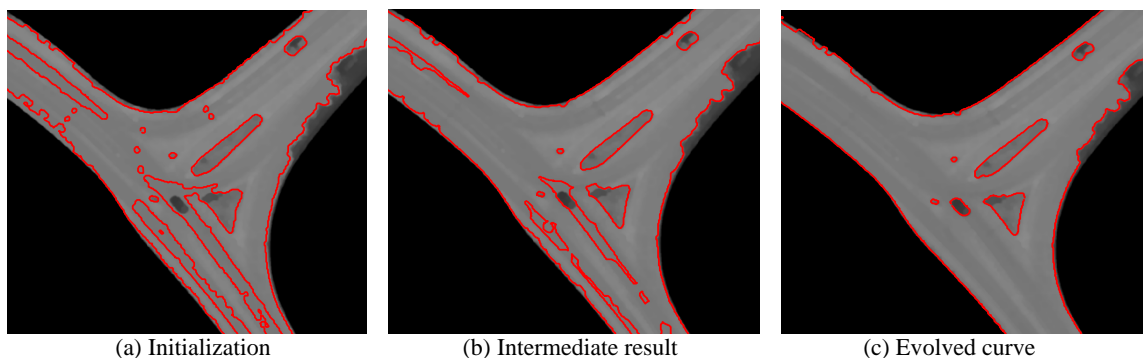


Figure 3-29: (a) The zero level curve of the corresponding initial level set function. (b) The intermediate result of the zero level curve evolution with  $\lambda=4$ ,  $\mu=0.13$ ,  $\nu=1.5$  and the time step  $\tau = 2.0$  ( $n=50$ ). (c) The zero level curve of the final level set function ( $n=265$ ).

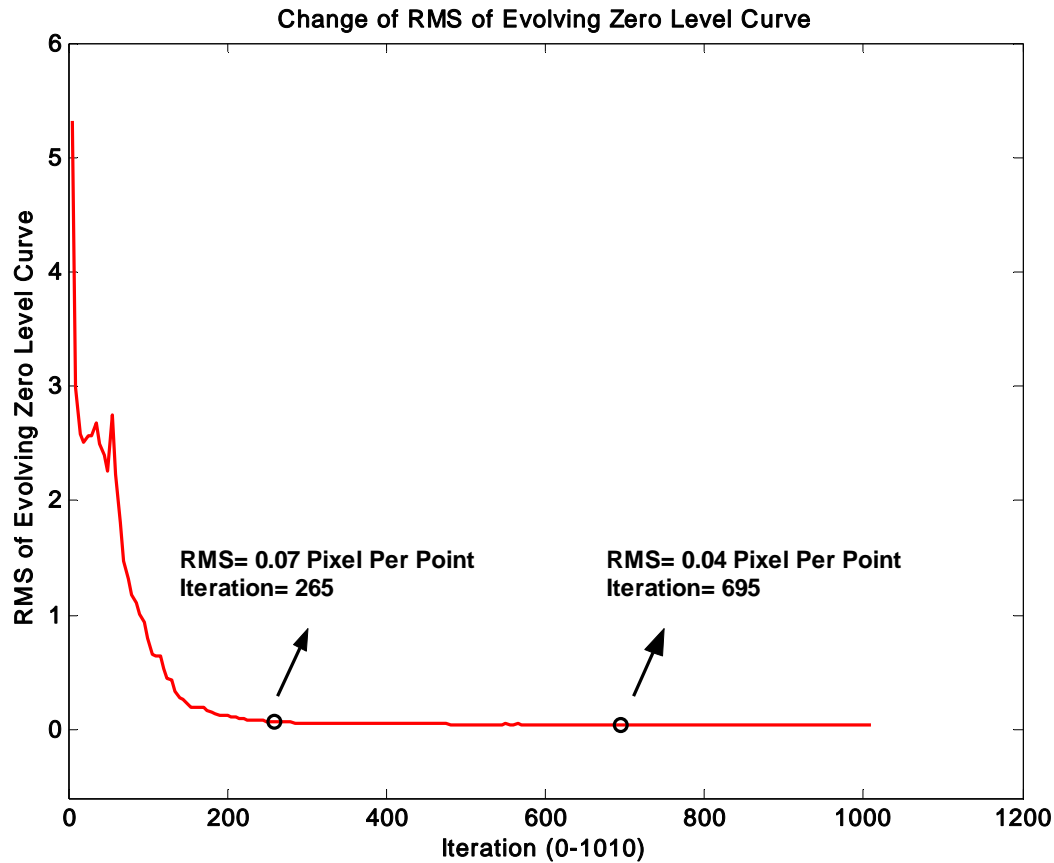


Figure 3-30: Illustrating fluctuations in the RMS of the interfaces during evolution

Since island candidates must be located within the junction outline, those curves that lie on the junction outline are removed (Fig. 3-32). Furthermore, islands possess boundaries with a small curvature variation, so the contours with high curvature variations are eliminated (Fig. 3-33). Each curve needs to be approximated first to become smooth using cubic spline technique (Fig. 3-34) so that the slight variation of curvature values caused by small disturbances is avoided.

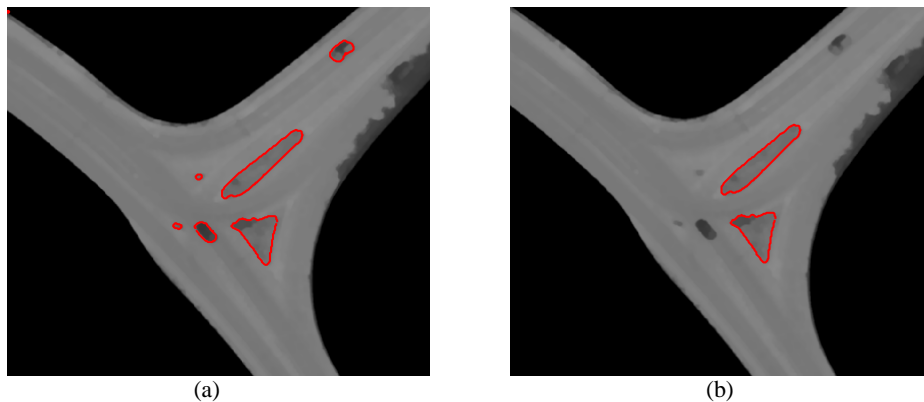


Figure 3-31: (a) Closed curves are retained as island candidates. (b) Two cars having areas of 13 and 11 m<sup>2</sup> are eliminated. The remaining islands have areas of 67 and 52 m<sup>2</sup>.

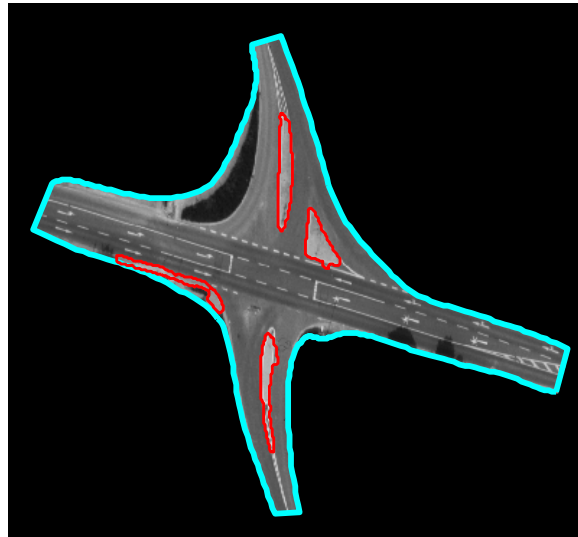


Figure 3-32: Illustration of the topological constraint. One of the obtained contours (left side) at some parts is located on the junction outline.

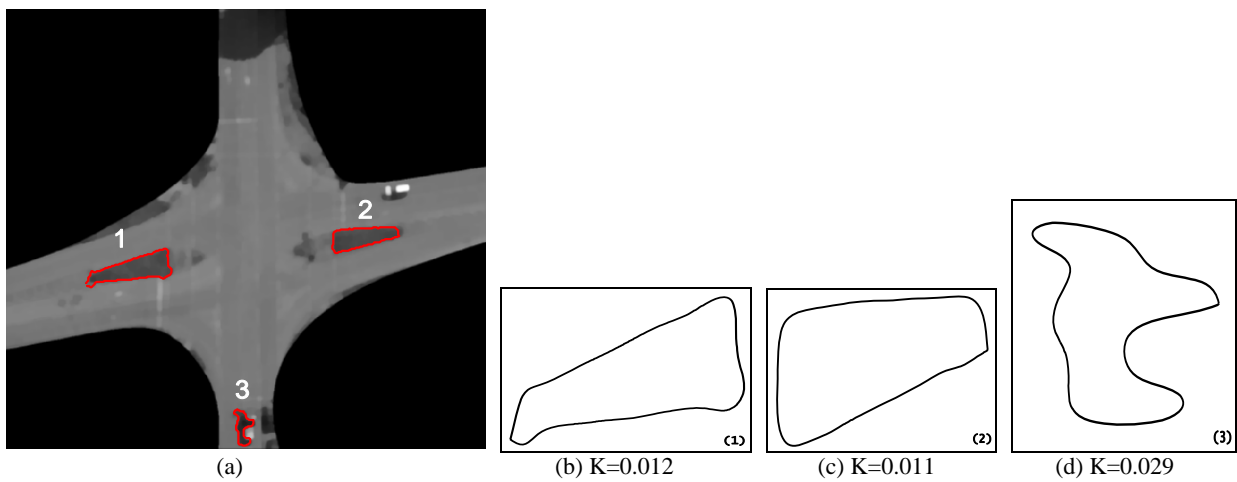


Figure 3-33: Illustration of the curvature constraint. (a) Islands labeled with numbers before applying curvature constraint. (b), (c) and (d) display the approximated curves 1, 2 and 3 and their computed mean curvature. The closed curve in (d) is not considered as an island as its mean curvature value is too high.

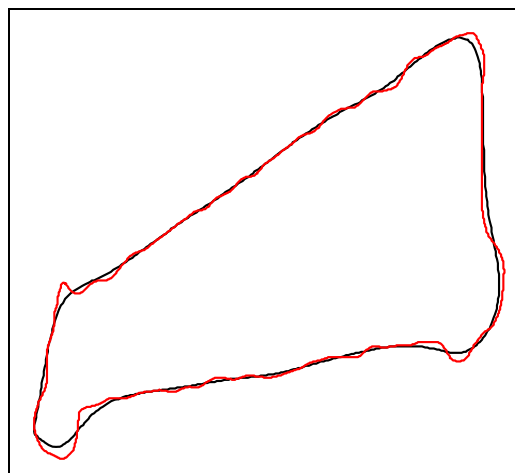


Figure 3-34: The evolved curve (red) for island 1 is approximated using cubic spline approximation technique (black) with a smoothness degree of 0.99 chosen within the range 0-1 so that the original shape is maintained.

### 3.4. Workflow for Roundabout

We defined different classes of road junctions and recognized roundabouts as subclass of complex junctions as both classes share the same characteristics. Therefore, the junction model used so far to extract simple and complex road junctions should be valid as well for roundabouts. In contrast to complex junctions, however, the island placed in the central area of roundabouts is much larger, which underlines the necessity to modify the current strategy (Fig. 3-35). The change is made in the island extraction step so that the central island is extracted at an early stage of the whole extraction process after analyzing the geospatial database, because a correctly extracted central island facilitates later stage of the roundabout reconstruction. Although road arm extraction is the same as used earlier, it can also benefit from the central island outline. In the reconstruction step, the snake external force field is modified based on the shape of the central island to assure a correct reconstruction result.

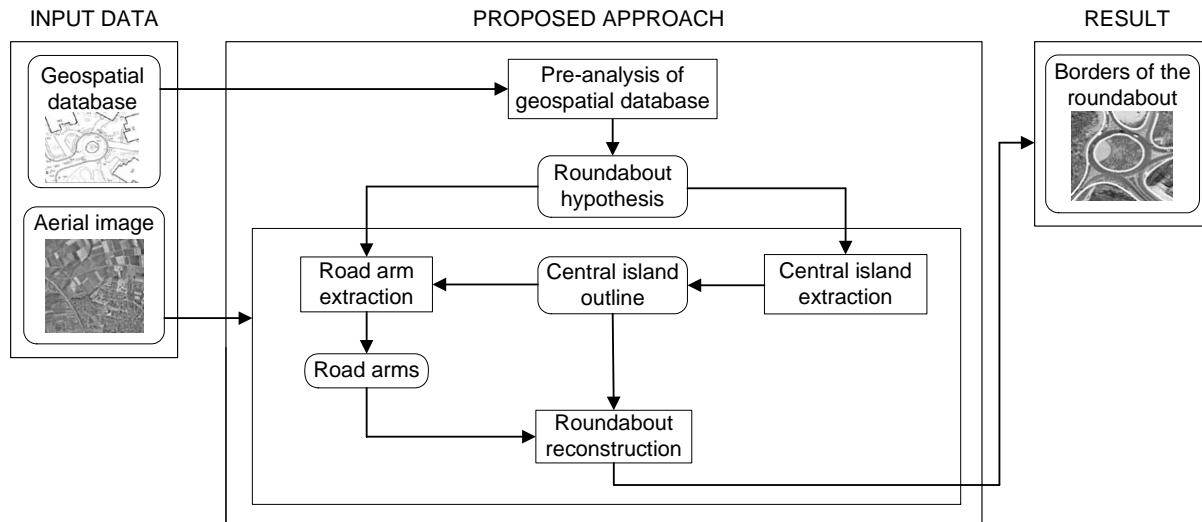


Figure 3-35: Workflow of roundabout extraction

#### 3.4.1 Pre-analysis of Geospatial Database

In existing geospatial databases, roundabouts are usually represented in one of two ways:

- As a point object when the diameter of the inscribed circle is small (Fig. 3-36-a). The actual threshold varies in different geospatial databases. For ATKIS the value is 30 m.
- As an area object when the diameter of the inscribed circle is larger than the threshold (Fig. 3-36-b).

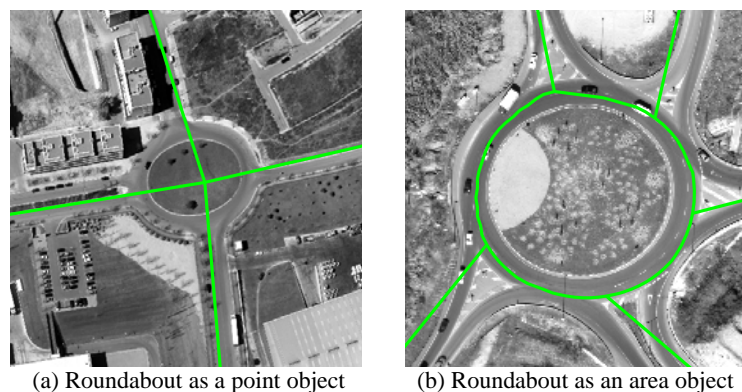


Figure 3-36: Vector data superimposed on the images

In addition to the information we derive for the extraction of road arms such as road width, road class and surface material of crossing roads, the diameter of the inscribed circle and the width of the circulating roadway are approximately determined. It is noted that the width of the circulating roadway depends mainly on the number of entry lanes. According to construction standards, the roadway must be at least as wide as the maximum entry width and generally should not exceed 1.2 times the maximum entry width [U.S. Federal Highway Administration 2000]. Figure 3-37 illustrates the relationship between these geometric parameters. In case that a roundabout appears as a point object, and is to be reconstructed with the developed method, attributive information must be included in the geospatial

database implying that the node represents a small roundabout. This means that the diameter of the inscribed circle is below the threshold that has been defined in the geospatial database.

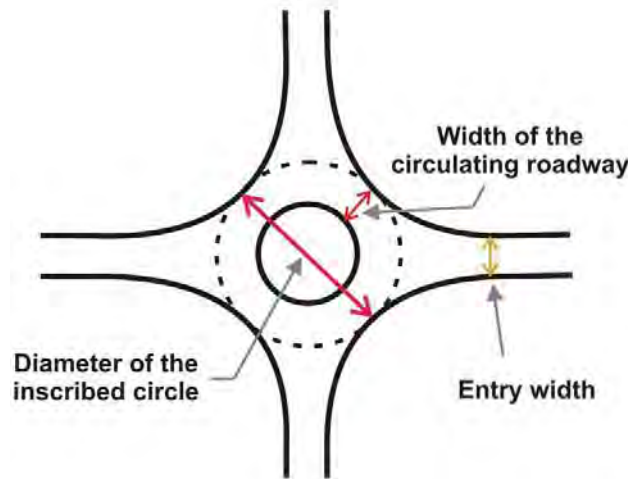


Figure 3-37: Illustration of the relationship between roundabout geometric parameters

### 3.4.2 Extraction of Central Island

Extraction of the central island is crucial to the extraction of the roundabout outline. Since islands in complex junctions are of small size, the junction outline is extracted independently, whereas in roundabouts, a correct extraction of the central island considerably facilitates the extraction of the outline. The reason is that the central island when enlarged influences the shape of the roundabout outline. Because of this, initial detection of the central island can give a good idea of how the outline appears in the image. Our method to detect central islands is based on the level sets we have used earlier to detect small islands (sections 2.2.4 and 3.3.4.2). Furthermore, we propose a hybrid evolution strategy to overcome disturbances.

#### 3.4.2.1 Initialization and Hybrid Curve Evolution

Although the level set formulation used is similar to the one used for the detection of small islands, the initialization of level sets and curve evolution strategy is different. For the extraction of large central islands in roundabouts, we cannot rely on the result of expansion or shrinking evolution alone. For example, if we decide to perform only the shrinkage curve evolution, it frequently occurs that cars and trucks block the movement of the evolving curve and consequently some parts of the island boundaries cannot be delineated (Fig. 3-38-b). In this case, the result of the ellipse fitting lies outside the island area (Fig. 3-38-d). For this experiment and other examples of central island detection we used the same set of control parameters,  $\lambda=4$ ,  $\mu=0.13$ ,  $\nu=2$  and the time step  $\tau = 2.0$ , for the evolution equation (Eq. 2.41). Since either evolution type alone has its own limitations, we employ a hybrid evolution strategy to overcome various kinds of disturbances often present inside and outside the central island.

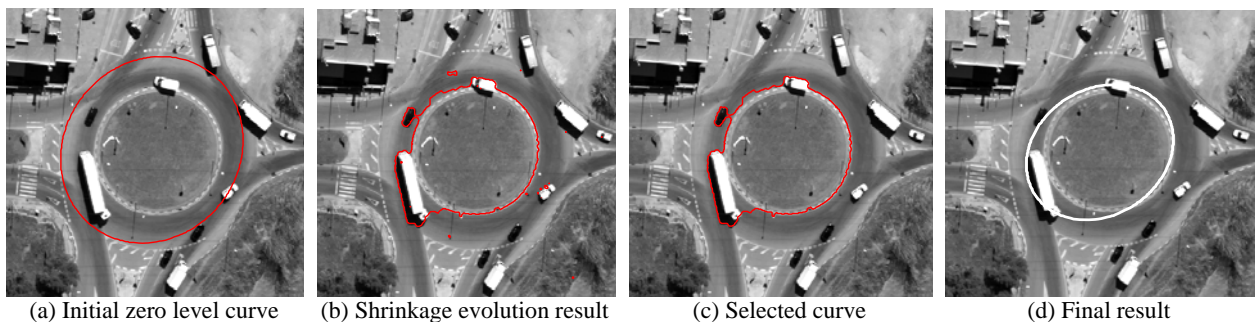


Figure 3-38: Showing the effect of disturbances when only one type of evolution is carried out. (a) Initial zero level curve superimposed on the image. (b) Evolved curves with the set of control parameters  $\lambda=4$ ,  $\mu=0.13$ ,  $\nu=2$  and the time step  $\tau = 2.0$ . These parameter settings are chosen for all experiments in this section. (c) The largest closed curve selected from evolved curves in (b). (d) Island is extracted by fitting an ellipse to the selected curve in (c). The result of applying our proposed approach to detect the central island in this sample is illustrated in Chapter 4.

Often before the curve evolution begins, a pre-processing step is necessary to remove some fine features that might hinder the curve motion. First, a morphological closing operator is applied in order to remove dark spots (Fig. 3-39-c)

and subsequently the opening with the same structuring element is performed to eliminate small bright features (Fig. 3-39-d) followed by Gaussian smoothing (Fig. 3-39-e).

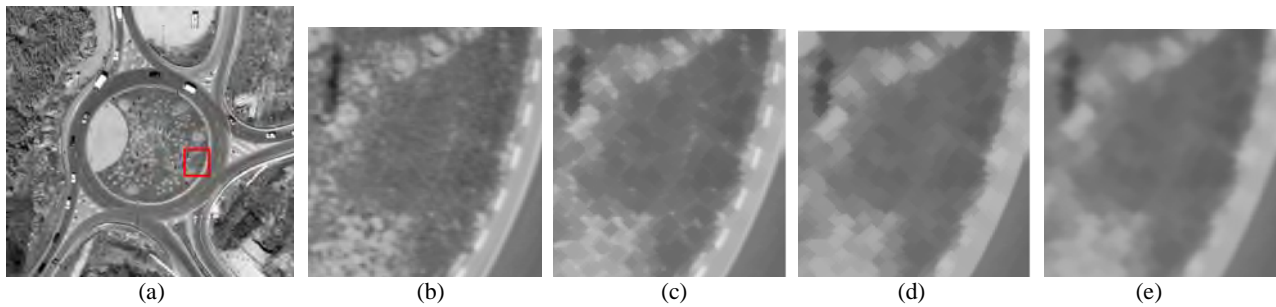


Figure 3-39: Illustrating preprocessing steps. (a) Original image. (b) A cut-out marked in the red box in (a). In (c) and (d), a disk structuring element of size 2 is used for the morphological operations, closing and opening respectively. In (e), Gaussian smoothing with disk structuring element of size 3 and standard deviation 2 is applied.

First, the extraction strategy when roundabouts appear as area objects is described. After locating vertices of the polygonal area identified as a roundabout object in the geospatial data base, we enlarge the polygon so that its increased area is one-tenth more than its initial area (Fig. 3-40-a), thereby making sure that the new polygon is located outside the central island. Hence, an ellipse is fitted to the obtained vertices as central islands are of ellipsoidal shape (Fig. 3-40-b) and subsequently shrinkage evolution begins using level sets. Among obtained closed curves in Figure 3-40-c, the one with the largest area is selected as the initial guess for the island. This island candidate is subject to further processing.

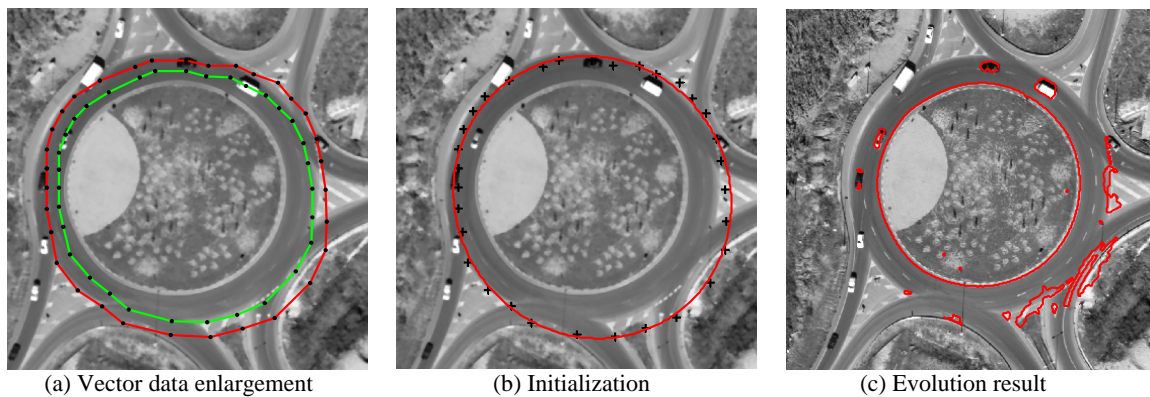


Figure 3-40: Illustrating initialization and shrinkage curve evolution. (a) Polygonal vector data (green) and its enlargement (red). Black dots represent vertices. (b) Initial zero level curve as an ellipse fitted to vertices. (c) Evolved zero level curves obtained after 1335 iterations.

Therefore, we make the initial polygon obtained from vector data smaller so that its area is reduced to half (Fig. 3-41-a). Subsequently, an ellipse is fitted to the obtained vertices (Fig. 3-41-b) and expansion curve evolution begins until the evolution is stopped (Fig. 3-41-c). The largest closed curve is most likely the desired solution due to the fact that the island is the largest object within the computational domain.

This closed curve, however, can not be regarded as the island because many disturbing features like trees and various structures exist inside the island, which can block the motion of the evolving curve toward the island boundary. Therefore, we have to be able to create leakages at some points along the boundary of disturbing features where zero level curves have stopped in order to pass over them. Assuming that disturbing objects inside the island don't contain smooth boundaries, cubic spline approximation is carried out to provide leakages (Fig. 3-42-a). Subsequently, expansion evolution and spline approximation are repeatedly carried out (Fig. 3-42-b) until no change in the position of the curve is reported. Again, the largest closed curve is regard as island (Fig. 3-42-c). The central island is usually enclosed by a raised curb which facilitates its extraction and prevents the evolving curve of leaking outside.

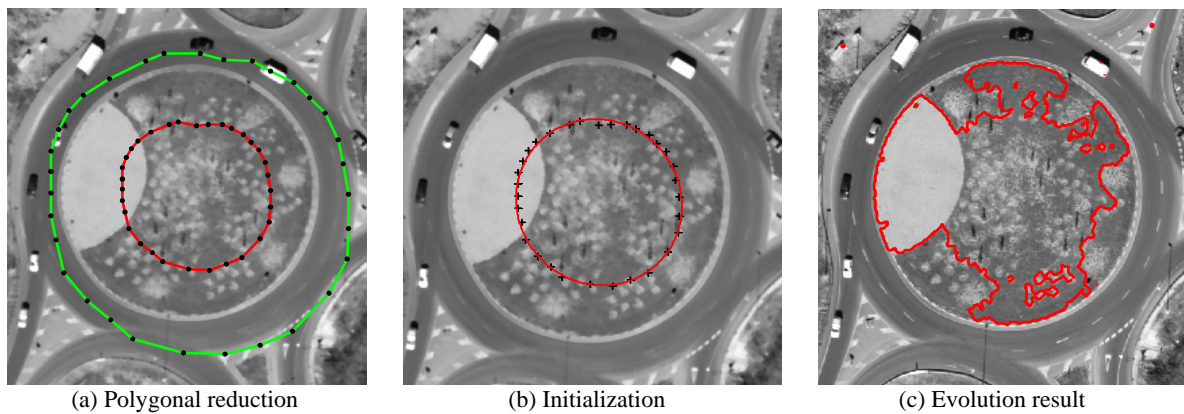


Figure 3-41: Describing initialization and expansion curve evolution. (a) Polygonal vector data (green) and its reduced polygon (red). (b) An ellipse is fitted to the obtain vertices and used as an initial zero level curve. (c) Expansion evolution results after 1330 iterations.

Now that the results of island detection from the iterative expansion and shrinkage curve evolution are obtained, we compare the image positions of the resulting curves and select those points which are close to each other (Fig. 3-43-a), thereby eliminating curve positions that are not located on the island boundaries. Selection of points is based on the closeness of points in such a way that points having a distance below a certain threshold are selected (Fig. 3-43-b). The final result is obtained when an ellipse is fitted to the selected points (Fig. 3-43-c).

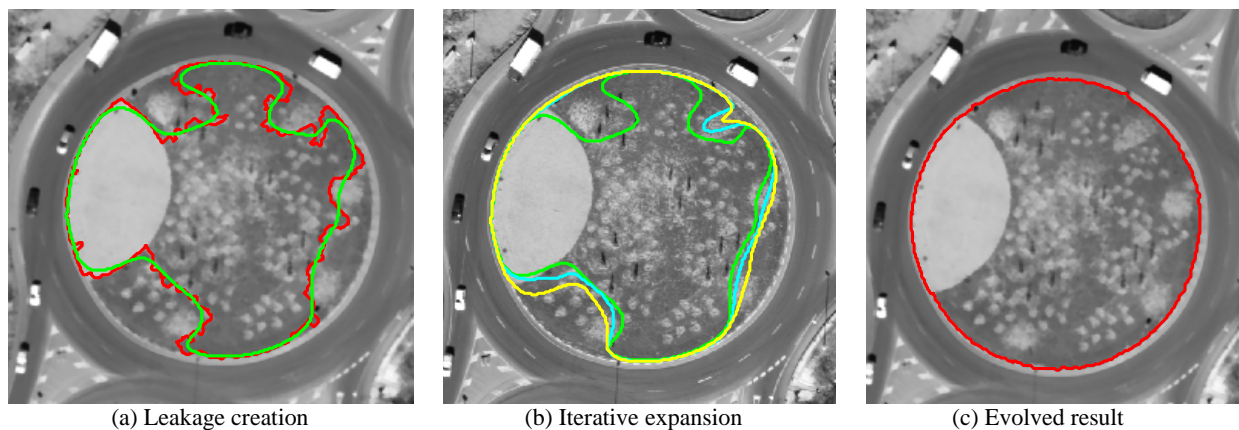


Figure 3-42: Illustrating leakage creation and iterative expansion curve evolution. (a) Selected red curve from figure 3-41-c and its approximated curve by cubic spline technique (green). (b) The approximated results of iterative expansion curve evolution in different colors. Green curve is the same curve as in (a) and cyan and yellow shows the results of two successive expansions. (c) The largest closed curve after the iterative expansion evolution stopped.

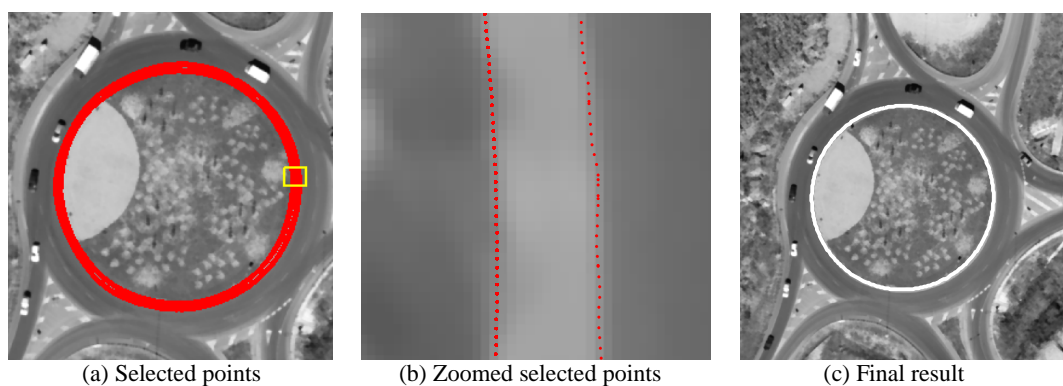


Figure 3-43: (a) Points selected from the iterative expansion and shrinkage curve evolution results when they are close enough. (b) Selected points within a smaller area specified in a yellow box in (a). The distance between points from two groups of results is less than 2 m. (c) The resulting island after fitting an ellipse to the selected points.

When a roundabout appears as a point object in the geospatial database (Fig. 3-44-a), the same hybrid evolution strategy is used but with a different initialization because we know that the diameter of the inscribed circle is below a known

threshold but how small it is, is unknown. This brings some limitations for the shrinkage curve evolution. In order to apply the shrinkage evolution, the initial zero level curve must be placed outside the island. Since the approximate diameter of the inscribed circle is unknown, we define three successive circles (Fig. 3-44-b) on each of which the shrinkage curve evolution is carried out separately. Intermediate and final results of shrinkage evolution on each initial curve from the smallest to the largest circle are depicted in Figure 3-45.

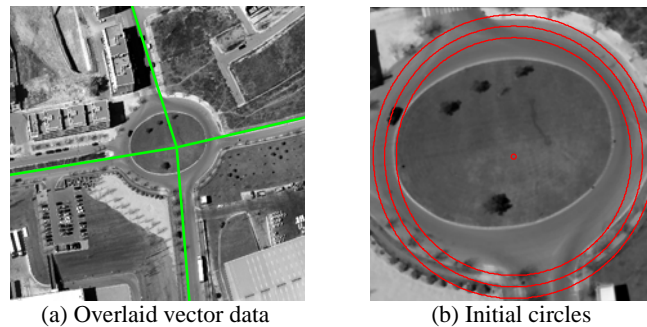


Figure 3-44: (a) Vector data overlaid on the image. (b) Three successive circles with an interval of 3 m in their diameters. The node indicates derived roundabout position in the vector data around which circles exterior to the island are defined. Among three circles, the smallest circle is not located entirely outside the central island.

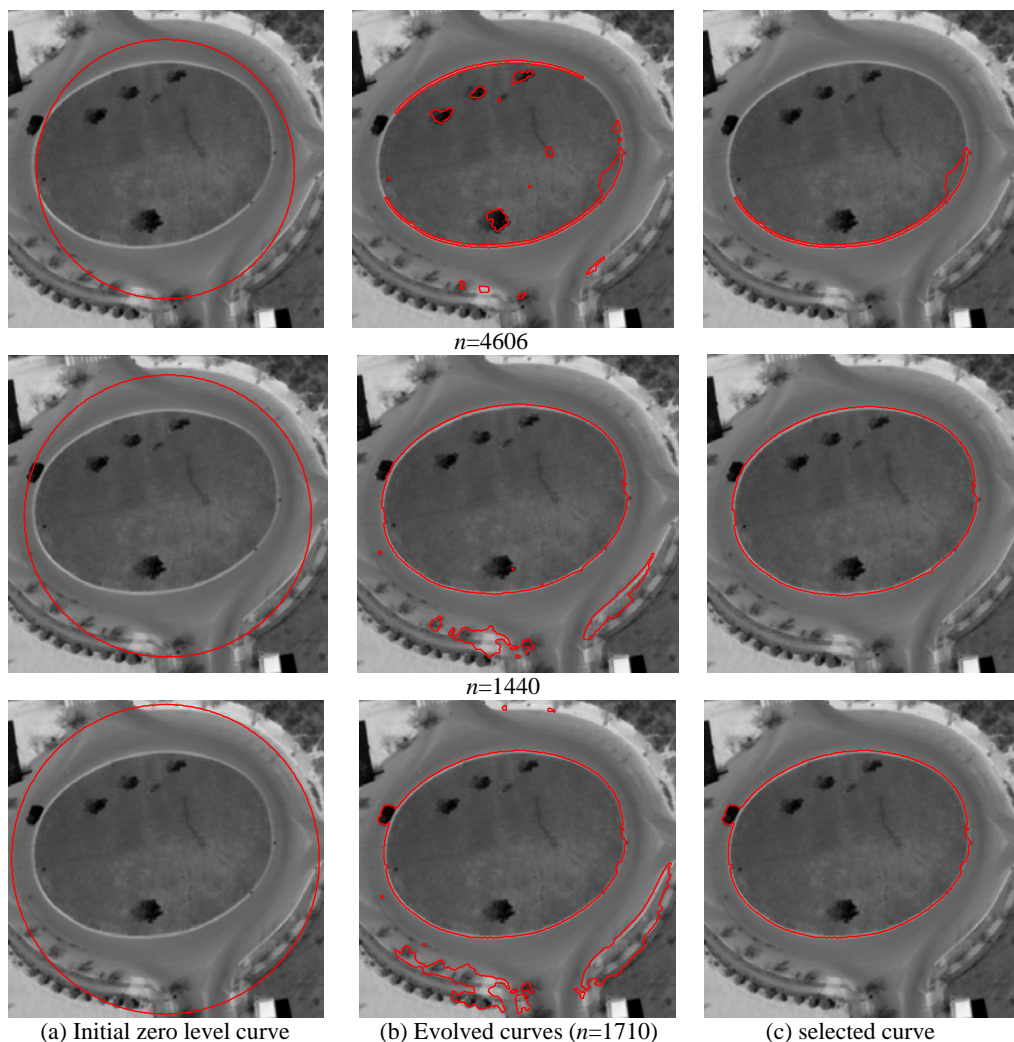


Figure 3-45: Shrinkage evolution on exterior circles. (a) Circles diameters are 31, 34 and 37 m from top to the bottom row respectively. (b) The results of the shrinking evolution. (c) The largest closed curve.  $n$  denotes the number of iterations.

In the next step, the iterative expansion evolution is carried out similar to the method described before with the exception that the initial curve is defined as a circle around the roundabout node so that it must be placed inside the island (Fig. 3-46). The diameter of the circle need be less than the threshold based on which islands are regarded as

point or area objects in the database. By experiment, it is safer to define a circle with a diameter as one-third of this threshold. The expansion result is compared with each group of shrinkage result separately and points that are close enough to each other are selected. These points are candidates on which an ellipse is fitted. In Figure 3-47, the fitting results for three groups of points are shown. The case with highest number of points is more likely to produce a correct result of island extraction.

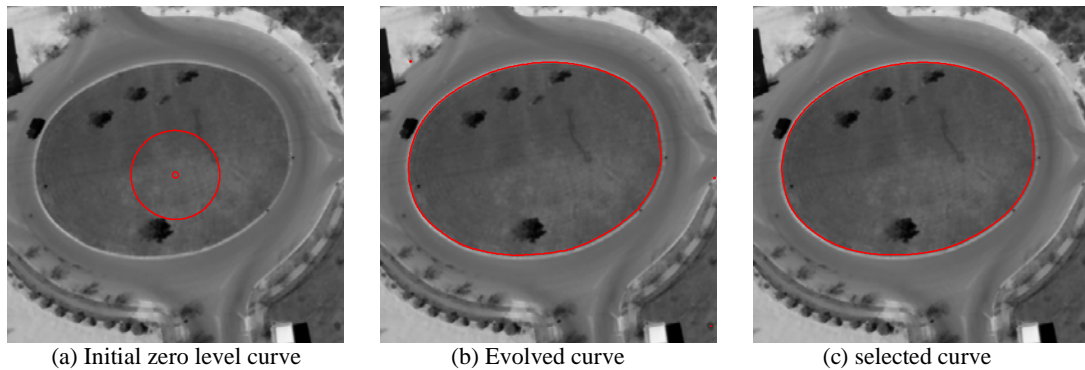


Figure 3-46: Iterative expansion evolution on the interior circle. (a) The diameter of the circle is 10 m. (b) The result of the iterative expansion evolution. (c) The largest closed curve.

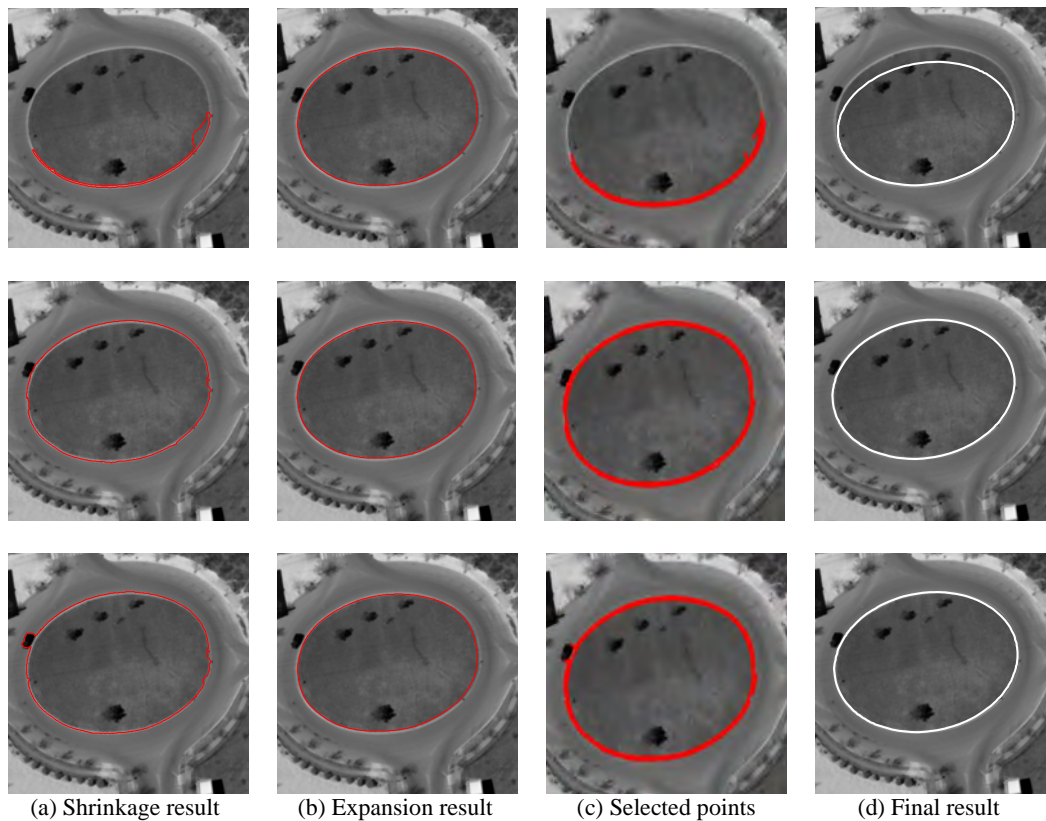


Figure 3-47: Steps for selecting appropriate points on which an ellipse is fitted. (a) Shrinkage results on the smallest, middle and largest circles shown at top, middle and bottom rows respectively. Column (b) shows the result of the iterative expansion evolution. (c) Selected points when two curves in (a) and (b) are compared. Column (d) displays the extracted islands. The bottom row includes the highest number of selected points and consequently the best choice.

### 3.4.2.2 Central island verification

Due to the importance of a correct result of island extraction for the reconstruction, verification is performed next. Islands can be verified using the existing information derived from the geospatial database. As is shown in Figure 3-48, when a roundabout appears as an area object, the diameter of its central island ( $D1$ ) obtained from the extraction process should not differ from that obtained from the geospatial database ( $D2$ ). In an ideal situation, the difference ( $\Delta D$ ) corresponds to the width of the circulating roadway (Fig. 3-48):

$$\begin{aligned}\Delta D &= D2 - D1, \\ \Delta D &= W\end{aligned}\tag{3.5}$$

where  $W$  is the width of the circulating roadway.

In practice, due to the inaccuracy in digitizing a roundabout, polygonal vector data do not lie exactly in the middle of the circulating roadway but somewhere within the area specified by the circulating roadway. Therefore,  $\Delta D$  is expected to be within the range between 0 and  $2W$  ( $0 < \Delta D < 2W$ ).

When a roundabout appears as a point feature, the diameter of the extracted central island must fall within a predefined range whose highest value is the threshold below which a roundabout is regarded as a point object in the geospatial database and whose lowest value is the possible minimum diameter of a central island. An extracted island is verified after these checks are carried out so that incorrect results can be identified and eliminated.

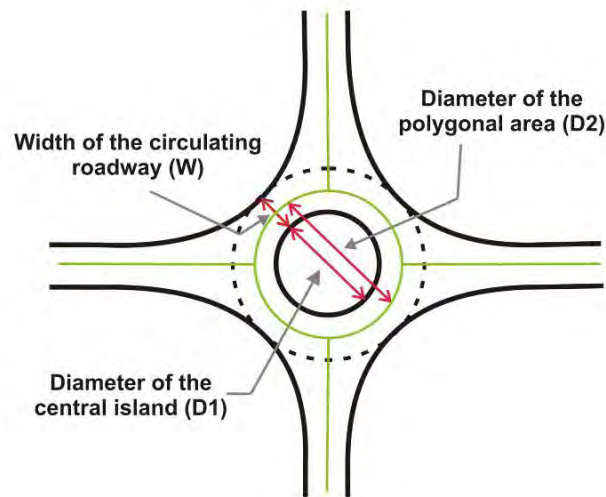


Figure 3-48 : Geometric relationship between roundabout parameters. Vector data is displayed in green.

### 3.4.2.3 Discussion

We proposed a hybrid evolution strategy used by level sets to detect central islands. The hybrid evolution strategy helps to overcome various kinds of disturbances. The main advantage of our method is its flexibility to detect islands of various sizes and shapes such as circle, ovals, etc. without being much affected by vehicles and various structures which often exist inside the island. Furthermore, results are reliable as they are verified using the information derived from the geospatial database. Depending on whether roundabouts appear as point or area objects, the initialization of the level set function and verification scheme are somewhat different, whereas the hybrid evolution strategy is the same in either case.

### 3.4.3 Road Arm Extraction

The approach used for the extraction of road arms in roundabouts is similar to the approach used for simple and complex junctions. In roundabouts, we can benefit from the obtained extracted central island to eliminate some road segments wrongly hypothesized on the circulating roadway. This problem can be observed in Figure 3-49 where two road segments are generated on the circulating roadway. These road segments are removed by checking if they are located partly inside the enlarged central island (Fig. 3-49-f).

### 3.4.4 Roundabout Reconstruction

The delineation of the roundabout outline is a challenging task. Difficulties of this task lie in the high variation of curvature along the outline contour and the large degree of disturbances caused by existing cars and trucks on the circulating roadway. The level of curvature variation depends on the size of the central island such that a larger central island imposes higher variation of curvature.

In Figure 3-50 an example is shown to describe the problem. As is shown, in order to detect the outline, we need to apply the balloon force in two different directions. In our snake model, however, the balloon force has been defined to be applied in only one direction pointing towards the junction center (inflation force). The answer to the question of when and in which direction to apply the balloon force (inflation or deflation) differs for different samples. As a result, several parameters need to be tuned on an ad hoc basis to address the described question, which is not desirable. To solve this problem, the external force field of the snake approach used so far, is modified based on the shape of the central island.

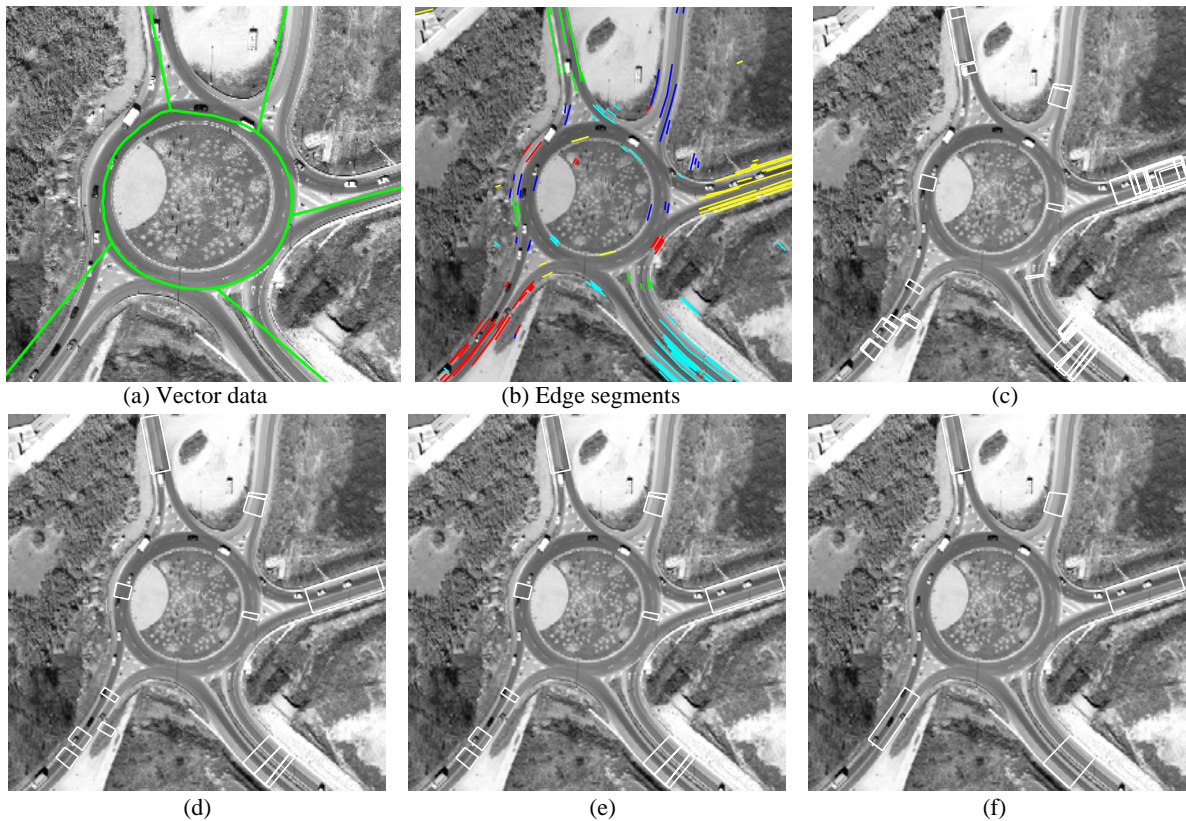


Figure 3-49: Road arm extraction in a roundabout. (a) Vector data overlaid on the image. (b) Five groups of edge segments in different colors obtained by applying parallelism, homogeneity and overlapping constraints. (c) Initial constructed road segment using anti-parallelism and width constraints. (d) Resulting segments after applying contrast constraint and removing overlapping segments. (e) Verified road segments including two wrong segments on the circulating roadway. (f) Road arms.

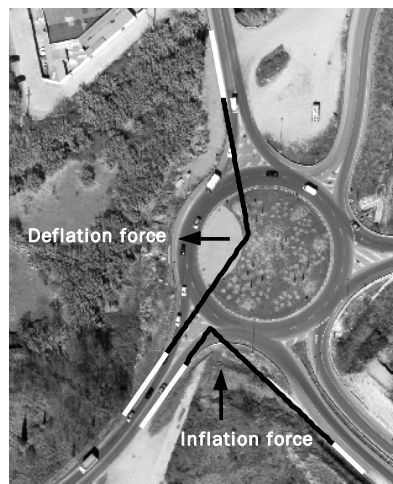


Figure 3-50: Showing two different directions in which the balloon force needs to be applied. The directions are specified by black arrows. Black lines are initial snakes and white lines display road arms.

#### 3.4.4.1 Shape-based Modification of the External Force Field

The GVF force field leads snakes towards image boundaries. It can also be modified based on the shape of the central island in order to lead the snakes to the roundabout outline. When assuming that the shape of the outline corresponds to the shape of the enlarged island, the island is enlarged to an extent depending on the width of the circulating roadway and subsequently the external force field is modified based the enlarged island. The modified force field is able to draw the initial snakes towards the outline even if they are located far away from the solution.

The enlarged island is clipped from the image, i.e. intensity values in this area are assigned zero (Fig. 3-51-a). In the clipped area external force field does not exist, so snakes located in this force-free area cannot move toward the outline.

To fix this problem, we need to manipulate the external force field in the clipped area so that snakes located in this area are guided towards the outline. To achieve this goal, a signed distance function is introduced to replace the clipped region. The main feature of this function is that whose GVF points directly from the center toward the boundary of the clipped region so that snakes situated in this area are drawn toward the outline of the roundabout.

To generate this signed distance function, the border of the enlarged central island is regarded as the reference (Fig. 3-51-b). Successive concentric layers at a specific distance interval from the reference to the center point are defined. Conversely proportional to the distance of each layer to the reference, an intensity value is calculated and assigned to the respected layer, i.e. layers closer to the reference curve are brighter and vice versa. The obtained intensity-step image has a gradual increase of intensity values from the center point toward the reference curve (Fig. 3-51-c) and consequently its GVF field points directly outward (Fig. 3-51-d). Finally, the GVF of the step image replaces the GVF of the original image in the corresponding area (Fig. 3-52). It should be noted that the enlarged central island must not pass over the border of the roundabout outline, in which case the final curves also pass through the roundabout outline as they are guided by the modified force field. To avoid this problem, the size of the enlargement must be less than the estimated width of the circulating roadway.

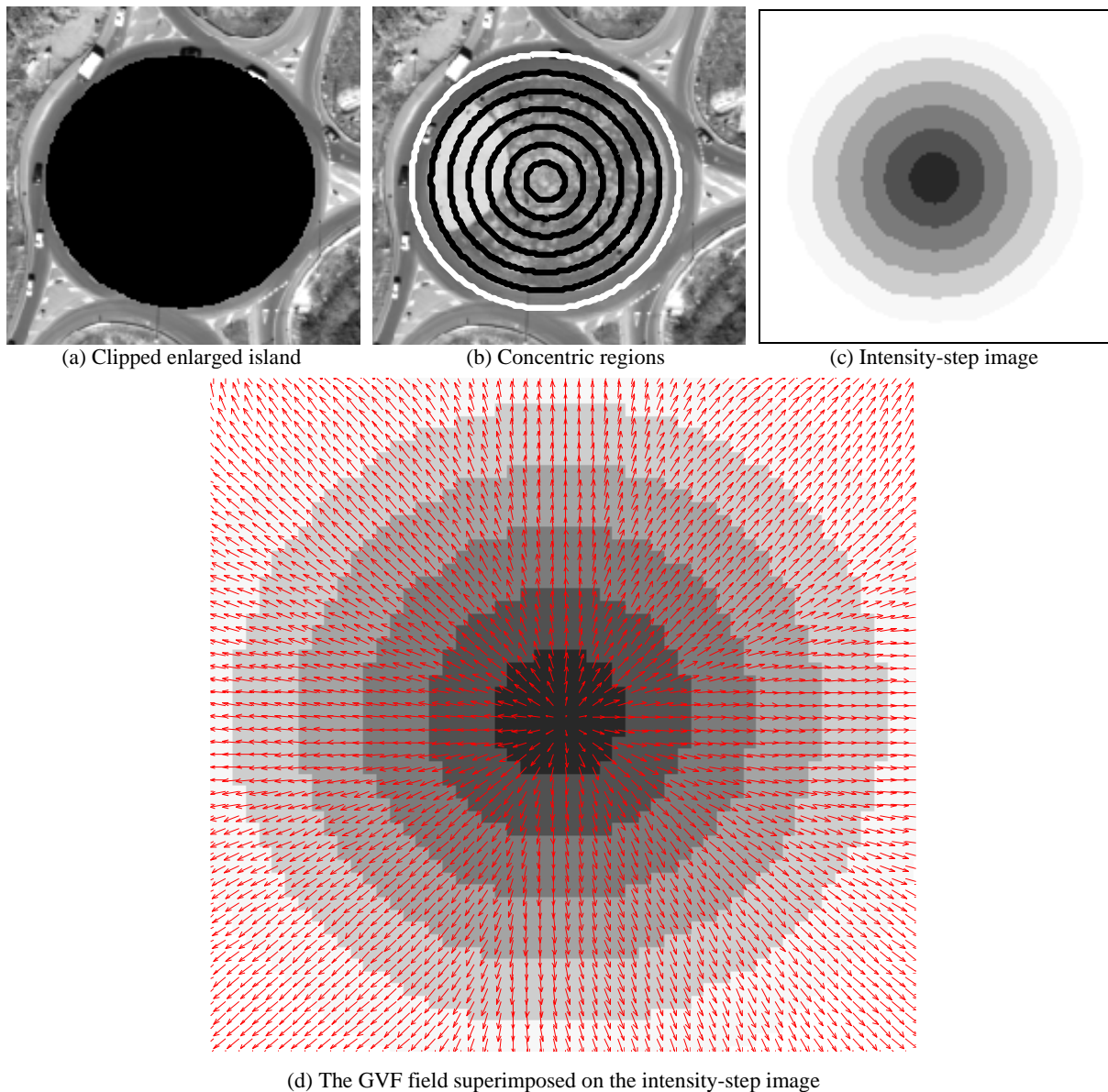


Figure 3-51: (a) The central island is enlarged and clipped on the image. The clipped area is shown in black. (b) The white curve is the reference for the signed distance function computation and black curves specify concentric regions. Black curves are generated at equidistance intervals. (c) Intensity-step image generated from the signed distance function. (d) The step image on which the GVF is superimposed. GVF vectors point from the center towards the image borders

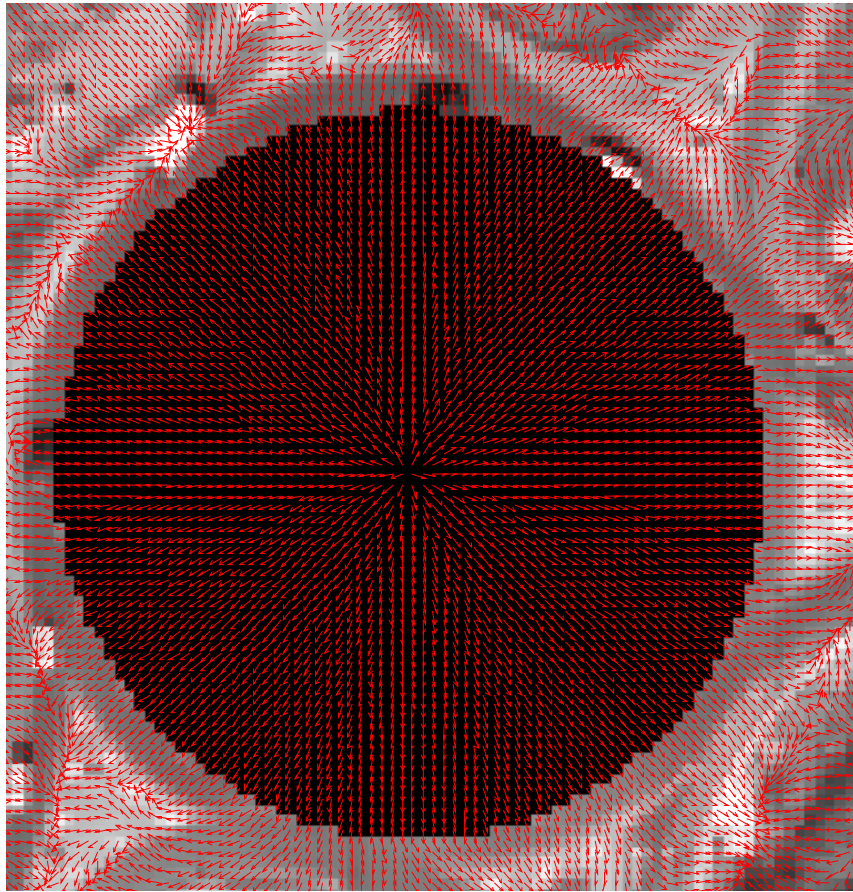


Figure 3-52: Modified external force field. GVF vectors point from the centre towards the image borders.

### 3.4.4.2 Outline Delineation

Our proposed snake model (section 3.3.3.1) was exploited to detect the roundabout outline with the exception that the external force field is modified based on the shape of the central island. The modified force field pulls the snakes toward the outline even if the initialization is far away from true borders. Furthermore, with this modified force field, various kinds of disturbances such as trees and vehicles often present within and outside the central island are overcome. In Figure 3-53, an example illustrating the improved results using our proposed modified force field is displayed. In Figure 3-53-a, the initialization is shown. The intersection lines meet in the middle of the central island far from the solution. In Figure 3-53-b, optimized result is shown when the GVF is not modified. In Figure 3-53-c, the improved results are displayed when the GVF is modified.

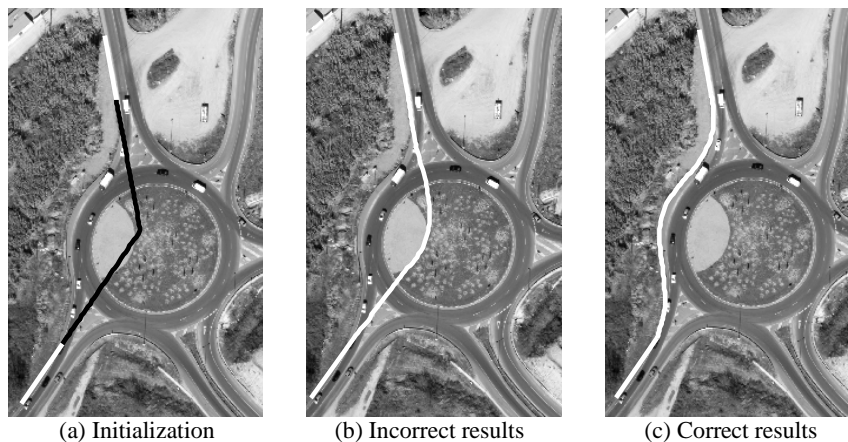


Figure 3-53: An example illustrating the effect of the modified external force field. (a) Intersection lines (black) used initial snakes. (b) Results when the GVF is not modified. (c) Improved results after the GVF is modified.



## 4. Results and Evaluation

In this chapter, we present results of testing our proposed approach on a variety of image samples. First, examples for intermediate and final results are displayed to explain the performance of our approach qualitatively. Then, the scheme for quantitative evaluation used in this work as well as quality measures are illustrated and the results are discussed.

### 4.1. Test Images and Context

For our experiments, we used black-and-white aerial Digital Mapping Camera (DMC) orthoimagery with a ground resolution of 0.1 m. The images depict rural and suburban areas of Germany. Because the number of junctions in one scene is generally low, junctions are selected from a large number of images. Besides the image, Basis DLM of the Authoritative Topographic Cartographic Information System of Germany (ATKIS) as external vector data is used. The content of the Basis DLM is approximately equivalent to that of topographic map 1:25000. In this database, roads are modeled as linear objects and junctions as point objects. Roundabouts are represented as point objects or area objects depending on the diameter of the central island. In cases that roundabouts appear as point objects, attributive information is also included to differentiate between roundabouts and junctions. The required planimetric accuracy for a road and road junction object is defined as  $\pm 3\text{m}$ .

### 4.2. Extraction Results

In this thesis, road junctions are categorized into three different classes of which two are dealt with, namely simple and complex including roundabouts. In following sections, first the main problem related to the road arm extraction is discussed. Then, results of the extraction of either kind of junction are displayed and discussed individually. We apply our approach on simple and complex junctions including roundabouts with the same set of control parameters for the snake model (see section 3.3.3.2). If the list of islands at the end is empty, the junction is considered to belong to the simple class.

#### 4.2.1 Road Arms

Road arms as a part of our proposed road junction model provide fixed boundary conditions necessary for the snake model. Road arms can be generated by a single road segment or by linking several road segments provided that they are collinear. Since road segments are generated based on detected edge segments, in examples where edge segments cannot be detected, road segments cannot be constructed. Disturbances such as trees and their shadows, poor contrast between the road surface and the surrounding environment and crowds of vehicles on the road are three main reasons why edge segment cannot be detected (Fig. 4-1). Furthermore, crowds of vehicles on the road surface violate the radiometric conditions for the construction of road segments (Fig. 4-1, bottom-row).

In roundabouts, in addition to disturbances mentioned above, dividers with a large radiometric difference with the neighboring roads can violate the radiometric constraints (Fig. 4-2). Our method cannot handle such cases.

In such examples, prior information about geometric characteristics of the dividers is of help to detect and exclude the divider from the road arm extraction process.

#### 4.2.2 Simple Junctions

In the following some exemplary results for simple junctions are given and discussed. In Figures 4-3, 4-4, 4-5, 4-6 and 4-7 two issues are discussed: the effect of various kinds of road markings on the snake evolution, poor contrast caused by secondary roads crossing the junction area. Poor contrast in an image of low radiometric quality is illustrated in Figure 4-8. Various kinds of disturbances caused by trees, vehicles, street lights and power lines and their shadows are shown and discussed in Figures 4-9, 4-10, 4-11, 4-12 and 4-13. Variation in radiometric characteristics of the junction central area as well as sharp curvature of the junction borders are shown in Figure 4-13. Finally, Figure 4-14 displays a case with a high curvature variation on the junction border along with intermediate steps.

Figure 4-3 depicts the sequence of snake optimization steps leading to the delineation of the junction. As can be seen in the intermediate result (Fig. 4-3-d), an unpaved road leaving the vertical road at the top affects the movement of snakes during optimization especially at the top-right side of the junction border. Balloon forces pull the snakes back to detect the true boundary. As mentioned in Chapter 3, unlike complex junctions in that the curvature at the junction border changes smoothly, in simple ones the curvature graph often contains a sharp peak implying that very dense snake vertices are needed compared to complex junctions in order to detect the curved part correctly. Lack of dense snake vertices causes the curve to become straight at early iterations. Rather than applying the required dense point spacing, this case is recognized by analysing the curvature graph constantly and the problem is solved by applying the balloon force. In this way no distinction needs to be made at this point of the processing between simple and complex junctions, and the method is more robust against disturbances.

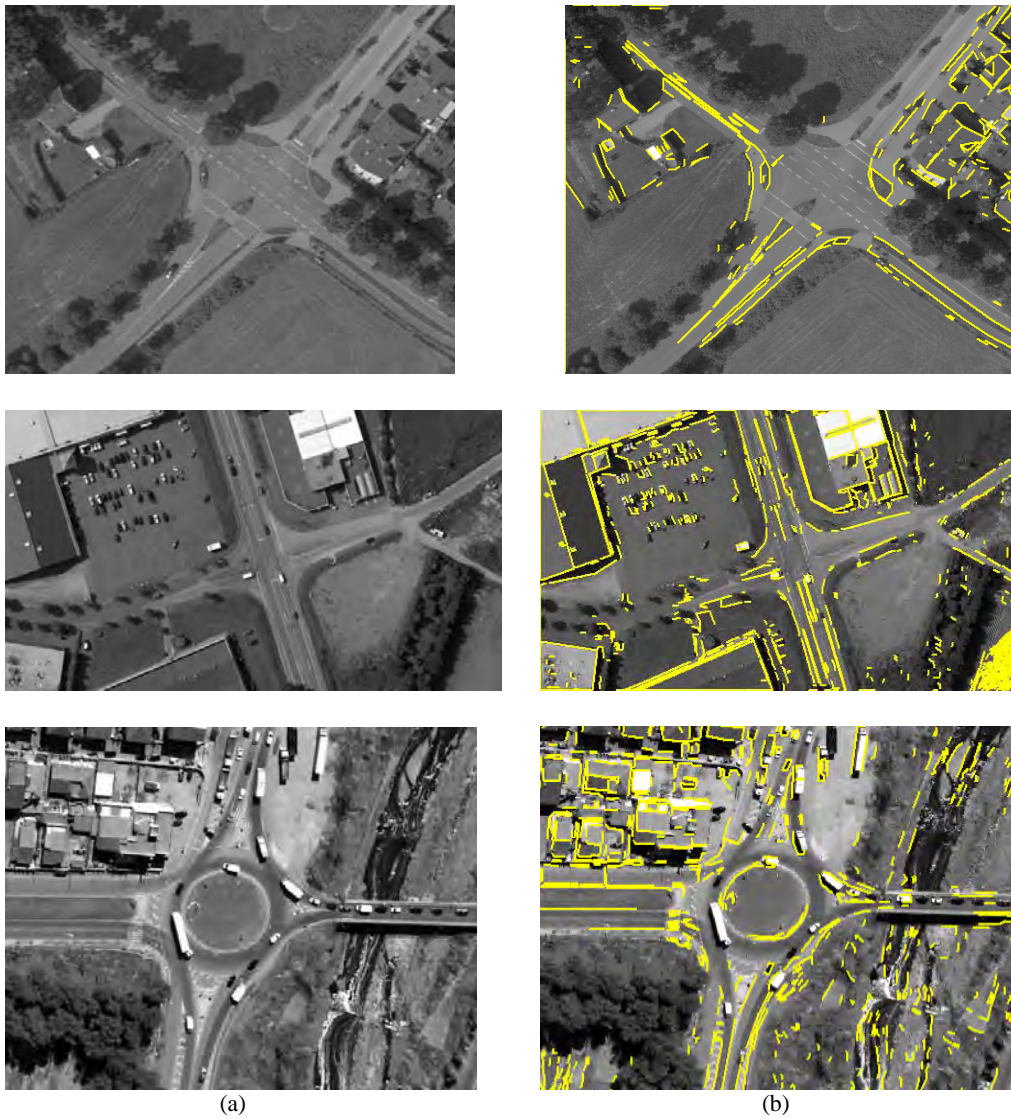


Figure 4-1: Illustrating disturbances and their effects on the road arm extraction. Column (a) displays original images. Column (b) shows edge segments after overlapping and parallelism constraints are applied. Top, middle and bottom-rows show the effect of trees and their shadows, poor contrast and vehicles respectively. In the top-row, trees and their shadow occlude road sides in the left, right and bottom roads. In the middle-row, edge segments have not been detected at the left road as the road surface does not contrast sufficiently with the car park area. In the bottom-row example, because of crowds of vehicles present on the top road, edge segments can not be detected well and also radiometric conditions for the generation of road segments do not hold.



Figure 4-2: An example where our approach fails to extract the road arm due to a wide divider that exists within the roads in the bottom.

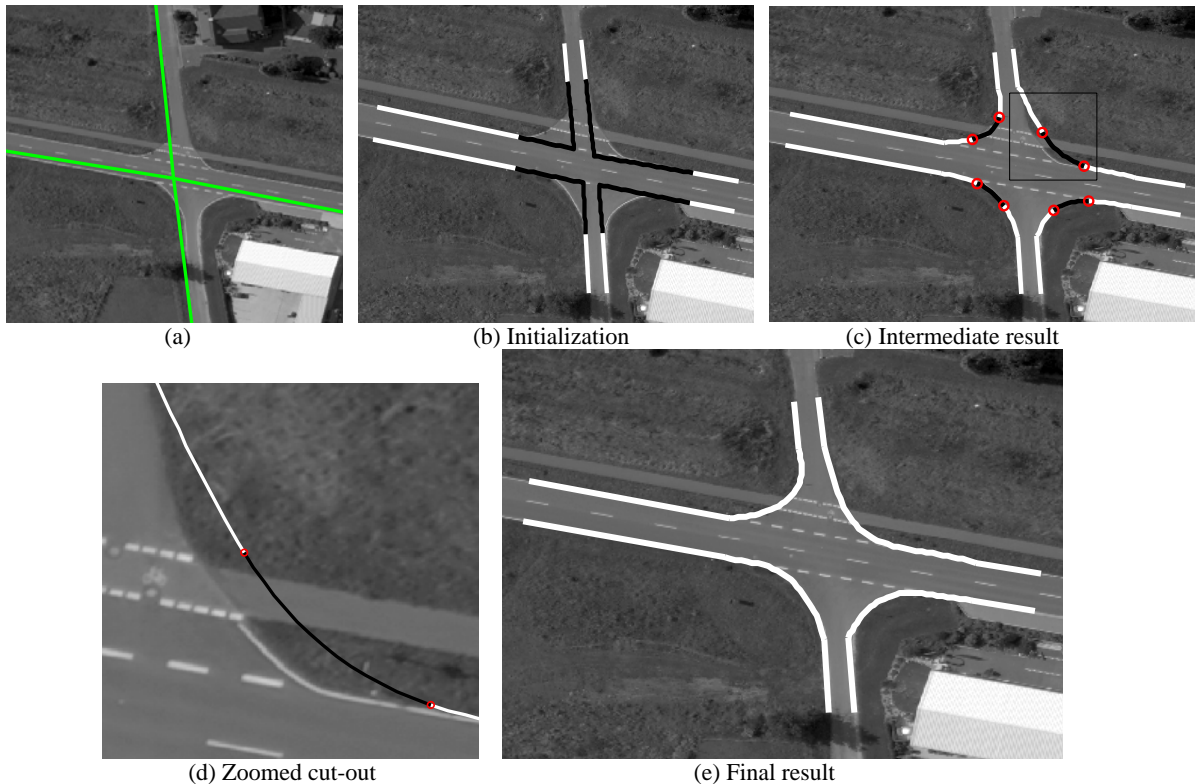


Figure 4-3: Illustrating the extraction of a simple junction extraction. (a) Vector data overlaid on the original image. (b) Road arms (white) from which intersection lines (black) are obtained. Black curves represent initial curves. (c) White curves imply active snake vertices and black curves are passive. Red points show force boundaries separating active and passive parts. The black box marked in (c) is enlarged in (d). (e) Extracted junction.

In Figures 4-4, 4-5 and 4-6, the effect of road markings on the performance of the approach is illustrated. Generally, road markings can be beneficial to the junction reconstruction process when located on the junction border in which case they strengthen the contrast between the junction border and the surrounding area. In contrast, such road markings often present in the junction central area as stop lines and warning lines can disturb the snake optimization if they are aligned with the movement direction of the snake. In such a case, the optimized curve lies slightly inside the junction central area (Figs. 4-4-g and 4-5-f).

Stop and warning lines, however, do not influence the evolving snakes in two cases:

- When they lie approximately perpendicular to the snake movement direction (Fig. 4-4-f)
- When there is a good contrast between the junction central area and the surroundings (Fig. 4-5-g)

The junction's geometrical shape is another factor which can affect the quality of the extraction. When the intersection angle between two adjacent roads is sharper, the initial snakes lie largely inside the junction central area and are consequently more likely to be caught by road markings. This property is best described in Figure 4-6-b where the initial snake at the bottom-left border is not located inside the junction but approximately on the border, which makes it unlikely to be trapped by the road markings (Figs. 4-6-b, c and d).

This problem can also be observed in Figure 4-4-b where the initial curve at the left border is less inside the junction and consequently it can overcome road markings (Fig. 4-4-f) whereas at the right border in Figure 4-4-g, the curve is drawn somewhat inside the junction central area.

Compared to the examples presented in Figures 4-4 and 4-5 where road markings are the major disturbing sources, in the example shown in Figure 4-6, the snake vertices are affected less by road markings and more by unpaved roads, in other words, instead of getting trapped by road markings, the contours are pulled outside the junction area (Fig. 4-6-c). In this case, the balloon force is applied in order to lead the curve toward the desired boundary at the junction border. The effect of unpaved roads leaving the junction area is resolved in all three samples.

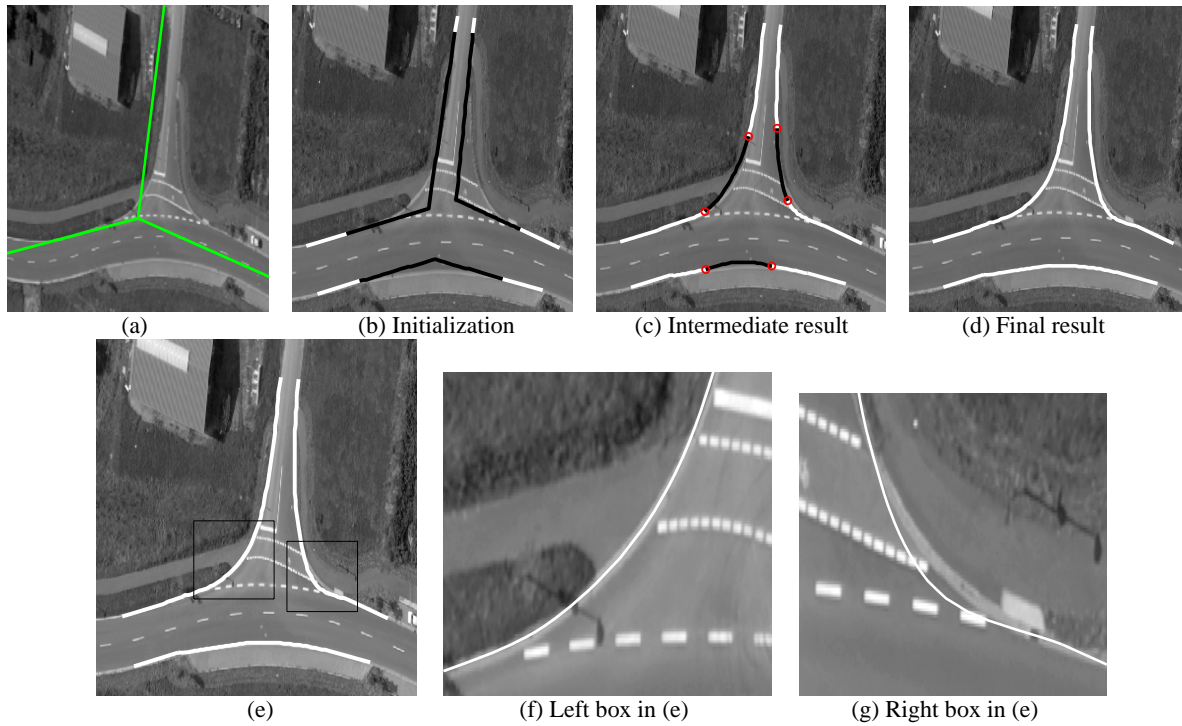


Figure 4-4: Illustrating the effect of road markings. (a) Vector data. (b) Initial snakes in black. (c) Snakes during evolution. (d) Extracted junction. Both scenes in (f) and (g) contain similar contrast and road markings. However, a better result is seen in (f). The reason is that, in (g), the warning lines are closer to each other involving more snake vertices. As a result, the curve is entered the junction area. In (f), stop and warning lines are close to each other at the top, however, they don't disturb the snake optimization because they are approximately perpendicular to the snake's movement direction.

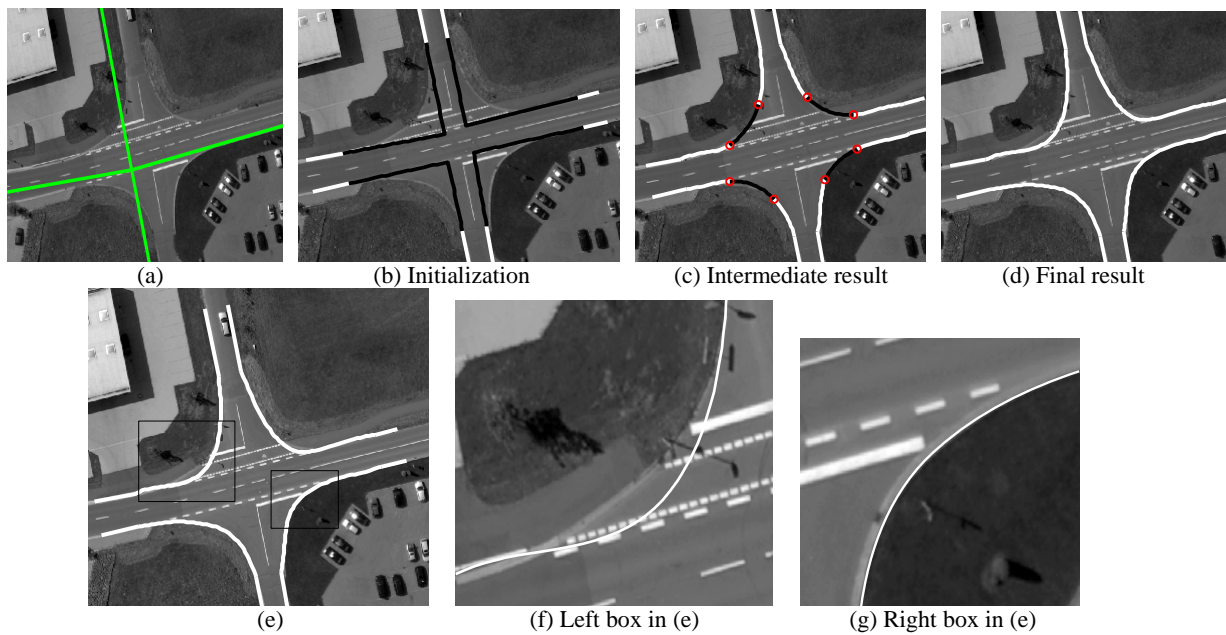


Figure 4-5: Illustrating the effect of road markings. (a) Vector data. (b) Initial snakes in black. (c) Snakes during evolution. (d) Extracted junction. The final curve in (f) is drawn inside the junction area due to the road markings and insufficient contrast. In (g), however, a correct detection was reached because of a good contrast. Initialization does not play a role here because it is the same for both junction borders.

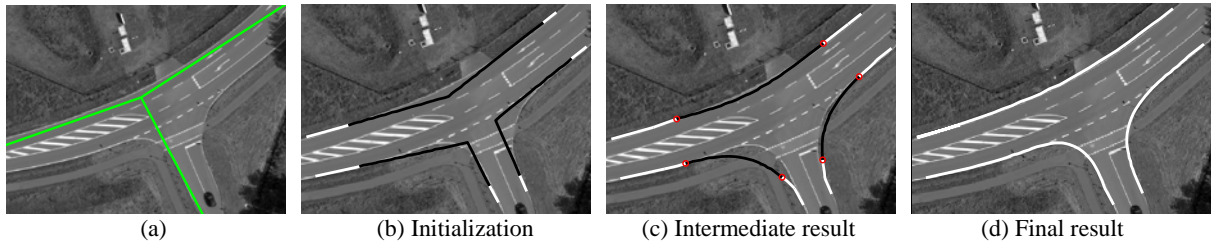


Figure 4-6: (a) Vector data. (b) Initial snakes in black and road arms in white. In (c) balloon forces are applied to passive parts (black) resulting in correct detection of junction borders in (d).

Figure 4-7 illustrates the case in which cross walks are present in the junction area. The junction area has a poor contrast to the surroundings. Furthermore, there is an unpaved road between two crosswalks. In the places where the unpaved road intersects the junction, the contrast is too low, and consequently the evolving curve can leak into the surrounding area through these low-contrast locations. All these problems can be overcome with our method. Since cross walks are aligned with the initial curves, they don't influence the snake's movement. When a contour leaks into the surrounding area and subsequently becomes straight due to the strong internal force, the balloon force pushes it back on the right track. The reasons why leakages can occur are as follows:

- Poor contrast between the junction area and the surrounding environment
- Sparse snake vertices
- Poor initialization when initial curves are located outside the junction area (Fig. 4-15-b)

In this example, two factors cause leakages: poor contrast and sparse snake vertices (Fig. 4-7-c).

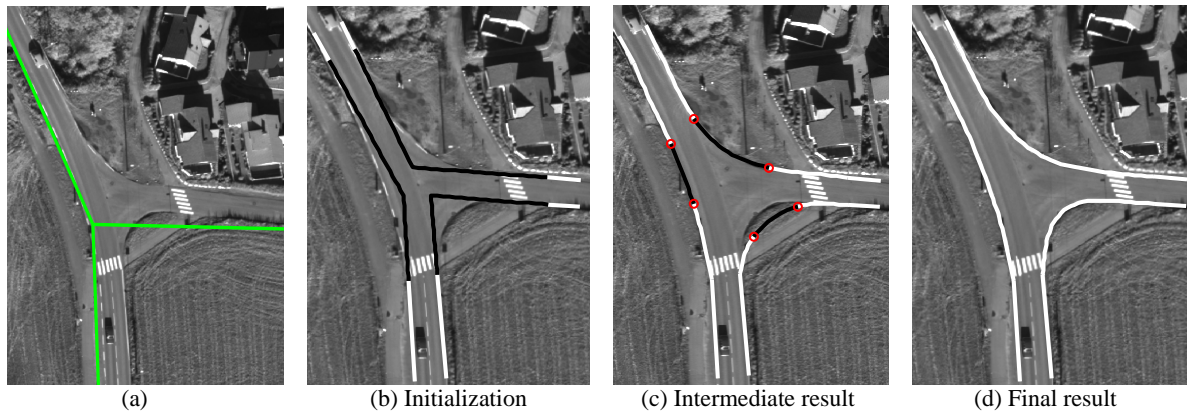


Figure 4-7: (a) Vector data. (b) Initial snakes in black and road arms in white. In (c) snake vertices are not affected by the cross walks. Furthermore, the effect of the small unpaved road at the bottom-right junction border is removed using the balloon force. (d) Extracted junction.

In Figure 4-8, the junction central area lacks sufficient contrast to the surrounding environment at the bottom-left border. As a result, the snake is attracted inside the junction area until it optimizes in a place where a better contrast exists (Figs. 4-8-c and d).

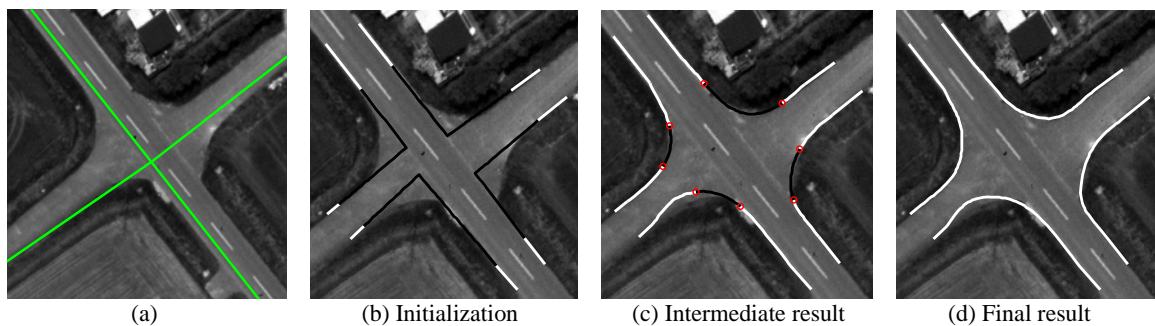


Figure 4-8: (a) Vector data. (b) Initial snakes in black and road arms in white. (c) Snakes during evolution. (d) Extracted junction. In (d) the contour at the bottom is somewhat entered the junction area due to poor contrast with the background.

In another example in Figure 4-9, besides a high variation of curvature, the junction border is partly shaded by trees, as can be seen in the bottom junction border. Furthermore, the contrast of the image is low. As a result, the snake is unable

to locate the entire border but a large part. In contrary, at the top junction border, trees do not exist, so a complete delineation of the junction boundary is reached.

In cases where a high variation of curvature does not exist, however, the effect of trees as well as their shadows can be easily resolved. In Figure 4-10, the major part of the bottom border is covered by trees. Furthermore, a car is present close the left border as well as a street light at the top. The paths, at the left and right borders, leave the roads. The left one causes a leakage during the snake optimization. The effect of the leakage is removed at intermediate stages when the balloon force is applied (Fig. 4-10-c). Therefore, none of the mentioned factors affect the quality of the final result (Fig. 4-10-d).

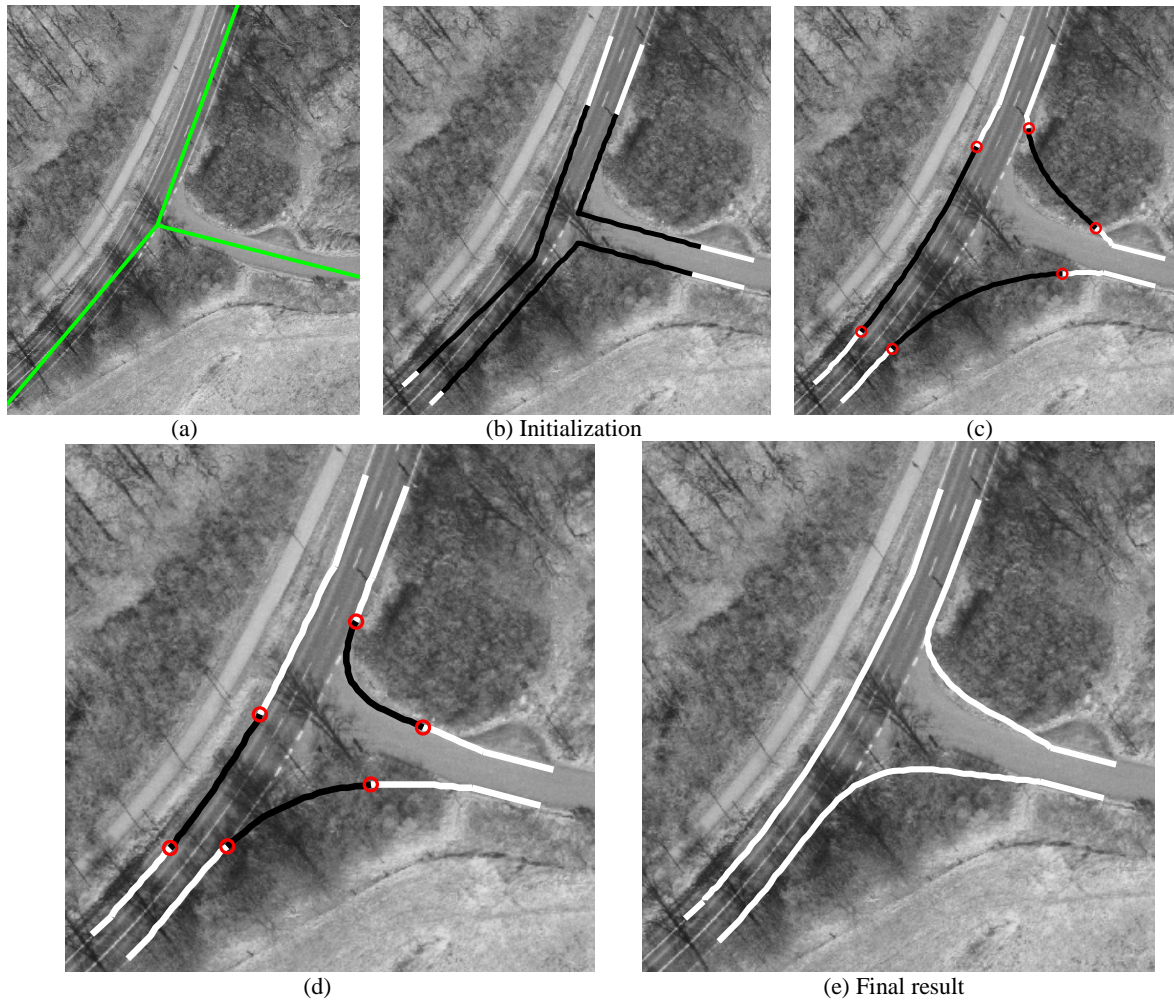


Figure 4-9: Illustrating disturbances caused by trees. (a) Vector data. (b) Initial curve at the bottom junction border is located nearly on the border. (c) Intermediate results where the balloon force has not been applied yet. (d) Intermediate results where balloon forces help recover the top-right border but the bottom border is partly captured due to the trees and their shadows. (e) Extracted junction

In Figure 4-11, another example is presented in which a large part of the junction border is covered by shadows. As the intermediate results (Figs. 4-11-c, d and e) are shown, the snake passes through the shadow region and detects the junction border successfully (Fig. 4-11-f).

Let another example illustrates that shadows from trees, vehicles and street lights can be handled by our method as is shown in Figure 4-12.

In special cases, as is shown in Figure 4-13, along the junction border within a short distance, the curvature can fluctuate sharply. Furthermore, next to this region shadows exist in this example. This situation is displayed at the bottom junction border where a power line construction as well as street lights and their shadows occlude the border. Due to the flexibility of our snake method, the curved junction border is detected.

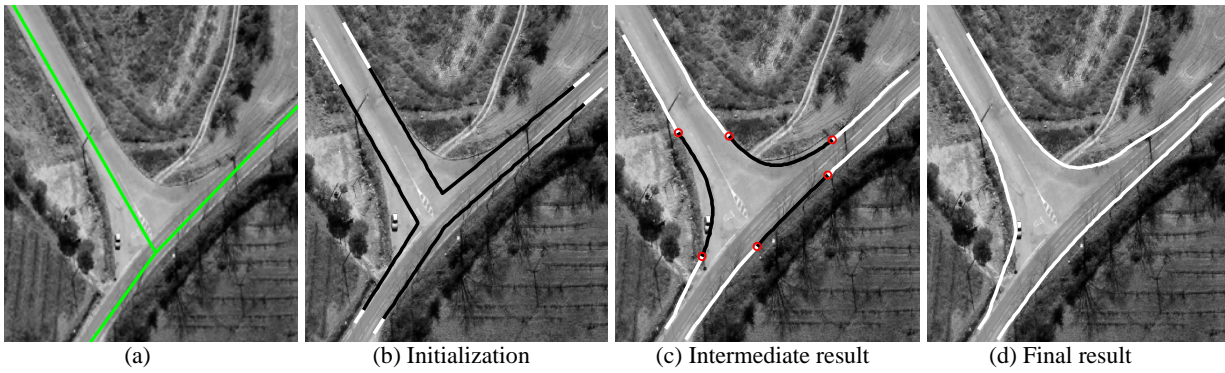


Figure 4-10: Shows the case in which various kinds disturbances like cars and trees exist. (a) Vector data. (b) Initial snakes in black and road arms in white. (c) Snakes during evolution. (d) The final result proves that our method can handle these disturbances.

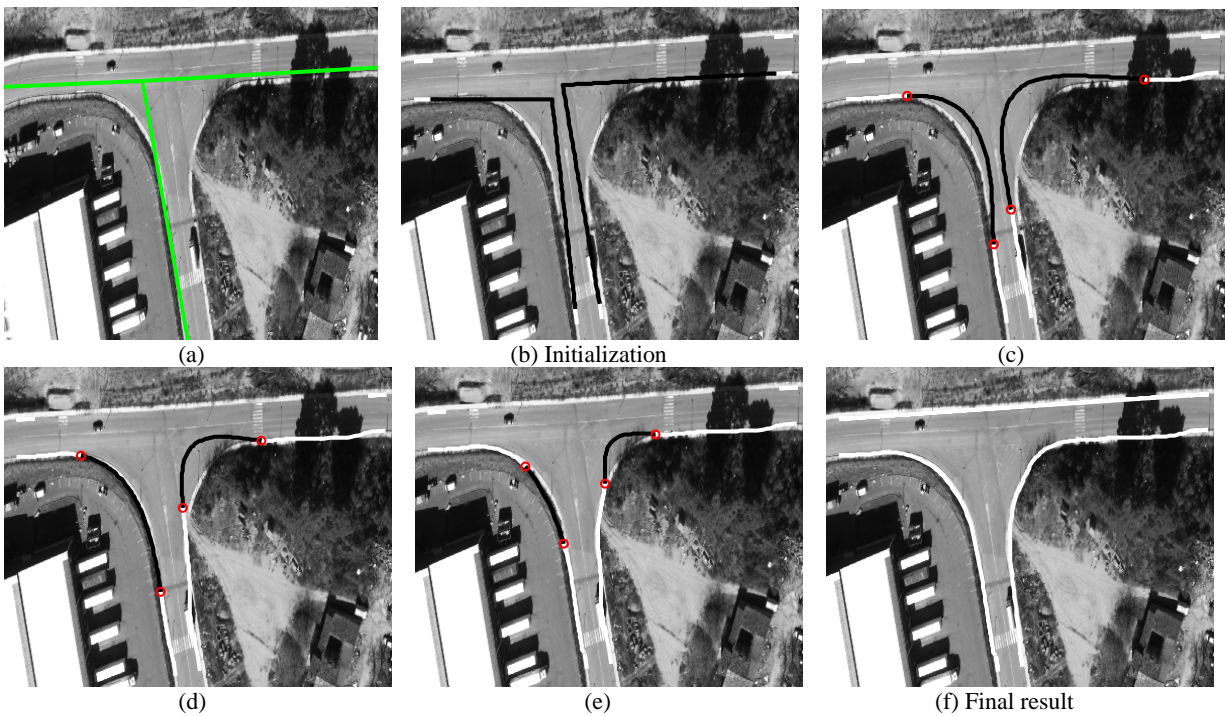


Figure 4-11: Illustrating a junction whose border is occluded by shadows. (a) Vector data. (b) Initial snakes in black and road arms in white. (c-e) Show intermediate results. The snake passes through a large body of shadow at the right junction border. (f) Extracted junction.

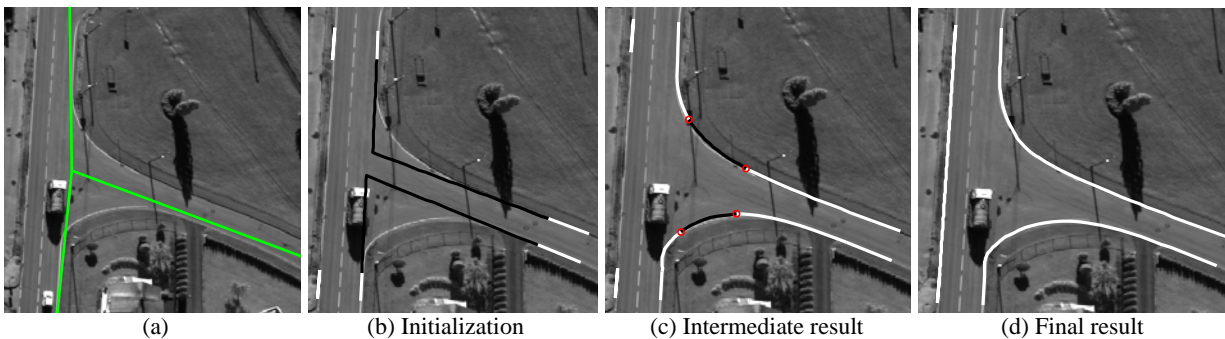


Figure 4-12: Shows the case in which shadows from different sources exist. (a) Vector data. (b) Initial snakes in black and road arms in white. (c) Snakes during evolution. (d) The final result indicates that shadows can be overcome by our snake method.

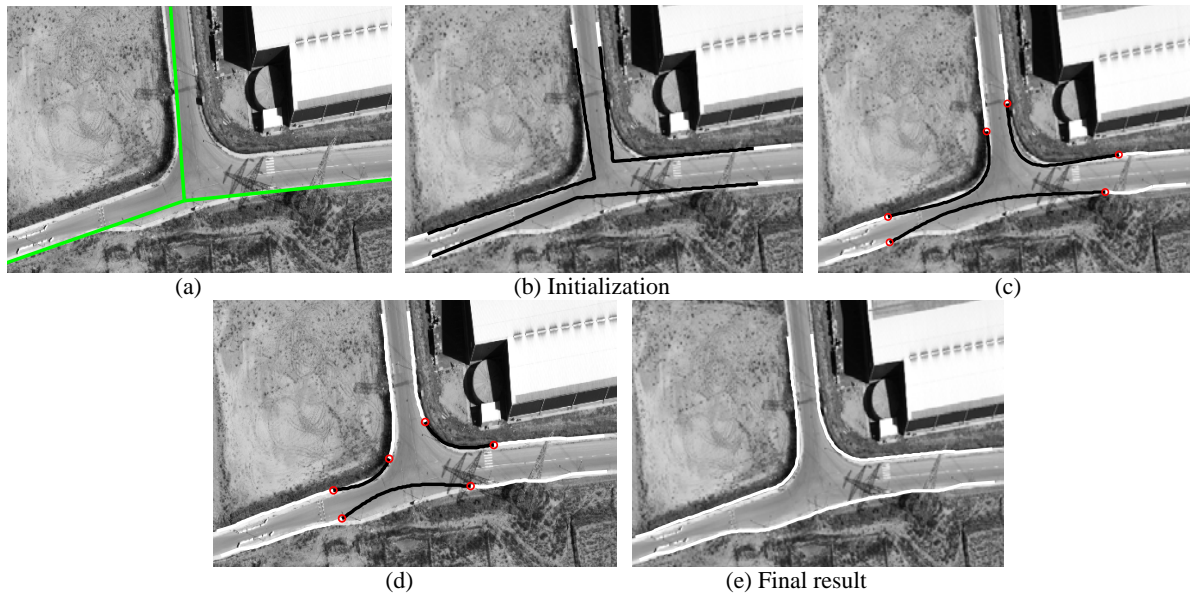


Figure 4-13: Describing the case in which the curvature changes within a short distance and shadows from power lines and street lights occlude the junction border. (a) Vector data. (b) Initial snakes in black and road arms in white. (c-d) show the snakes during evolution. (d) The final result indicates that shadows can be overcome by our snake method.

In Figure 4-14, the junction borders at the top and bottom have a very high curvature. The challenge in this example is that the initial snake lies considerably far from the junction border. Furthermore, the junction area represents two areas with different radiometric properties such that the area at the top is brighter than the one at the bottom. As a result, it is hard to pull the initial curve back toward the junction border at that area. Our snake method is able to handle such a situation. However, the speed of convergence for the snake at the top is slower than that at the bottom (Figs. 4-14-c and d).

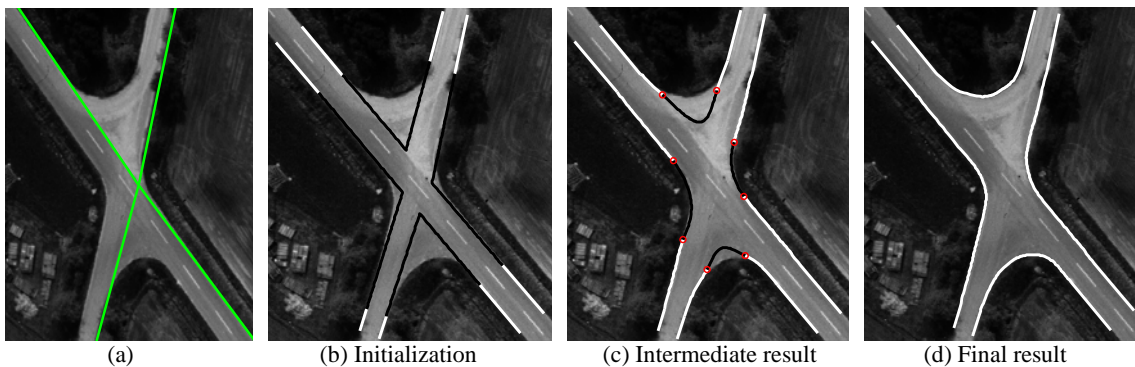


Figure 4-14: (a) Vector data. In (b), initial curves at the top and bottom are very far away from the borders. In (c), the passive part of the ziplock snake (black) at the top is much farther from the junction border than that in the bottom, because different radiometric properties at the top hinder the snake motion. Therefore, a higher number of iterations is needed to recover the border. (d) Extracted junction.

A far initialization can occur when there is a high curvature variation at the junction border, as it is the case in Figure 4-15-b at the top-left junction border, the initial curve lies outside the junction area. Furthermore, the initial snake is approximately straight. As a result, it becomes straight in the first iterations. Here, the balloon force is applied in several successive instances of snake evolution and leads to a correct capture of the junction border (Figs. 4-15-c, d, e and f).

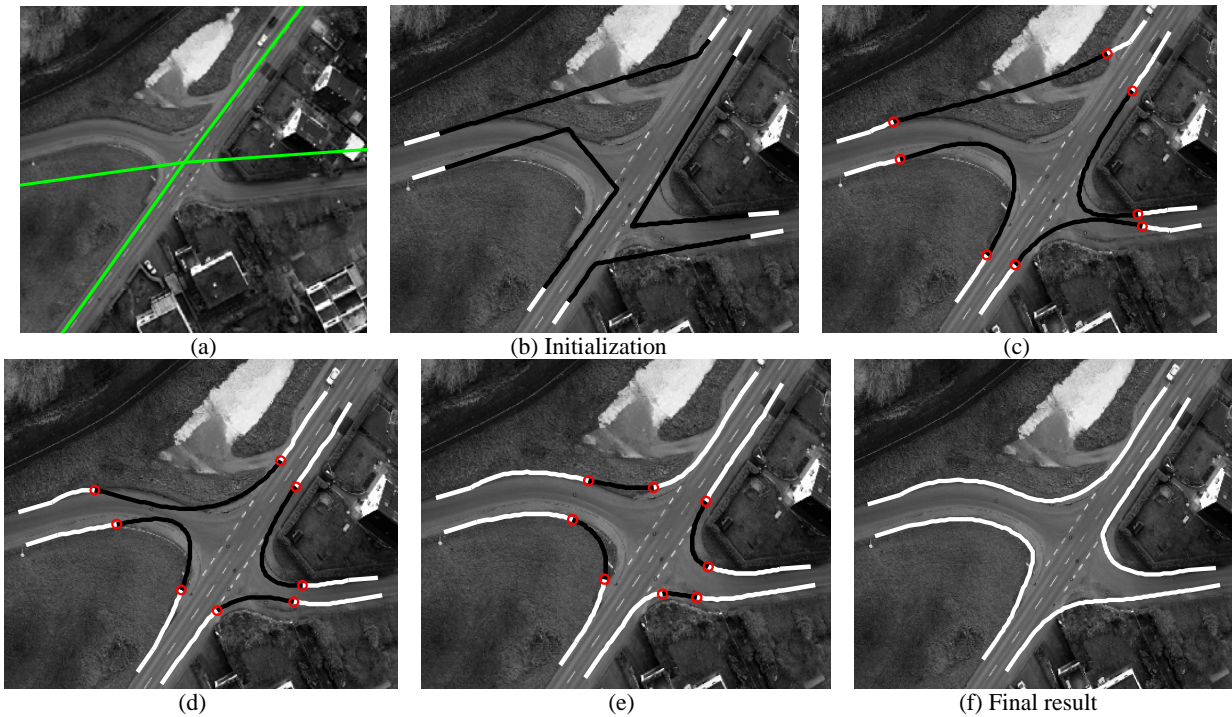


Figure 4-15: (a) Vector data superimposed on the image. (b) Initial curves at bottom-left junction border are modified. (c), (d) and (e) are intermediate results. In (c) the balloon force has been applied only on the bottom-right border whereas in (d) and (e) the balloon force is applied on all borders. (f) Extracted junction.

#### 4.2.2.1 Discussion

We showed the potential of our approach by testing it on several simple junctions. The obtained results demonstrate that various kinds of disturbances present along the junction border as well as inside the central area of the junction can be overcome. Furthermore, cases with high variation of curvature along the junction border can be handled successfully by applying the balloon force. Strong road markings present in the junction central area might sometime draw the snake slightly inside, but in most cases road marking have no effect on the quality of the final results. As shown in some samples, single vehicles and their shadows do not disturb our snakes. However, a row of cars may mislead the snake inside the junction.

#### 4.2.3 Complex Junctions

Complex junctions contain traffic islands in their central area. This is a fundamental difference between simple and complex junctions. Islands are designed to regulate the traffic in the junction area. For this reason, when approaching the junction area from a far distance, the width of crossing roads often increases gradually. This means that the junction border is longer than that in simple junctions but its curvature changes more smoothly. Furthermore, a variety of road markings often exists in the junction area. In all experiments for detecting islands, the same set of control parameters for our level set formulation was chosen (see Chapter3, Fig. 3-29).

Except for the example presented in Figure 4-23 where traffic islands appear brighter than the background, in the rest of examples islands appear darker than the background. Figures 4-16 and 4-17 show two typical examples of the island detection where no disturbing feature is present. Examples in which islands are occluded by various disturbing features such as traffic signs and trees situated inside the islands and their shadows are represented in Figures 4-18, 4-20 and 4-21. The problem of poor contrast between the islands and the surroundings is shown and discussed in Figures 4-22 and 4-23. Finally, the issue of the size of the island is discussed in Figure 4-23.

In all examples of complex junctions, in addition to the problems related to the extraction of traffic islands, similar problems to the ones described in simple junctions for the extraction of the junction borders are seen frequently. We mention such problems in each sample.

Figure 4-16 illustrates the capability of our snake-based method to delineate junction borders even from a very far distance. Trees and their shadows have been resolved at the top-left border. Furthermore, there is a car park at the left side, which means no contrast or edges exist at the place where cars enter the road from the car park. Due to the proper initialization by intersection lines (Fig. 4-16-b), this part has been processed successfully. Three successive instances of the snake evolution are displayed in Figures 4-16-d, e and f.

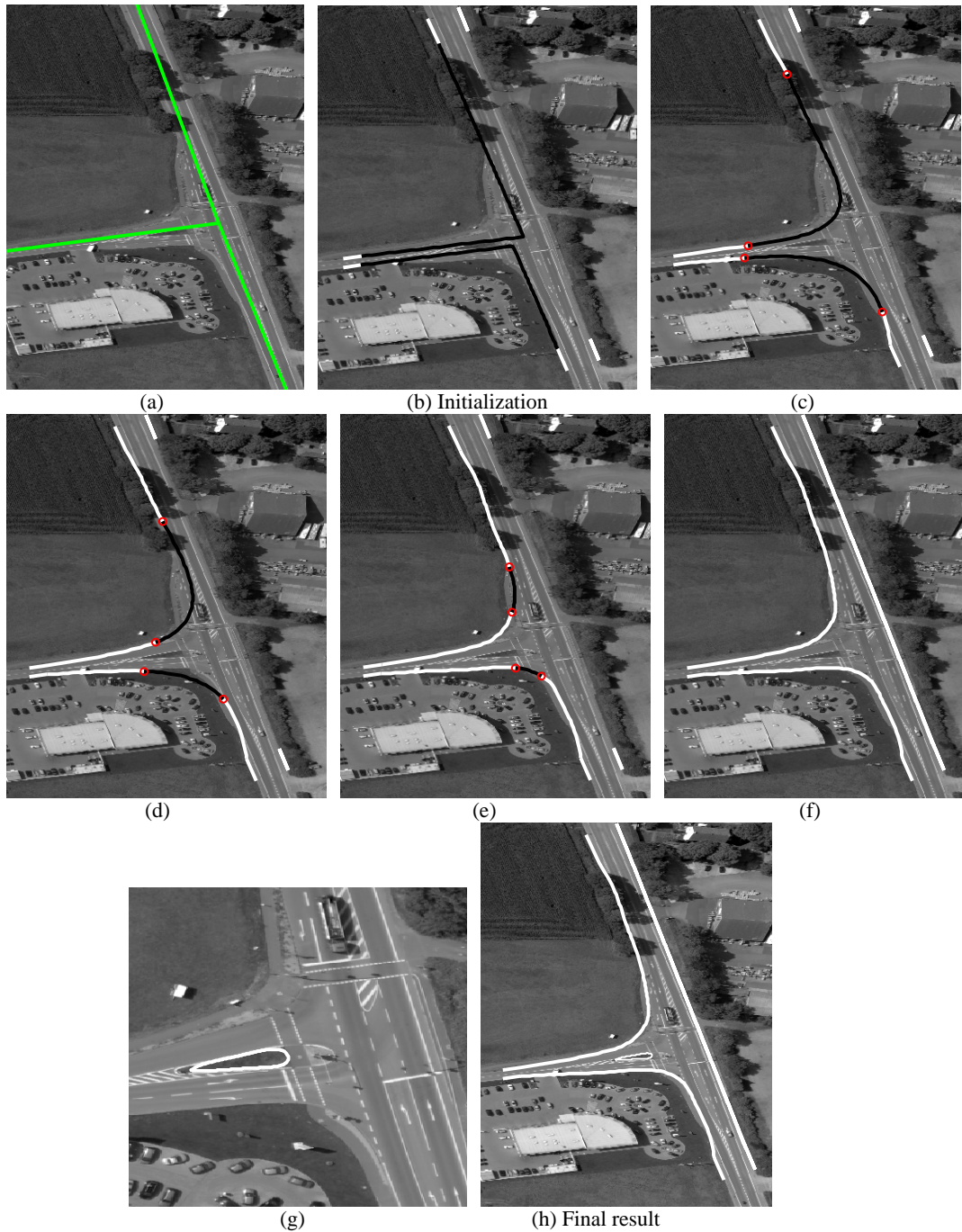


Figure 4-16: Describing an example in which a car park and tree shadows are present in the scene. Furthermore, junction borders are captured from a far distances. (a) Vector data. (b) Initial snakes in black and road arms in white. (c), (d) and (e) show intermediate results of the evolution. (f) Junction outline. (g) Captured island. (h) Reconstructed complex junction.

In Figure 4-17, the island can be easily extracted. However, a low contrast between the junction border and the surrounding area at the bottom-left border causes the snake to detect some parts of the surrounding area as the junction border. This detected part of the surroundings, however, is hardly distinguishable from the junction surface by a human operator.

In Figure 4-18, consecutive steps for the extraction of a complex junction are described. Although traffic islands are slightly occluded by traffic signs and their shadows, they are extracted successfully.

In case one of the associated road sides from two neighboring road arms is located on the road side and another on a road marking, inconsistency occurs. In our approach, this inconsistency cannot be overcome (Fig. 4-19). In this example, the right part of the road border has been extracted correctly but the left part lies somewhat within the road (Fig. 4-19-b).

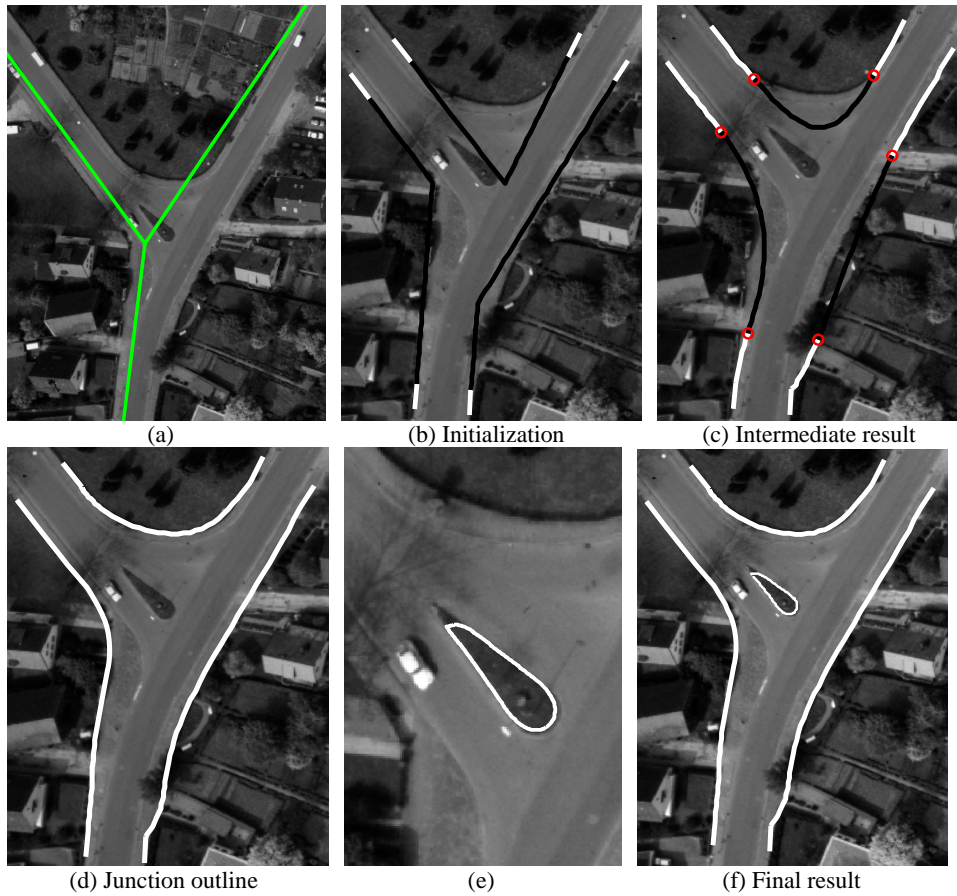


Figure 4-17: (a) Vector data. (b) Initial snakes in black and road arms in white. (c) Snakes during evolution. In (d), the bottom-left junction border is detected incorrectly due to the poor contrast. (e) Extracted island. (f) Detected islands and the junction outline are superimposed on the original image.

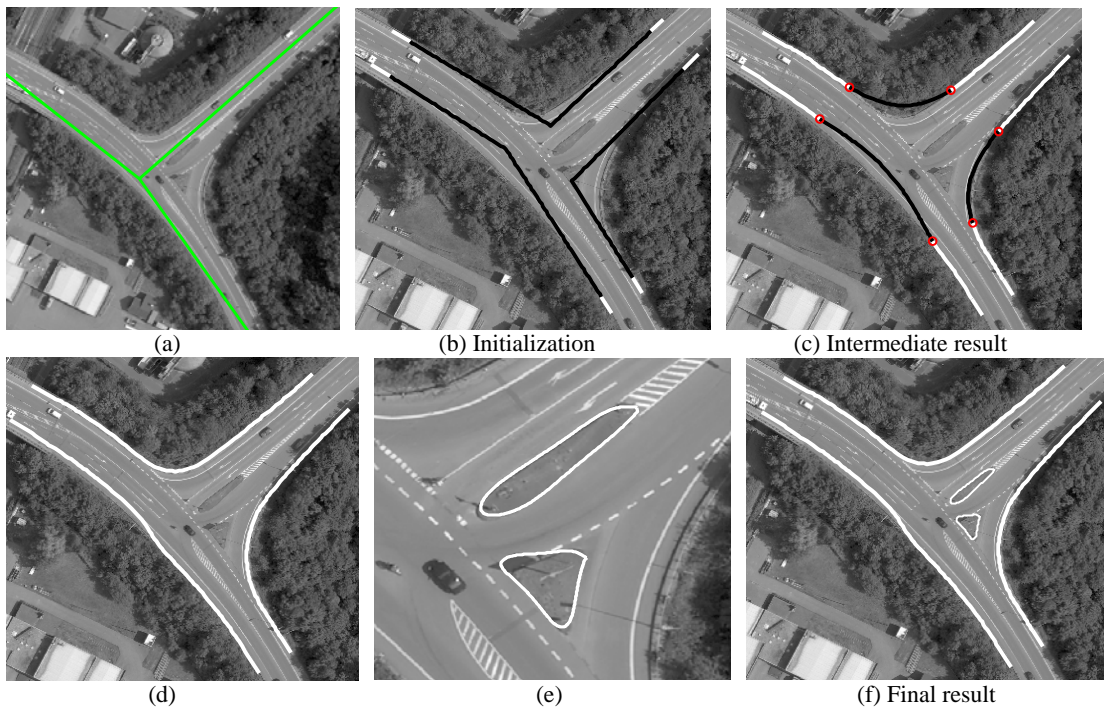


Figure 4-18: Illustrating successive steps for the extraction of a complex junction. (a) Vector data. (b) Initial snakes in black and road arms in white. (c) Snakes during evolution. (d) Junction outline. (e) Detected islands. (f) Detected islands and the junction outline are superimposed on the original image.

The same problem can occur when in one of the neighboring roads, road sides cannot be extracted because of occlusions or disturbances. These problems can only be addressed by a more sophisticated road model including width constraints and disturbing objects.

Figure 4-20 describes another example of a complex junction in which the island includes a few trees inside. Trees can affect the quality of the island extraction if they are very tall and stand close to the island border. In such a case, tree shadows are considered by level sets as a part of the island surface. In this example, however, the described problem is not severe.

Figure 4-21 displays a complex scene including tall trees and their shadows inside the islands and along the junction border. The major problem for the extraction of islands is that tree shadows occlude the island border in a large part. Consequently, shadowed areas are considered as part of the islands. Since shadows do not have a specific geometric form, they cause the extracted islands not to have a smooth boundary even after applying cubic spline approximation (Fig. 4-21-f). As can be seen in Figure 4-21-h, tree shadows beside the border cause the extraction result to be far from the true island boundaries.



Figure 4-19: Incorrectly extracted road border. Marked box in (a) shows the area where inconsistency occurs. This area is displayed in detail in (b).

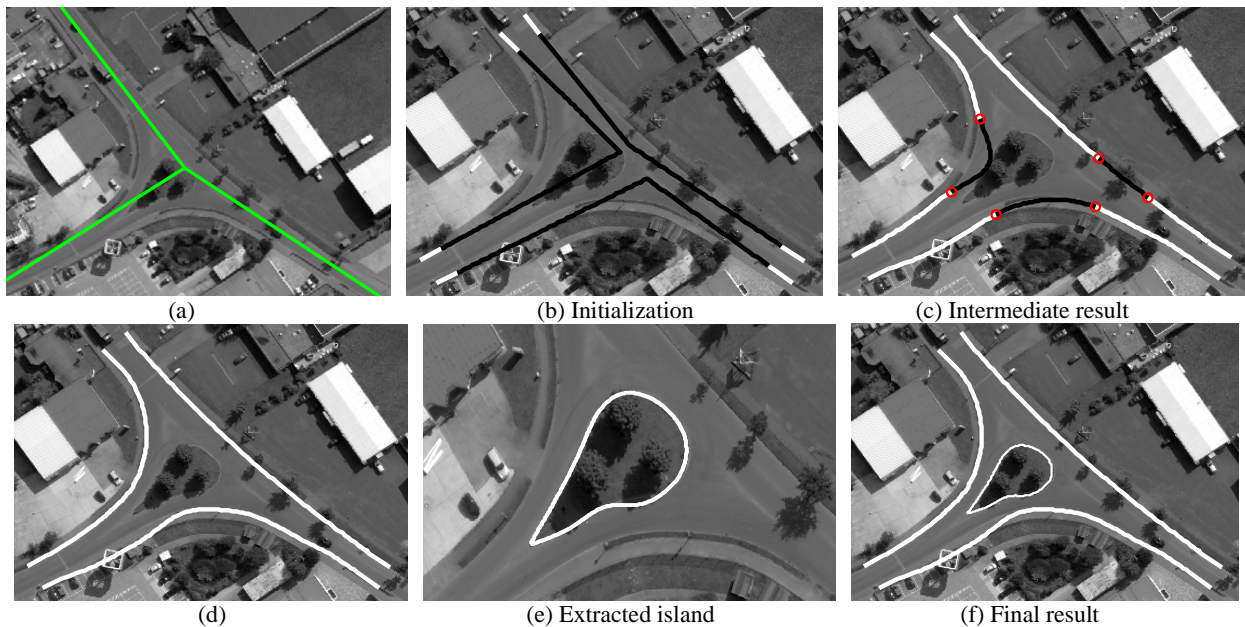


Figure 4-20: (a) Vector data. (b) Initial snakes in black and road arms in white. (c) Snakes during evolution. (d) Junction outline. In (e), the island is detected correctly even if some trees exist inside the island. Despite a poor contrast in the whole image and the presence of a row of trees and their shadows beside the junction border at the top-right, the final result in (f) is visually of a good quality.

For the extraction of islands, we assume that there is good contrast between the island surface and the surrounding asphalt. This precondition, however, does not always hold (see Fig. 4-23).

The problem can also be seen in Figure 4-22-e where the island is almost washed out after pre-processing. Furthermore, the junction area contains two parts having a remarkable radiometric contrast. As a result, when the snake begins

progressing from the start point at the right side, it gets stuck in the border between the two regions. However, at the end, the internal force pulls it back toward the junction border. The problem and the snake evolution are shown in Figures 4-22-c and d. The bottom-right border (Figure 4-22-f) lacks smoothness at the top where it is connected to the road arm side. The reason is that, near the road arm side, a sharp boundary attracts the snake slightly downside.

Figure 4-23 illustrates an example in which one of the available islands (the bottom island) is an elongated area having a very narrow width (1 m) and a weak contrast to the surrounding asphalt area. In the pre-processing step, the size of islands is further reduced and the contrast is weakened to reduce the effect of disturbing factors. Therefore, the island is almost washed out and cannot be recovered. The other three islands, however, were extracted successfully.

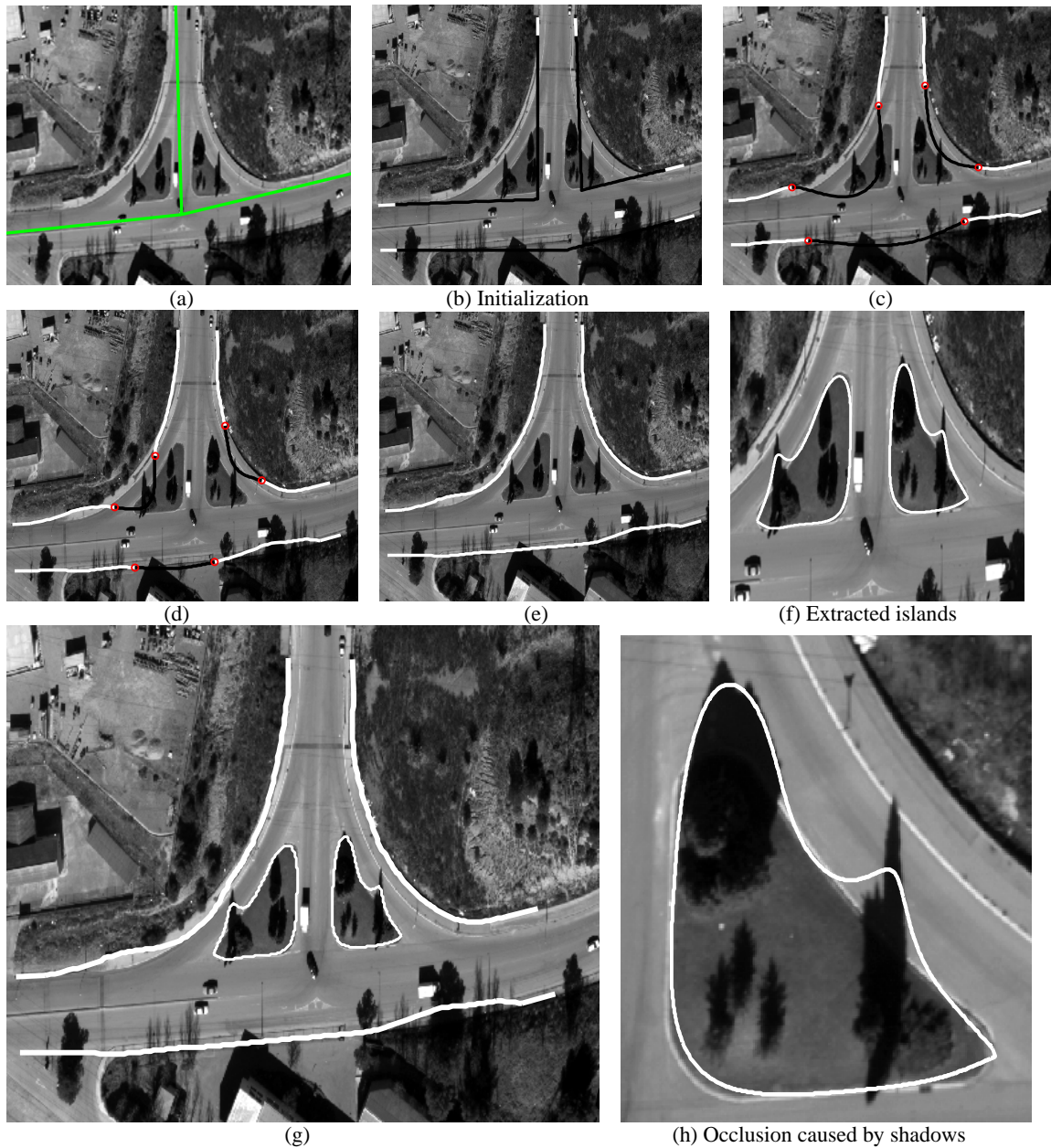


Figure 4-21: (a) Vector data. (b) Initial snakes in black and road arms in white. In (c) and (d), intermediate results describe how the snake passes over the islands toward the junction border. (e) Junction outline. (f) The island border is not smooth due to tree shadows. (g) Final result. (h) Incorrect result of island detection due to tree shadows.

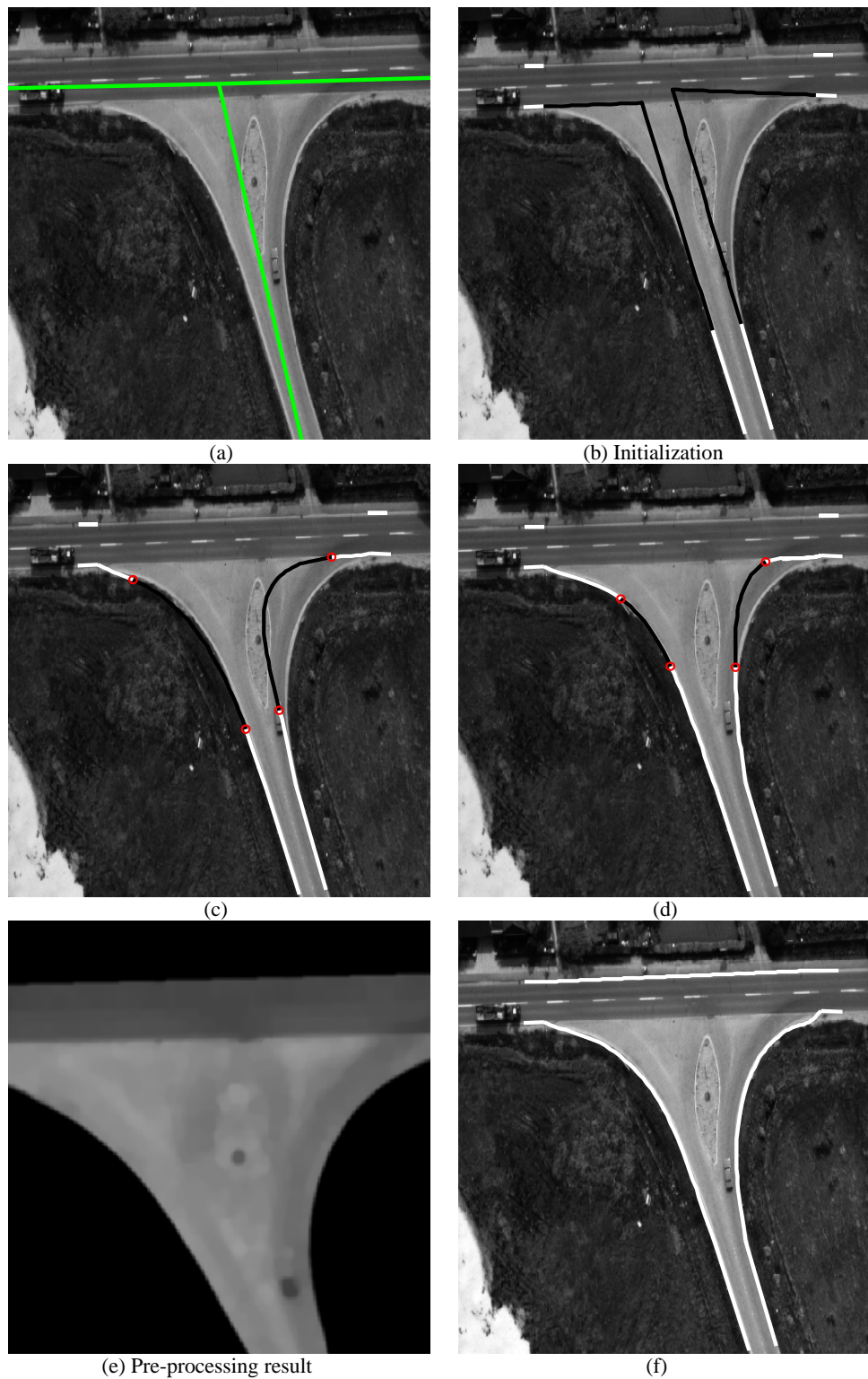


Figure 4-22: Illustrating a failure case of island extraction due to poor contrast. (a) Vector data. (b) Initial snakes in black and road arms in white. (c) and (d) show intermediate results of the evolution. In (e) the island cannot be recognized after pre-processing with human eyes. (f) Final result.

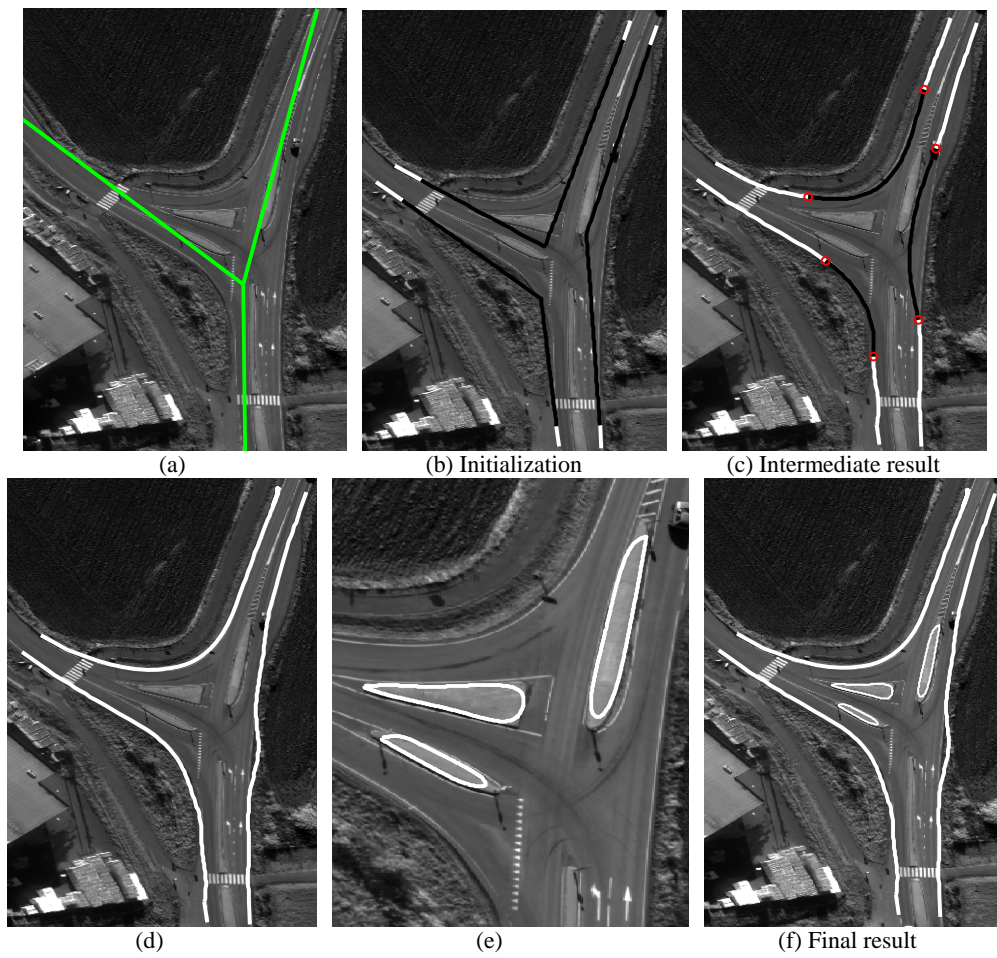


Figure 4-23: (a) Vector data. (b) Initial snakes in black and road arms in white. (c) Snakes during evolution. (d) Junction outline. (e) Detected islands. (f) The traffic island in the bottom has not been extracted. In this sample, a variety of disturbing factors such as cross walks, an unpaved road and vegetation close to the junction border at the right are present. The vegetation, which appears similar to edges, also causes a little deviation of the curve from the desired border (f).

#### 4.2.3.1 Discussion

Complex junctions differentiate themselves from simple ones by traffic islands. These small islands are captured in most of cases, but when occluded by trees or their shadows, they may not be extracted correctly. This is the main drawback of the level set approach. Poor contrast is another reason why islands can not be detected. The size of the island is another factor determining whether the island can be detected, i.e. too small an island is almost wiped out in the pre-processing step, so it cannot be extracted.

#### 4.2.3.2 Roundabout

We employ level sets combined with a hybrid evolution strategy for the extraction of central islands and our proposed snake-based method to capture the borders of roundabouts. Furthermore, the external force of the snake is modified based on the shape of the central island to assure a correct delineation of roundabout borders.

In following sections, five different examples are represented and various steps leading to the extraction of central islands as well as borders are illustrated.

#### Central Island

For the extraction of roundabouts, central islands are important components to be extracted first. We have tested our method for the extraction of central islands on several samples with the same set of control parameters for the used level sets (see section 3.4.2.1), some of which are shown below. Different steps of this task were described in detail in Chapter 3, section (3.4.2.1). First, we discuss two samples in which central islands are large enough to be considered as area objects in the geospatial database. After wards one sample where the central island appears as a point object in the topographic database is presented. Two further examples are also shown without describing intermediate steps of the extraction. Finally, an example where our evolution strategy is not able to detect the central island is illustrated.

In Figure 4-24, the effect of vehicles on the evolution is discussed whereas disturbances present inside the central island are illustrated in Figures 4-25, 4-26. In Figure 4-24-c, vehicles close to the island border block the movement of the

evolving curves toward the island boundaries. However, the island is detected along its border where vehicles are not present. This problem can be easily solved when we make use of the results of both expansion and shrinkage curve evolution. As is shown in Figure 4-24-e, the points located far away from the island boundary are removed, thereby resulting in a correct result of extraction (Fig. 4-24-f). There are cases in which disturbing features are present within the central island. Figure 4-25 describes one of those examples in which trees and coarse size text exist inside the island. Furthermore, the island border is partially occluded by tree shadows. In Figure 4-25-f, it is shown that our proposed iterative expansion curve evolution method is able to handle such a difficult situation.

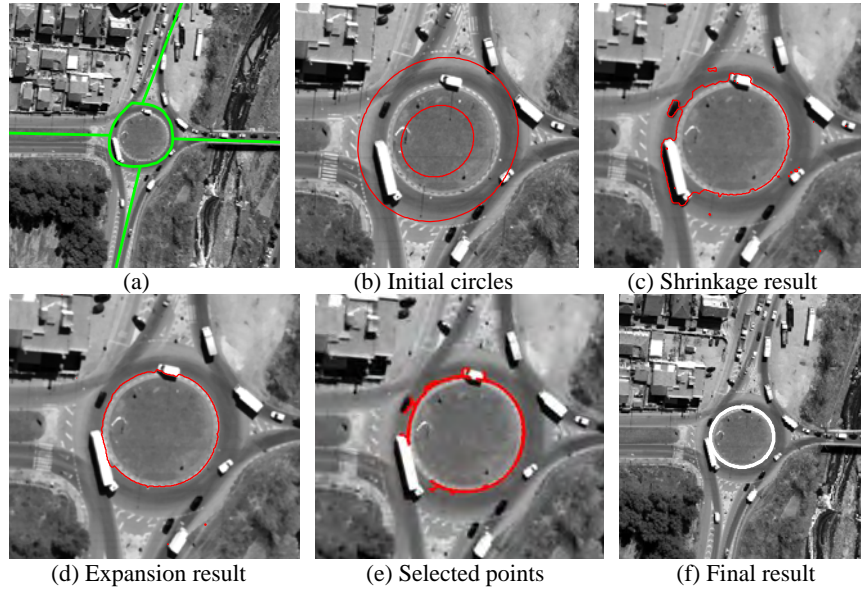


Figure 4-24: Successive steps illustrating the extraction of the central island. (a) Vector data. (b) Initial zero level curves as interior and exterior circles in relation to the central island. (c) Evolved zero level curves obtained after applying shrinkage evolution on the exterior circle. (d) Evolved zero level curves obtained after applying iterative expansion evolution on the interior circle. (e) Describes the points chosen when the results from (c) and (d) are close enough to each other. (f) The fitted ellipse to the chosen points transferred into the original image.

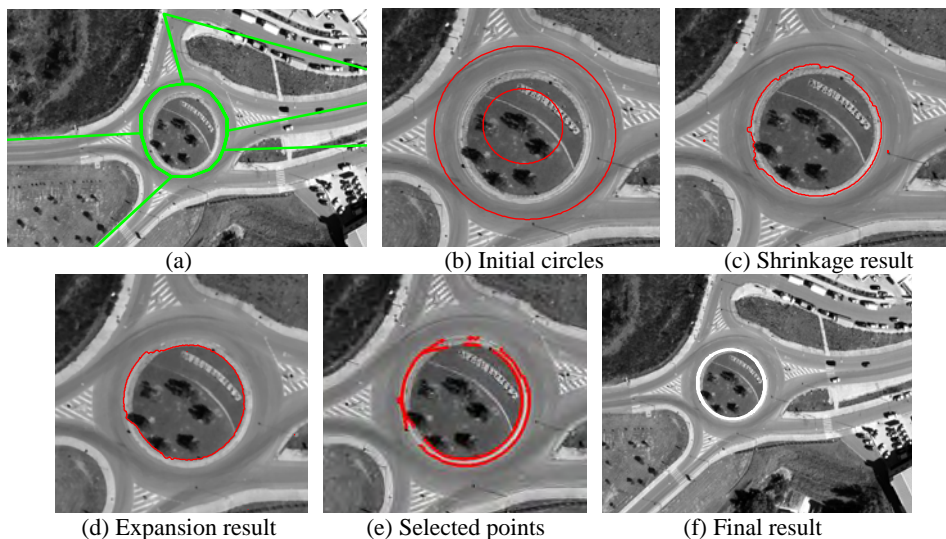


Figure 4-25: Describing consecutive steps to the central island extraction. (a) Vector data. (b) Initial zero level curves as interior and exterior circles in relation to the central island. (c) Evolved zero level curves obtained after applying shrinkage evolution on the exterior circle. (d) Evolved zero level curves obtained after applying iterative expansion evolution on the interior circle. (e) Describes the points chosen when the results from (c) and (d) are close enough to each other. (f) The fitted ellipse to the chosen points transferred into the original image.

As mentioned in Chapter 3, for smaller roundabouts, central islands are represented as point objects in the geospatial database. In Figure 4-26, the central island is identified in the geospatial database as a point object (Fig. 4-26-a), so three successive circles are defined around the point obtained from the vector data (Fig. 4-26-b). Shrinkage curve evolution is applied on each circle. The results of shrinkage evolution are shown in Figures 4-26-c, d and e. In Figure 4-

26-f, the interior circle is defined and expanded iteratively until it reaches a stable state (Fig. 4-26-g). The curve in Figure 4-26-g is compared with the curves in Figures 4-26-c, d and e individually. The case in which the compared curves are sufficiently close to each other is chosen and close points from both curves are selected (Fig. 4-26-h). Finally, an ellipse is fitted to these points (Fig. 4-26-i). In this example, in the central island, there are bushes as well as two areas with a sharp contrast relative to each other. The final result proves the robustness of our proposed iterative expansion method. Here, the usefulness of defining three successive circles can be seen because the smallest circle lies partly inside the island border, and consequently it shrinks away from the island boundary, which is not desirable. However, with the two other larger circles, we can detect the island boundary, because they enclose the island.

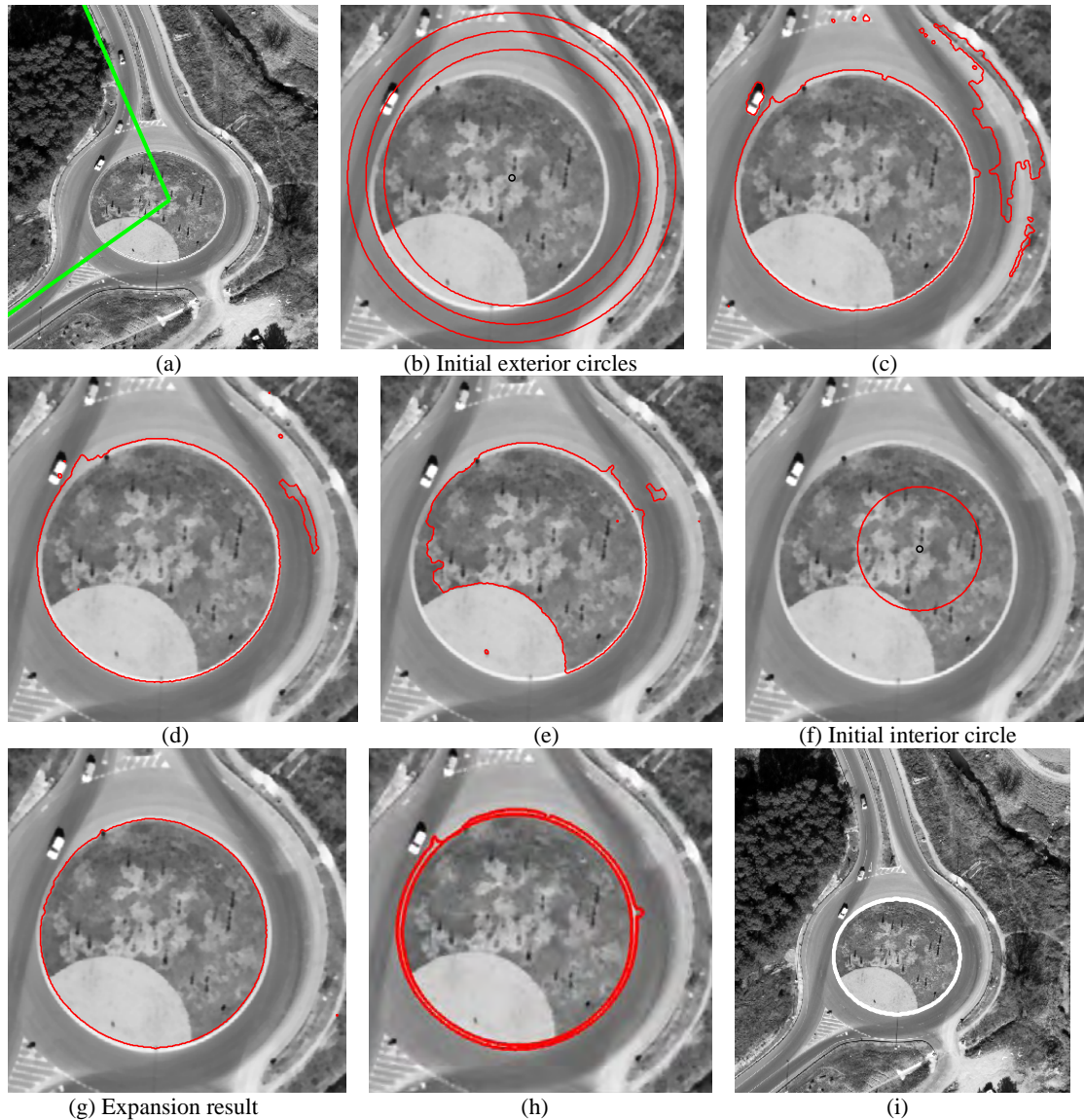


Figure 4-26: (a) Vector data. (b) Three successive circles as initial zero level curves for the shrinkage evolution. (c), (d) and (e) are the results of shrinkage evolution for the largest, middle and smallest circles respectively. (f) Initial zero level curve appears as a circle situated inside the central island. (g) The result of iterative expansion evolution. (h) Selected points. (i) Extracted central island.

Figure 4-27 shows two further examples for our method. The example at the top row shows two areas with a sharp contrast with each other inside the central island. Furthermore, the darker area includes some small bushes. With our proposed iterative expansion curve evolution strategy, the effect of these disturbing features is eliminated.

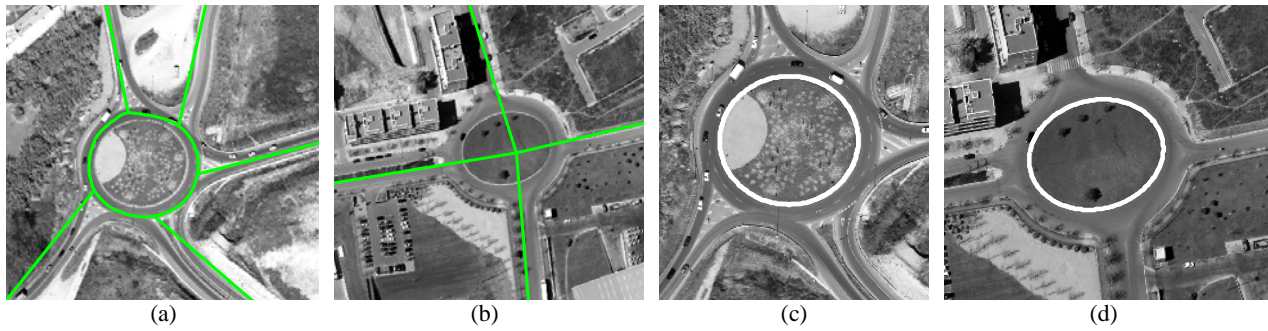


Figure 4-27: Two further examples of central island extraction. (a) and (b) show vector data superimposed on the image. (c) and (d) show the extracted central islands.

In Figure 4-28, one example is shown where our hybrid evolution strategy fails to detect the central island. The reason is that large trees and their shadows heavily occluded the island border such that the expanding curve leaks outside the island and converges to undesirable features. Therefore, our evolution strategy cannot overcome large disturbances on the island border.



Figure 4-28: Illustrating an example in which the central island cannot be extracted due to heavy occlusions caused by trees and their shadows.

### Roundabout Border

The same examples chosen in the previous section to describe steps for the detection of central islands are used also in this section to illustrate the extraction of roundabout borders. In Figure 4-29, disturbances like vehicles are discussed. In Figure 4-30, two problems of poor initialization and sharp curvature of the border are illustrated. Finally, three examples in which the roundabout borders include high curvature variation are represented and discussed (Figs. 4-31, 32 and 33).

Road arms are extracted automatically in three examples (Figs. 4-30, 4-31, 4-32). Nevertheless, in two other samples the road arm extraction breaks down (Figs. 4-29, 4-33), so road arms are provided manually in order to be able to evaluate the performance of our approach for the delineation of roundabout borders.

Figure 4-29 shows a scene highly disturbed by vehicles. Using the modified external force field of the snake, we overcome vehicles exist on the circulating roadway. However, vehicles outside the influence area of the modified force field can degrade the quality of the final result especially if roundabout borders lack sufficient contrast with the surroundings. As is shown in Figures 4-29-c, d and e, a vehicle at the bottom-left border has drawn the curve somewhat inside the road. Nevertheless, single vehicles on the crossing roads do not affect the curve movement if a good contrast exists between the roads and the surroundings.

In Figure 4-30, all borders are extracted correctly except for the right-middle border. The reason is that this border has a concave shape with a very sharp curvature. As a result, a much stronger balloon force is needed to push the curve back towards the boundary. Furthermore, borders whose initializations are very far, as is the case for top-right border, can be detected correctly.

In Figure 4-31, high variation of curvature at opposite borders is overcome. During evolution, the snake at the right side detects the related border sooner than that at the left side (Fig. 4-31-d). The reason is that, at the right side, the balloon force accelerates the movement of the snake toward the border whereas at the left the balloon force is applied opposite

to the direction in which the modified force field acts. Therefore, the left curve needs higher number of iterations to detect the associated border.

In Figure 4-32, the challenging part is the capture of the roundabout border that has a high variation of curvature (left border). Furthermore, disturbances such as vehicles and features inside the central island are present in the scene. This situation can be handled with the snake external force field modified based the shape of the central island. The border at the bottom, however, cannot be correctly captured as its curvature is too high.

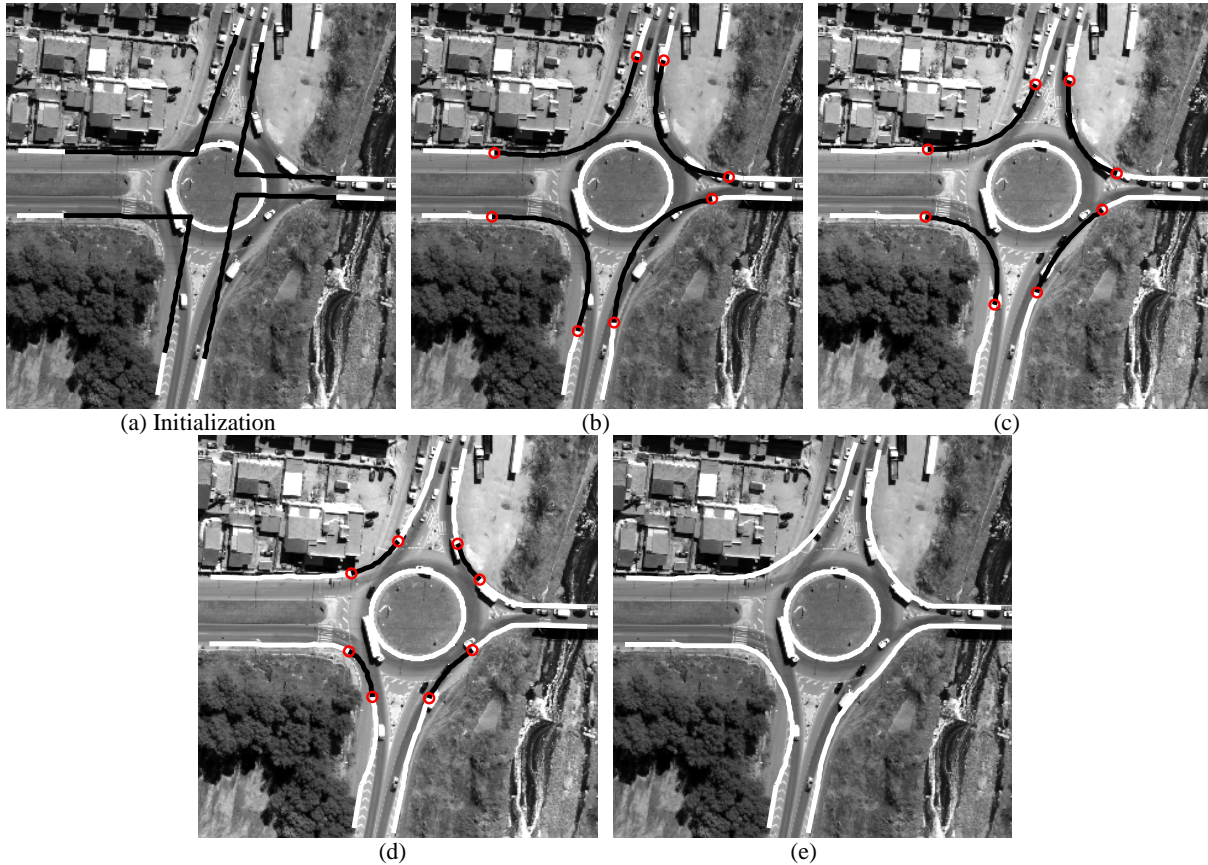


Figure 4-29: Illustrating the delineation of roundabout borders. (a) Initial snakes in black and road arms in white. In (b), (c) and (d) the evolving curves are shown. (e) Reconstructed roundabout. The vehicle at the bottom-left border has attracted the curve slightly inside the road where contrast is poor.

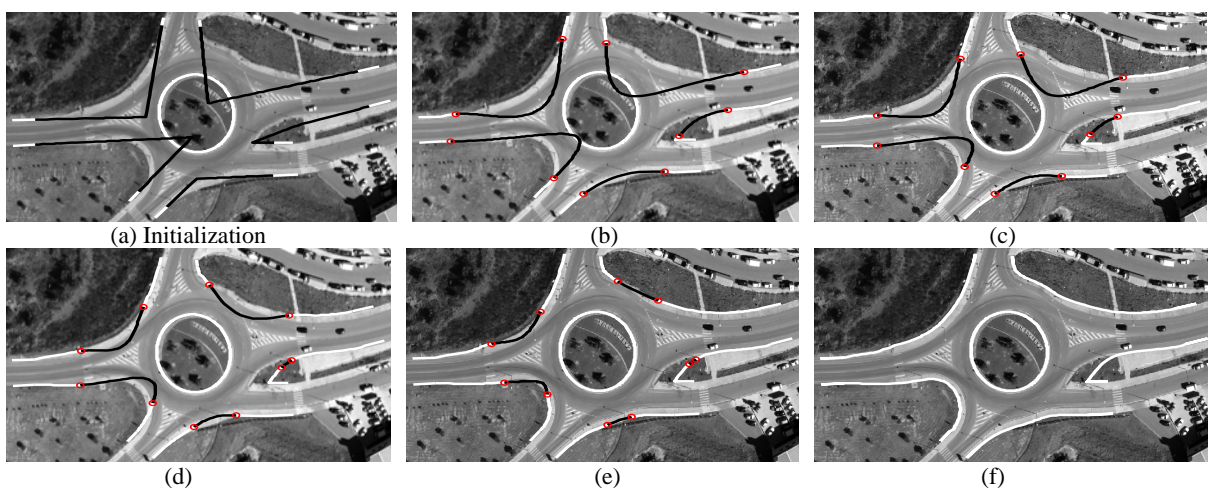


Figure 4-30: (a) Initial snakes in black and road arms in white. In (b), (c), (d) and (e) the evolving curves are shown. (f) Reconstructed roundabout. The right-middle border has not been recovered due to a sharp curvature.

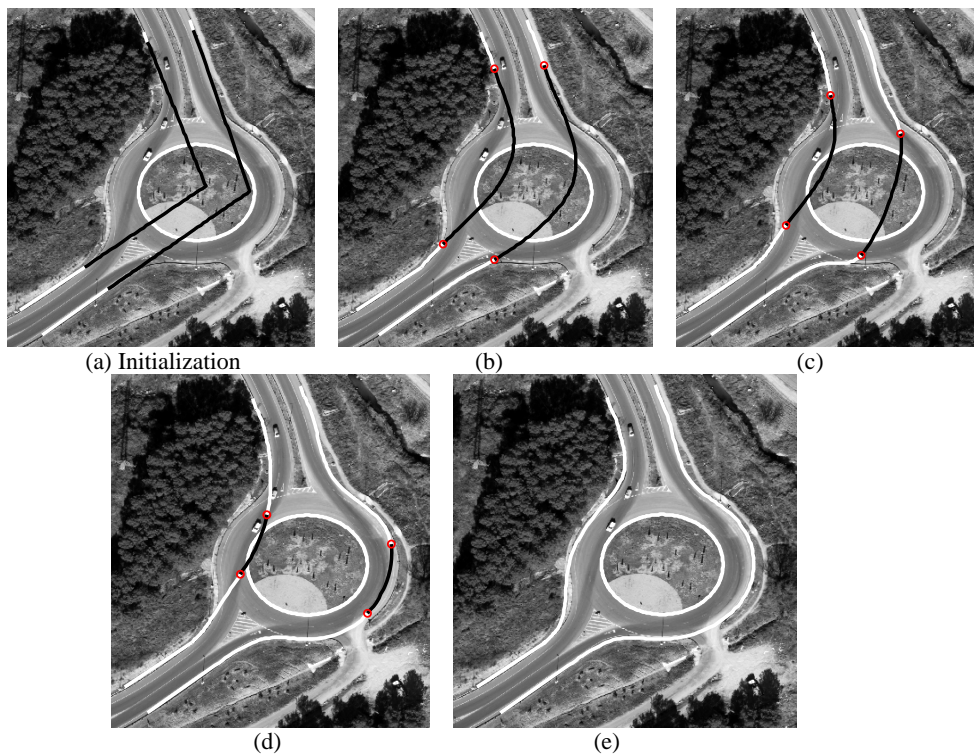


Figure 4-31: Illustrating the capture of roundabout outline. (a) Initial snakes in black and road arms in white. In (b), (c) and (d) evolving curves are shown. In (d), the right snake has converged to the border whereas the left snake is still on the border of the central island. (e) Reconstructed roundabout.

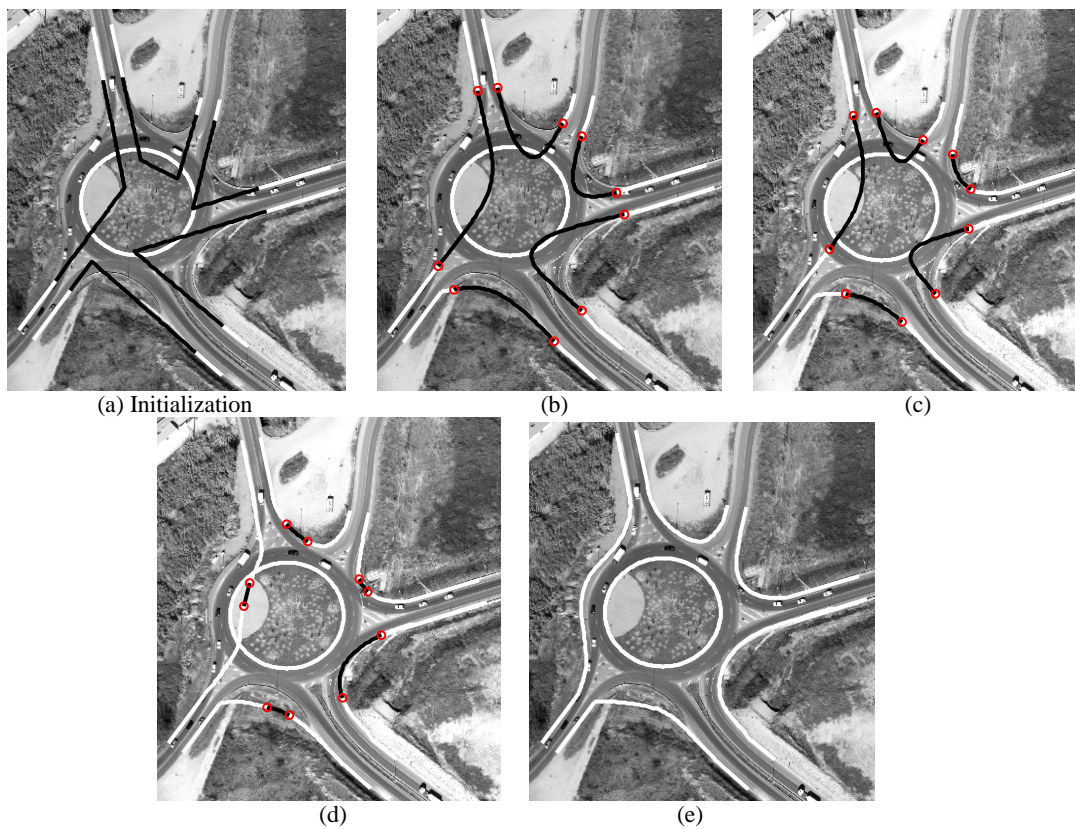


Figure 4-32: Illustrating the capture of roundabout outline. (a) Initial snakes in black and road arms in white. In (b), (c) and (d) evolving curves are shown. (e) Reconstructed roundabout.

In Figure 4-33, all four borders include sharp curvature variations. In particular, the top-right border, which its initial curve is very far away from the solution (Fig. 4-33-a), cannot be recovered unless our proposed force field is applied.

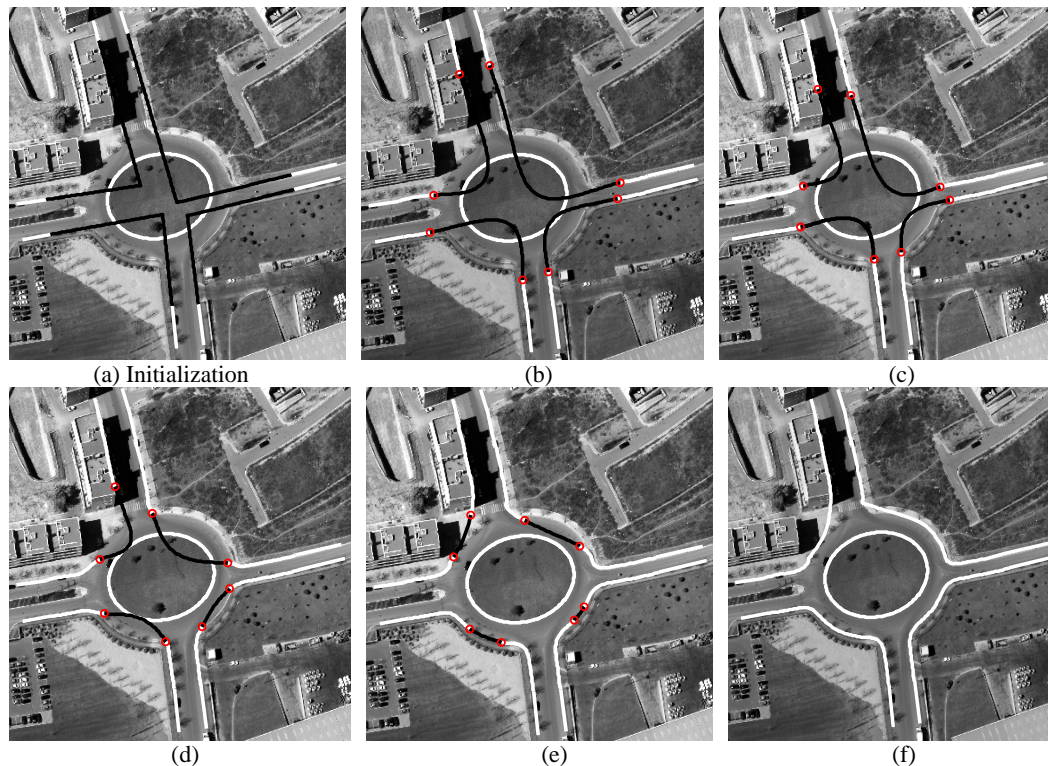


Figure 4-33: (a) Initial snakes in black and road arms in white. In (b), (c), (d) and (e) evolving curves are shown. (f) Reconstructed roundabout.

## Discussion

Central islands in all roundabout samples are extracted successfully. With a hybrid evolution strategy, the effect of various kinds of disturbances appearing inside and outside the central island can be removed. Although small shadows of trees on the island border does not affect the detection result, large shadows, appearing mainly in urban areas, may cause the evolving curve penetrate outside the central island. For the reconstruction of roundabouts, the modification of the external force field proved to be efficient. The modified force field helps to overcome high variation of curvature in roundabout borders. Furthermore, disturbances originated from various sources such as vehicles and their shadows and features inside the central islands are overcome in the reconstruction step.

## 4.3. Quantitative External Evaluation

In order to quantitatively evaluate the performance of the approach, we compared the extraction results to the manually plotted road junction areas used as reference data. The comparison was carried out by matching the extraction results to the reference data using the so-called *buffer method* [Heipke et al. 1998]. The buffer width can be defined according to the required extraction accuracy for a specific application. Although the buffer width can be defined using the required accuracy of ATKIS, which for a road object is defined as 3m, we decided to set the value within the range of 0.5 m to 3 m, i.e. 5 pixels to 30 pixels in concert with the image resolution of 0.1 m. This allows to assess the relevance of the approach for applications that demand varying degrees of accuracy. A smaller value of the buffer width is chosen for an application that requires more accurate extraction results.

An extracted object is assumed to be correct if the maximum distance between the extracted object and its corresponding reference does not exceed the buffer width (Fig. 4-34-a). Furthermore, a reference object is assumed to be matched if the maximum deviation from the extracted object is within the buffer width (Fig. 4-34-b). Two examples in which the extraction result and reference data are unmatched are described in Figures 4-34-c and 4-34-d respectively. Based on these assumptions the following quality measures were used in our work:

- **Completeness:** is the ratio of the number of matched reference objects to the reference number of objects.
- **Correctness:** is the ratio of the number of correctly extracted objects to the number of extracted objects.
- **Geometric accuracy:** is the average distance between the correctly extracted objects and its corresponding reference, which is expressed as Root Mean Square (RMS) value.

The geometrical measure (RMS) is computed using the coordinate differences between the vertices in one dataset and their nearest correspondence on the other dataset as follows:

$$D_j = \frac{\sum_{i=1}^n d_i}{n} ; j=1, 2, \dots, m \quad (4.1)$$

$$RMS = \sqrt{\frac{\sum_{j=1}^m D_j^2}{m}} \quad (4.2)$$

where  $d_i$  denotes the distance between the correctly extracted object and its corresponding reference data at the vertex  $i$  and  $D_j$  is the average of  $d_i$  computed at all vertices in each object.  $j$  denotes the object index.  $n$  stands for the number of vertices in the matched object, and  $m$  is the number of matched objects.

The distance between vertices either in the reference data or in the extracted object corresponds to one pixel, i.e. 10 cm in object space. The quality measures are computed in object space and for three different object classes individually, namely road border in simple and complex junction including roundabouts, traffic islands in complex junctions excluding roundabouts and central islands in roundabouts, because for each class of objects a different extraction strategy was used.

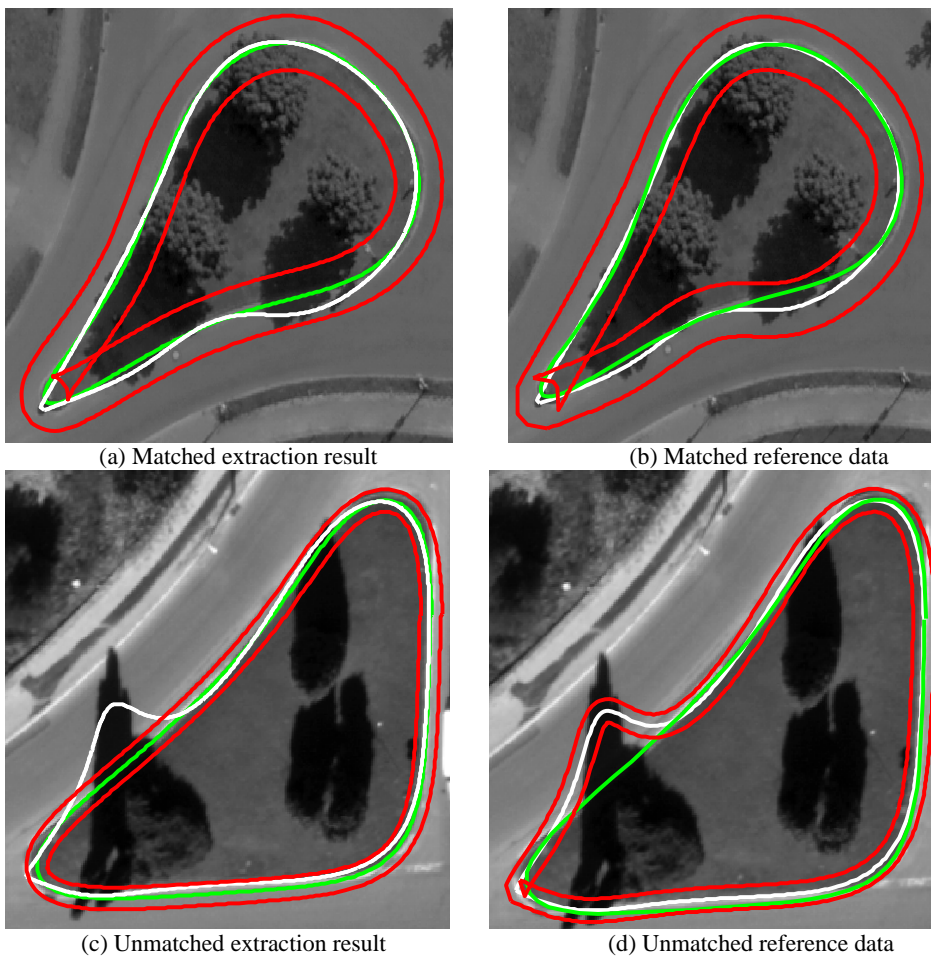


Figure 4-34: Illustrating the buffer method in image samples. In all figures, reference data is depicted in green and the extraction result in white. The buffer area is bordered with red lines.

### 4.3.1 Border of junctions

Road border is resulted by connecting the junction border to the associated road sides. We tested the proposed approach on 40 samples comprising simple and complex junctions and 10 roundabouts. From these samples a number of 143 road borders are resulted. Table 4-1 lists the evaluation results of our proposed approach for the extraction of junction borders with different buffer widths. From the buffer width value 0.5 m to 3 m, the completeness of the road border extraction have increased implying that the results are more complete for higher buffer width values. The geometrical accuracy increases inversely proportional to the buffer width value so that results obtained with a value of 0.5 are more accurate than those obtained with a larger buffer width value. For the buffer width value 0.5 m, the completeness is rather low. The reason is that a slight deviation of the extraction results from the true boundaries exceeding the buffer

width occurs frequently due to disturbances and sometimes also due to road markings. One example describing such a problem is given in Figures 4-5-e and 4-5-f where the top-left road border has entered slightly inside the junction area. However, the deviation from the junction border is less than 1 m and thus shows up as an error for the smallest buffer width. For the buffer widths of 2 m and 3 m, a significantly higher quantity of completeness have been achieved, which points out the validity of our approach for many practical applications.

Table 4-1: Evaluation results for road borders

Buffer width (m)	0.5	1	2	3
Reference number of road borders	143	143	143	143
Completeness	51%	61%	73%	78%
Geometric accuracy (m)	0.31	0.41	0.54	0.59

## 4.3.2 Islands

Small traffic islands and central islands of roundabouts are captured using the same level set formulation. However, the initialisation and some post-processing steps are different. For this reason, the evaluation of the extraction approach for central islands and small islands is carried out separately.

### 4.3.2.1 Traffic Islands in Complex Junctions

Traffic islands appear in the middle area of complex road junctions. Among 17 traffic islands that exist in the selected nine complex junction samples, two islands could not be detected. The same quality measures as adopted for road borders are taken for the evaluation of small traffic islands (Table 4-2). The buffer width values, however, are limited to 0.3 and 0.5 m due to the small size of islands. Likely disturbances, which deteriorate the geometrical accuracy of the detection, are of two kinds for the islands: first, tree shadows situated inside the islands (Fig. 4-21-h), second, vehicles beside the islands and their shadows. Our level sets method cannot overcome these disturbances.

Table 4-2: Evaluation results for traffic islands

Buffer width (m)	0.3	0.5
Reference number of islands	17	17
Completeness	65%	71%
Correctness	60%	87%
Geometric accuracy (m)	0.18	0.22

### 4.3.2.2 Central Islands in Roundabouts

Evaluation results for the extraction of central islands in roundabouts are shown in Table 4-3 for two different buffer widths. In four samples, central islands are represented as point objects and in six other samples as area objects. Central islands of roundabouts were extracted with high quantities of completeness and correctness for the buffer width of 0.5 m implying the effectiveness of our hybrid evolution strategy to detect central islands. In the buffer width value 1 m, all of central islands were extracted correctly.

Table 4-3: Evaluation results for central islands

Buffer width (m)	0.5	1
Reference number of central islands	10	10
Completeness	90%	100%
Correctness	90%	100%
Geometric accuracy (m)	0.26	0.35

We achieved a good evaluation result in the extraction of central islands, which proves the robustness of our method.

## 4.4. Summary

In this chapter, we introduced the input data and presented various examples of simple and complex junction extraction. Various types of disturbances and their effects on the performance of the approach as well as issues related to the island extraction were described and discussed. Several examples of central island extraction along with intermediate results were presented to show the robustness of the hybrid evolution strategy. Furthermore, the reconstruction of roundabouts was shown to demonstrate the effectiveness of our shape-based modified external force field. To evaluate our approach, we used several quality measures to assess completeness and correctness as well as geometric accuracy. We divided road junctions into their constituent components, namely road borders, traffic islands and central islands, each of which was evaluated separately. Quality measures were computed for different buffer widths and explanations on the quality of the results were provided. The evaluation results prove the suitability of our approach for many practical applications.

## 5. Conclusions and Outlook

This thesis describes a new approach to the extraction of road junctions. Compared to existing research works, it comprises a detailed modeling of junctions including islands. Our approach makes use of parametric active contours and level sets in combination with a road extraction method to capture road junctions. It utilizes a priori information derived from an existing topographic database and eventually results in detailed extraction of road junctions.

From the topographic database geometric, radiometric and topological information of the junction are derived. This information gives a rough idea of the junction. Using the junction center point, we focus our attention on a limited image region. First, edges are detected and road segment hypotheses are generated using several geometric and radiometric criteria. Furthermore, road markings if present in the scene are detected in order to verify the obtained road segments. Road arms are obtained after road segments with similar geometric properties are linked. The resulting road arms supply initial conditions for the road junction extraction. We propose a novel snake model that employs the ziplock snake concept and integrates it with a new external force field. This new force field is a combination of the balloon force and the GVF. The GVF increase the capture range of snakes and provides a dense force field assuring a stable optimization. Furthermore, the balloon force is associated with geometric characteristics of junction borders. These characteristics are incorporated into our snake model implicitly. The balloon force helps to overcome high variations of curvature in junction borders and lack of sufficient contrast between the junction central area and the surroundings. Before snake optimization starts, initial snakes are decreased based on the junction geometrical shape to assure a close global initialization. Next, the junction outline is delineated. Due to the strong internal snake energy, a number of disturbances can be overcome, e.g. trees, shadows from various sources and single vehicle. The obtained junction outline defines an area within which traffic islands may exist. A level set approach is used to detect these islands. Initialization of the level sets is carried out using segmentation results. Such region-based initialization needs less computation time and is flexible in practice. In order to select islands from the evolved curves, some geometric and topological constraints are introduced based on the properties of islands. This type of evolution strategy, however, is not applicable for roundabouts. Since the shape of a roundabout is heavily affected by the shape of its central island, we need initially to detect the central island followed by the modification of the snake external force field in order to handle cases with a high variation of curvature including all kinds of possible disturbances. The central island is detected using level sets with a hybrid evolution strategy. This hybrid strategy includes two steps: shrinking and iterative expansion curve evolution. Eventually, the central island is obtained after some post-processing. The external snake force field is modified using a signed distance function so that initial snakes are pulled toward the outline even from far distances. The reason is that force arrows at any location on the modified force field point to the roundabout outline. A signed distance function is computed from the contour of the enlarged central island and its GVF substitutes the corresponding region in the original external force field.

Many tests of the approach have been carried out using digital aerial images with a ground resolution of 0.1 m depicting different landscapes. The experiments show that for the buffer width of 3 m, 78% of road borders in rural and suburban areas are reliably extracted, and the achieved geometric accuracy is better than 0.59 m. The achieved geometrical accuracy for traffic islands is 0.22 m with 87% of them been correctly extracted for the buffer width 0.5 m. A better assessment result is expected for central islands such that for the buffer width 1 m, all of them were extracted with the geometric accuracy of 0.35 m.

Extracted road junctions can be used for the reconstruction of road networks in large scales. As road maps are used in a variety of applications such as traffic and fleet management, intelligent transportation systems, car navigation systems, and internet-based map services etc., all these applications benefit from the result of our work indirectly. Furthermore, future car navigation systems require detailed and accurate road maps [Brenner 2008]. As traffic islands are a level of detail in road maps, they can also be used in car navigation systems.

### 5.1. Discussion and Conclusions

The most outstanding feature of our approach is the integration of information derived from an existing geospatial database with active contours to extract simple and complex road junctions.

The core of this work is to investigate the potential of active contours to capture complex topographic objects using existing topographic databases. It was shown that active contours are efficient techniques for the extraction of road junctions. Furthermore, the utilization of a topographic database is proved to be beneficial to the extraction.

Main issues are discussed as follow:

- Road junction class

Junctions belong to a different class of topographic objects than roads. They are of a variety of geometrical shapes. Furthermore, they include islands in their central area, which makes their extraction hard as less geometric and radiometric constraints can be applied for their capture. However, roads are fundamental components of junctions since the geometrical shape of junctions is affected by the number of crossing roads and their widths. Furthermore, in our work, they provide initial positions and directions used to initialize the snake model. Modeling of junctions without

reliance on the crossing roads needs more investigation and perhaps a quite different approach. The importance of such a research is that the quality of the crossing roads can be assessed using the extracted road junctions.

- The balloon force and parameterization

Junction borders contain varying degrees of curvature such that the curvature has its highest value in the middle of junction borders. To capture the junction borders in places with a high curvature, a dense snake vertices is needed to better describe the complexity of the contour, whereas in boundaries with a low curvature as well as in straight lines less vertices is required. Too few snake vertices in high-curvature boundaries cause the snake to become straight after a few iterations. In such cases, the balloon force can push the snake toward the junction center until it converges to the desired boundary. As was shown in some samples, the balloon force can compensate the effect of a constant number of snake vertices along a boundary with varying degrees of curvature.

- Snake internal force and disturbances

Disturbances are nearly always present in the central area of junctions where the definition of geometric and radiometric constraints is difficult. Snakes are well suited to overcome disturbances and variation of radiometric properties if a strong internal energy and a correct initialization is provided. Our snake model has these characteristics. Occlusions caused by shadows from trees, street lights, traffic lights and traffic boards can be resolved easily. We demonstrate this advantage in several samples. Road markings are useful road surface features used to verify road arm extraction results and to assist the snake in detecting junction borders. However, markings can be quite misleading in central area of junction where they appear as stop line or warning lines. With a proper selection of snake spacing and internal snake energy, they don't have a major effect on the quality of final results. However, row of cars behind the traffic light close to a road side might cause the snake to yield incorrect results. To handle such complex scenes, cars need to be modeled and integrated with the current approach.

- Disturbances and the extraction of traffic islands

Although islands and junction borders are occluded by similar disturbing factors, the way chosen to overcome disturbances for each of them is not the same. Unlike junction borders where strong internal snake energy is used to overcome disturbances, in traffic islands, the internal energy of the level sets is used not to overcome disturbances but to assure a stable numerical computation during the evolution. Instead, a pre-processing procedure including morphological operators with a rather large structuring element is applied to eliminate road markings and small shadows, which proved to be useful in most of cases. However, large shadow areas cast on the island border caused mainly by tall trees situated inside islands might lead to incorrect detection results. This is the weakest part of the approach for the extraction of traffic islands. Incorporation of the island's shape information into the level sets equations may improve the final results.

In roundabouts, disturbances such as bushes, sparse trees and their shadow, vehicles and their shadows are handled using an evolution strategy in which a combined shrinkage and expansion curve evolution is carried out. Several tests on samples describing various kinds of disturbances show the efficiency and robustness of our evolution approach. In city areas, however, the extraction of central islands seems to be challenging as they contain many different structures inside. Another possible problem is that a row of vehicles all round the central island may block the movement of the evolving curve. It is another reason emphasizing the necessity to model vehicles in urban regions.

- Region-based initialization of level sets

Initialization of level sets is of special importance. Poor initialization results in much more time to converge to the desired boundaries. Furthermore, initial curves detect every object when evolving, which is not desirable. A better solution is to segment the region of interest so that islands are roughly obtained. An initial level set function is constructed from these regions, which means that the zero level curve needs far less iterations to detect islands. Furthermore, some undesirable features are discarded at the segmentation step, which makes the initialization more flexible. The question of whether expansion or shrinking evolution is to be applied is handled automatically. It is noted that if islands are discarded in the segmentation step, they have no chance to be detected later. Therefore, a reliable segmentation method is crucial to the island extraction.

- Shaped-based modification of the external force field and roundabout reconstruction

Roundabouts contain a high variation of curvature in their outline. Furthermore, initial snakes may lie far from the outline inside the central island. Vehicles are often present in the circulating roadway as well. As a consequence, it is likely that initial snakes fail to detect the outline correctly. Unlike simple junctions where the balloon force is applied in only one direction toward the junction central area, in roundabouts, the balloon force sometimes needs to be applied in the opposite direction too. The question of when to apply the balloon force and in which direction is very complex requiring heuristic parameter settings. Our proposed solution is to modify the external force field based on the shape of central islands so that initial snakes are pulled towards the roundabout outline even if they are situated far from the border. In this way, the effect of all kinds of disturbances can be removed. In most cases, the detection of the roundabout outline heavily depends on the modified external force field. Therefore, a reliable detection of the central islands is crucial to our approach.

## 5.2. Outlook

Based on the obtained results, some directions of research can be investigated. The most interesting are the following:

- Incorporation of vehicles into the junction model is highly desirable. Vehicles can be used to verify the road arm hypotheses and consequently enhance the reliability of the results. It also helps find reasons for cases where the road arm extraction method fails especially in suburban areas where usually vehicles exist on roads and near road junctions.
- Our employed level set method in conjunction with the segmentation procedure overcomes small disturbances, e.g. shadows from street lights. However, in the presence of strong occlusions like large shadow areas on the island border, it cannot manage to overcome such disturbances and consequently, sometimes shadows are detected as parts of islands. Incorporation of the island shape information as prior knowledge into the level set formulation might improve the result, e.g. curvature profile of islands is a useful feature to be considered. Another solution might be the extraction of trees in order to exclude them from the scene.
- Lack of sufficient contrast between the island surface and the surrounding asphalt results in weak island edges. Since the level sets we use are based on edge information of objects, the evolving zero level curves might penetrate into the island surface from places where poor edge information exists and consequently islands cannot be extracted correctly. It seems that the incorporation of region-based evolution criteria such as radiometric properties of island regions in form of statistical parameters into the energy functional of level sets can at least partly solve the problem.
- As an alternative, parameterization in our snake model can be carried out dynamically by adding or deleting snake vertices based on the snake external energy and shape information of boundaries. The suitability of this method for high resolution imagery needs to be examined in future research work.
- Use of color information of high resolution aerial imagery can improve the performance of snakes and level sets. Furthermore, color information especially Near Infrared (NIR) band can be used to improve the segmentation results based on which region-based level set initialization is carried out.
- Applicability of our approach for processing of very high resolution aerial imagery with a ground resolution of a few cm is another research topic. This also helps to examine the behavior of our snake model in the images with varying ground resolutions.
- This work can be extended in order to reconstruct highly complex interchanges mainly appearing in expressways. Since, in interchanges, crossing roads do not intersect at grade, the incorporation of height data into the junction model is necessary. This requires the utilization of stereo images or Airborne Laser Scanning (ALS) data.
- A road network consists of roads connected by road junctions. In this work, road junctions as well as roads in a limited area near the road junctions are extracted. Further enhancement of the approach enables a complete reconstruction of the road network from high resolution aerial imagery.
- Updating the topographic database in another interesting research line. Newly-built roads are usually connected to the road network through road junctions. As a result, the identification of these roads and the result of their extraction in the junction area can be used for updating existing topographic databases.
- Extraction of road junction without relying on prior information from a topographic database is demanded considering that vector data is not always available. Furthermore, less-accurate vector data can sometimes mislead the extraction. As a result, fully automatic extraction of road junctions using only image data as input is desirable.
- Our work can be extended to urban areas if a more sophisticated road arm extraction approach is designed. In urban areas, extraction of roads based on edge segments is more likely to fail, because edge segments cannot often be detected due to the complexity of the scene. In an advanced road extraction method, spectral information and vehicles are possible features that should be considered.
- Investigations are needed to examine the potential of the presented concepts for the capture of other man-made as well as natural objects. For every snake-based method, a close initialization is crucial for successful object detection. Because of this, active contours must be used in conjunction with a method that can provide a close initialization. These initialization conditions might be supplied for man-made objects much easier than for natural objects. Therefore, this work has a high potential to extract other man-made objects such as roads, buildings, bridges, etc. The extraction of natural objects, however, can be conducted semi-automatically through the interaction of active contours with a user.



## References

- Baumgartner, A., 1998. Extraction of roads from aerial imagery based on grouping and local context. In: *IntArchPhRS.*, Vol. 32(3/1), pp. 196-201.
- Barsi, A., Heipke, C., Willrich, F., 2002. Junction Extraction by Artificial Neural Network System – JEANS. In: *IntArchPhRS.*, Vol. 34, Part 3B, pp. 18-21.
- Berger, M.O., Mohr, R., 1990. Towards autonomy in active contour models. In: *The 10<sup>th</sup> International Conference on Pattern Recognition*, Atlantic City, NJ, pp. 847-851.
- Boichis, N., Viglino, J.-M., Cocquerez, J.-P., 2000. Knowledge based system for the automatic extraction of road intersections from aerial images. In: *IntArchPhRS.*, Vol. XXXIII, Supplement B3, pp. 27-34.
- Boichis, N., Cocquerez, J.-P., Airault, S., 1998. A top down strategy for simple crossroads extraction. In: *IntArchPhRS.*, Vol. XXXII, part 2/1, pp. 19-26.
- Brenner, C., 2008. Geosensor networks- The case of navigation & driver assistance systems. In: *EuroSDR & ISPRS Hannover Workshop (presentation)*, Hannover, Germany (<http://www.ikg.uni-hannover.de/geosensor/presentation.html>).
- Bresson, X., Butz, T., and Thiran, J.-P., 2005. Anaconda: A new active contour oriented non deterministic approach. Technical Report TR-ITS-2005, Swiss Federal Institute of Technology, Lausanne, Switzerland.
- Bresson, X., Vandergheynst, P., and Thiran, J., 2006. A variational model for object segmentation using boundary information and statistical shape prior driven by the Mumford-Shah functional. *International Journal of Computer Vision*, Vol. 68(2), pp. 145-162.
- Bresson, X., Vandergheynst, P., and Thiran, J., 2003. A Priori Information in Image Segmentation: Energy Functional based on Shape Statistical Model and Image Information. In: *IEEE International Conference on Image Processing*, Vol. 3, pp. 428-428
- Caselles, V., Kimmel, R., and Sapiro, G., 1997. Geodesic active contours. In: *International Journal of Computer Vision*, Vol. 22(1), pp. 61-79.
- Caselles, V., Catta, F., Coll, T., Dibos, F., 1993. A geometric model for active contours in image processing. In: *Numer.Math.*, Vol. 66, pp. 1-31.
- Chan, T. and Vese, L., 2001. Active contours without edges. In: *IEEE Trans. Imag. Proc.*, Vol. 10(2), pp. 266-277.
- Cohen, L.D., 1991. On active contours models and balloons. In: *Computer Vision, Graphics, and Image Processing: Image Understanding*, Vol. 53(2), pp. 211-218.
- Courant, R., Hilbert, D., 1953. *Methods of Mathematical Physics*. Wiley-Interscience, New York.
- Dal Poz, A. P., Zanin, R. B., do Vale, G. M., 2006. Automated extraction of road network from medium-and high-resolution images. In: *Pattern Recognition and Image Analysis*. Vol. 16(2), pp. 239-248.
- De Gunst, M., 1996. Knowledge-based interpretation of aerial images for updating of road maps. Ph.D. thesis, Delft University of Technology, the Netherlands.
- Epstein, C.L. and Gage, M., 1987. The curve shortening flow. In: *Wave Motion: Theory, Modeling, and Computation*, Springer-Verlag, New York.
- Gautama, S., Goeman, W., D'Haeyer, J., 2004. Robust detection of road junctions in VHR images using an improved ridge detector. In: *IntArchPhRS.*, Vol. XXXV, Part B3, Istanbul, pp. 815-819.
- Gerke, M., 2006. Automatic Quality Assessment of Road Databases Using Remotely Sensed Imagery. *Wissenschaftliche Arbeiten der Fachrichtung Geodäsie und Geoinformatik der Universität Hannover*, No. 261; also in: *Deutsche Geodätische Kommission, Reihe C*, No. 599 , 105 p.
- Gomes, J. and Faugeras, O., 2000. Reconciling distance functions and level sets. In: *Journal of Visual Communication and Image Representation*, Vol. 11, pp. 209-223.
- Heipke C., Mayer H., Wiedemann C., Jamet O., 1998. External evaluation of automatically extracted road axes. In: *PFG 2*, pp. 81-94.
- Heipke, C., Steger, C., Multhammer, R., 1995. A hierarchical approach to automatic road extraction from aerial imagery. In: *McKeown D.M., Dowman I., (Eds.), Integrating Photogrammetric Techniques with Scene Analysis and Machine Vision II*, SPIE Proceedings (2486), pp. 222-231.
- Hinz, S., Baumgartner, A., Steger, C., Mayer, H., Eckstein, W., Ebner, H., Radig, B., 1999. Road extraction in rural and urban areas. In: *Semantic Modeling for the Acquisition of Topographic Information from Images and Maps*. In: *SMATI'99*. München, pp. 7-27.
- Kass, M., Witkin, A., Terzopoulos, D., 1988. Snakes: Active contour models. In: *International Journal of Computer Vision*, Vol. 1(4), pp. 321-331.
- Koutaki, G., Uchimura, K., Hu, Z., 2005. Automatic Road Extraction Based on Intersection Detection in Suburban Areas. In: *Journal of Imaging Science and Technology*. Vol. 49(2), pp. 163-169.
- Laptev, I., Mayer, H., Lindeberg, T., Eckstein, W., Steger, C., Baumgartner, A., 2000. Automatic extraction of roads from aerial images based on scale space and snakes. In: *Machine Vision and Applications*, Vol. 12(1), pp. 23-31.
- Laptev, I., 1997. Road extraction based on line extraction and snakes. Master Thesis, Computational Vision and Active Perception Laboratory (CVAP), Royal Institute of Technology (KTH), Stockholm, Sweden, 67 p.

- Li, H., Xu, C., Gui, C., Fox, M.D., 2005. Level Set Evolution without Re-initialization: A New Variational Formulation. In: Proceedings of IEEE conference on Computer Vision and Pattern Recognition(CVPR'05), IEEE Computer Society Press., pp. 430-436.
- Malladi, R., Sethian, J. A., Vemuri, B. C., 1995. Shape modeling with front propagation: a level set approach. In: IEEE Transactions on Pattern Analysis and Machine Intelligence, Vol. 17, pp. 158-175.
- Mayer, H., Laptev, I., Baumgartner, A., 1998. Multi-Scale and Snakes for Automatic Road Extraction. In: Proc. Fifth European Conference on Computer Vision, Freiburg, Germany, Vol. 1406 of Springer Verlag Lecture Notes in Computer Science, pp.720-733.
- Mayer, H., Laptev, I., Baumgartner, A., Steger, C., 1997. Automatic Road Extraction Based on Multiscale Modeling, Context, and Snakes. In: International Archives of Photogrammetry and Remote Sensing, Vol. 32(3-2W3), pp. 47-56.
- Neuenschwander, W.M., Fua, P., Iverson, L., Szekely, G., Kubler, O., 1997. Ziplock snakes. In: International Journal of Computer Vision, Vol. 25(3), pp. 191-201.
- Niu, X., 2006. A semi-automatic framework for highway extraction and vehicle detection based on a geometric deformable model. In: ISPRS Journal of Photogrammetry and Remote Sensing, Vol. 61, pp. 170-186.
- Osher, S. and Fedkiw, R., 2002. Level Set Methods and Dynamic Implicit Surfaces. Springer-Verlag, New York.
- Osher, S., and Sethian J.A., 1988. Fronts Propagating with Curvature-Dependent Speed: Algorithms Based on Hamilton-Jacobi Formulations. In: Journal of Computational Physics, Vol. 79(1), pp. 12-49.
- Péteri, R., and Ranchin, T., 2003. Multi-resolution Snakes for urban road extraction from Ikonos and Quickbird images. In: Proceedings of the 23rd Symposium of the European Association of Remote Sensing Laboratories (EARSeL) "Remote Sensing in Transition", Ghent, Belgium, pp. 69-76.
- Ridler, T.W., and Calvard, S., 1978. Picture thresholding using an interactive selection method. In: IEEE Trans. on Systems, Man, and Cybernetics, SMC-8(8), pp. 1264-1291.
- Shi, Y., Nakagawa, M., Shibasaki, R., 2004. Reconstruction of Next-generation 3D Digital Road Model By Using Air-borne Three Line Scanner Imagery. In: Japan Society of Photogrammetry and Remote Sensing Student Forum Proceeding, Jun-04.
- Steger, C., 1998. An unbiased detector of curvilinear structures. In: IEEE Transactions on Pattern Analysis and Machine Intelligence, Vol. 20(2), pp. 113-125.
- U.S. Federal Highway Administration, 2000. Roundabout: An Information guide. FHWA-RD-00-67 (<http://www.tfhr.gov/>).
- Vemuri, B. and Chen, Y., 2003. Joint image registration and segmentation. In: Geometric Level Set Methods in Imaging, Vision, and Graphics (textbook), Springer, pp. 251-269.
- Vosselman, G., Gunst, M.D., 1997. Updating Road Maps by Context Reasoning. In: Grün, A., Baltsavias, E.P., Henricsson, O. (Eds.), Automatic Extraction of Manmade Objects from Aerial and Space Images (II), Birkhäuser Verlag, Basel, pp. 267-276.
- Wiedemann, C., 1999. Completion of automatically extracted road networks based on the function of roads. In: IntArchPhRS. Vol. 32(3-2W5), pp. 209-215.
- Wiedemann C., 2002. Improvement of Road Crossing Extraction and External Evaluation of the Extraction Results. In: IntArchPhRS., Vol. 34, Part 3B, pp. 297-300.
- Xu, C. and Prince, J.L., 1998. Generalized Gradient Vector Flow External Forces for Active Contours. In: Signal processing, Vol. 71, pp. 131-139.
- Zhang, C., 2003. Updating of Cartographic Road Databases by Images Analysis. Ph.D. thesis, Institute of Geodesy and Photogrammetry, ETH Zurich, Switzerland, IGP Mitteilungen No. 79.
- Zhang, Q., Couloigner, I., 2004. A Wavelet approach to road extraction from High Spatial Resolution Remotely-Sensed Imagery. In: GEOMATICA, Vol. 58(1), pp. 33-39.
- Zhao, H., Chan, T., Merriman, B., and Osher, S., 1996. A variational level set approach to multiphase motion. In: Journal of Computational Physics, Vol. 127, pp. 179-195.

## Acknowledgements

This thesis would not have been realized without the assistance, guidance and support of many people, all of whom it is not possible to mention by name.

The first person I would like to thank is Professor Christian Heipke for his kind supervision and many good ideas. His serious and significant research has a great influence on my work. He provided the opportunity to obtain DAAD scholarship and helps me greatly to start my PhD study. It is hard to express how much I am obliged to him.

Many thanks go to my direct supervisor Dr. Kian Pakzad for his supervision and critical remarks. He has always been supportive to me in countless ways.

I would also like to thank Professor Helmut Mayer and Professor Monika Sester for serving on my thesis committee as examiners. Furthermore, I would like to thank them for their valuable comments and suggestions.

I would also like to thank all the people that read my thesis: Professor Uwe Sörgel, Dr. Sönke Müller and Gesine Böttcher.

Further, I would like to thank all the members of image analysis group from whose discussions I benefited a lot.

I dedicate this achievement to my parents as a minimal return to what they have done for me. I am and will be always grateful to them.

Last but not least, I would like to thank my wife, Nahid, for all the love, peace, encouragement, and inspiration she has brought to me during my study. I feel fortunate to have her in my life. She shares a great part of my achievement.

## Curriculum Vitae

Name	Mehdi Ravanbakhsh
May 12, 1973	Born in Bojnord, Iran
1979-1984	Primary School, Bojnord, Iran
1984-1987	Secondary School, Bojnord, Iran
1987-1992	High School, Bojnord, Iran
1992-1997	Department of Surveying, K.N.Toosi University of Technology, Tehran, Iran  Degree: B.Sc. in Surveying, Geodesy and Photogrammetry
1997-1999	Geomatics Department, Technical Faculty, Tehran University, Tehran, Iran  Degree: M.Sc. in Photogrammetry and Remote Sensing
2000-2001	Teaching Assistant at Islamic Azad University, Tehran, Iran
2001-2004	Lecturer & Supervisor, National Cartographic Center (NCC), Tehran, Iran
2004-2008	Institute of Photogrammetry and GeoInformation (IPI), Leibniz Universität Hannover, Hannover, Germany  Degree: Ph.D. in Photogrammetry and Computer Vision